

A Census of the β Pic Moving Group and Other Nearby Associations with Gaia*

K. L. LUHMAN^{1,2}

¹*Department of Astronomy and Astrophysics, The Pennsylvania State University, University Park, PA 16802, USA; kll207@psu.edu*

²*Center for Exoplanets and Habitable Worlds, The Pennsylvania State University, University Park, PA 16802, USA*

ABSTRACT

I have used the third data release of the Gaia mission to improve the reliability and completeness of membership samples in the β Pic moving group (BPMG) and other nearby associations with ages of 20–50 Myr (Sco Body, Carina, Columba, χ^1 For, Tuc-Hor, IC 2602, IC 2391, NGC 2547). I find that Carina, Columba, and χ^1 For are physically related and coeval, and that Carina is the closest fringe of a much larger association. Similarly, Tuc-Hor and IC 2602 form a coeval population that is spatially and kinematically continuous. Both results agree with hypotheses from Gagné et al. (2021). I have used the new catalogs to study the associations in terms of their initial mass functions, X-ray emission, ages, and circumstellar disks. For instance, using the model for Li depletion from Jeffries et al. (2023), I have derived an age of $24.7^{+0.9}_{-0.6}$ Myr for BPMG, which is similar to estimates from previous studies. In addition, I have used infrared photometry from the Wide-field Infrared Survey Explorer to check for excess emission from circumstellar disks among the members of the associations, which has resulted in a dramatic increase in the number of known disks around M stars at ages of 30–50 Myr and a significant improvement in measurements of excess fractions for those spectral types and ages. Most notably, I find that the W3 excess fraction for M0–M6 initially declines with age to a minimum in BPMG (<0.015), increases to a maximum in Carina/Columba/ χ^1 For ($0.041^{+0.009}_{-0.007}$, 34 Myr), and declines again in the oldest two associations (40–50 Myr). The origin of that peak and the nature of the M dwarf disks at >20 Myr are unclear.

1. INTRODUCTION

The discovery of a large debris disk around the nearby A star β Pic by the Infrared Astronomical Satellite (Smith & Terrile 1984; Aumann 1985) prompted an interest in measuring the age of the system. To do so, Barrado y Navascués et al. (1999) sought to identify additional stars that were born in the same molecular cloud as β Pic by examining the kinematics of stars that appeared to be comoving with it. Using data from the Hipparcos mission and other sources, they concluded that the M stars GJ 799 and GJ 803 were likely members of a moving group associated with β Pic (BPMG). Based on a comparison of the two stars to theoretical isochrones in a color-magnitude diagram (CMD), Barrado y Navascués et al. (1999) estimated an age of 20 ± 10 Myr, which was consistent with other age indicators for the stars. Through similar analysis of kinematics and signatures of youth, Zuckerman et al. (2001b) expanded the proposed membership of BPMG to 18 systems and subsequent studies have reached ~ 100 can-

didate members (Zuckerman et al. 2001b; Song et al. 2003; Kaisler et al. 2004; Zuckerman & Song 2004a; Torres et al. 2006; Lépine & Simon 2009; Teixeira et al. 2009a; Kiss et al. 2011; Schlieder et al. 2010, 2012a,b,c; Liu et al. 2013; Malo et al. 2013; Moór et al. 2013; Binks & Jeffries 2014, 2016; Gagné et al. 2014, 2015, 2018; Riedel et al. 2014; Shkolnik et al. 2017; Gagné & Faherty 2018; Lee & Song 2019; Lee et al. 2022; Stahl et al. 2022; Schneider et al. 2023; Lee et al. 2024). The internal kinematics, lithium abundances, and CMDs of those samples have been used to estimate the age of the association, where most values have ranged between 20–25 Myr (Zuckerman et al. 2001b; Ortega et al. 2002, 2004; Song et al. 2002; Mentuch et al. 2008; MacDonald & Mullan 2010; Yee & Jensen 2010; Binks & Jeffries 2014, 2016; Malo et al. 2014b; Mamajek & Bell 2014; Bell et al. 2015; Herczeg & Hillenbrand 2015; Nielsen et al. 2016; Shkolnik et al. 2017; Crundall et al. 2019; Miret-Roig et al. 2020; Galindo-Guil et al. 2022; Lee et al. 2022; Couture et al. 2023; Jeffries et al. 2023; Lee et al. 2024). Given their youth and proximity, members of BPMG are amenable to studies of primordial and debris disks (Spangler et al. 2001; Kalas et al. 2004; Liu et al. 2004; Chen et al. 2005, 2008; Schneider et al. 2006; Rebull et al. 2008; Plavchan et al. 2009; Schutz et al. 2009; Riviere-Marichalar et al. 2014; Moór et al. 2016, 2020; Binks & Jeffries 2017;

* Based on observations made with the Gaia mission, the Two Micron All Sky Survey, the Wide-field Infrared Survey Explorer, the NASA Infrared Telescope Facility, Cerro Tololo Inter-American Observatory, the Southern Astrophysical Research Telescope, Gemini Observatory, the and the eROSITA instrument on the Spectrum-Roentgen-Gamma mission.

Sissa et al. 2018; Tanner et al. 2020; Adam et al. 2021; Pawellek et al. 2021; Cronin-Coltsmann et al. 2022, 2023) and surveys for brown dwarf and planetary companions (Lowrance et al. 2000; Kasper et al. 2007; Biller et al. 2010; Lagrange et al. 2009, 2010, 2019; Mugrauer et al. 2010; Macintosh et al. 2015; Plavchan et al. 2020; Martioli et al. 2021; Wittrock et al. 2022, 2023; De Rosa et al. 2023; Franson et al. 2023; Mesa et al. 2023).

The Gaia mission is providing high-precision photometry, proper motions, and parallaxes for stars as faint as $G \sim 20$ (Perryman et al. 2001; de Bruijne 2012; Gaia Collaboration et al. 2016), which corresponds to substellar masses in nearby young associations. As a result, Gaia data have made it possible to significantly improve the reliability and completeness of membership catalogs for those associations. In the case of BPMG, Gagné & Faherty (2018) and Lee et al. (2022) have used Gaia to search for new members, each identifying more than 50 candidates. Lee et al. (2024) further assessed the membership of candidates from Gagné & Faherty (2018) and other surveys using Gaia data and radial velocities. Many of the candidates from Gaia lack measurements of age diagnostics or velocities, which are needed for confirmation of membership. In addition, although the available samples of proposed members share a core group of a few dozen stars, the samples can otherwise differ substantially.

In this paper, I attempt to perform a thorough census of BPMG using the third data release of Gaia (DR3, Gaia Collaboration et al. 2021, 2023) in conjunction with photometry, spectroscopy, and radial velocities from other sources. The resulting catalog of adopted members is used to characterize the association’s initial mass function (IMF), age, and disk population. To facilitate the interpretation of the disk census in BPMG, I also present new membership catalogs for additional nearby associations with ages of 20–50 Myr, consisting of Sco Body, Carina, Columba, χ^1 For, Tuc-Hor, IC 2602, IC 2391, and NGC 2547.

2. SEARCH FOR NEW MEMBERS OF BPMG

2.1. Identification of Candidate Members

The following data from Gaia DR3 have been employed in my survey of BPMG: photometry in bands at 3300–10500 Å (G), 3300–6800 Å (G_{BP}), and 6300–10500 Å (G_{RP}); proper motions and parallaxes ($G \lesssim 20$); and radial velocities ($G \lesssim 15$). I have adopted the geometric values of parallactic distances derived by Bailer-Jones et al. (2021) from the Gaia DR3 parallaxes. My survey also utilizes JHK_s photometry from the Point Source Catalog of the Two Micron All Sky Survey (2MASS, Skrutskie et al. 2003, 2006) and photometry at 3.4, 4.6, 12, and 22 μm (W1–W4) from the WISE All-Sky Source Catalog (Cutri et al. 2012a), the AllWISE Source Catalog, and the AllWISE Reject Catalog (Cutri et al. 2013a; Wright et al. 2013) of the Wide-field

Infrared Survey Explorer (WISE, Wright et al. 2010). I use the photometry from AllWISE for most Gaia sources, but a small fraction of the latter have close matches only in one of the other two WISE catalogs (Luhman 2022b). Because of potentially large errors in W1 and W2 for bright stars (Cutri et al. 2012b, 2013b), I have adopted data at $W1 < 8$ and $W2 < 7$ from the All-Sky Catalog instead of AllWISE and I have ignored all W2 data at $W2 < 6$, as done in Esplin et al. (2018).

In my previous surveys of young associations (e.g., Esplin & Luhman 2017; Luhman & Esplin 2020; Luhman 2022a), I have analyzed Gaia astrometry in terms of a “proper motion offset”, which is defined as the difference between the observed proper motion of a star and the motion expected at the celestial coordinates and parallactic distance of the star for a specified space velocity. This metric serves to reduce projection effects, which is important for an association like BPMG that is extended across a large area of sky. In my survey of BPMG, the proper motion offsets are calculated relative to the motions expected for a velocity of $U, V, W = -10, -16, -9 \text{ km s}^{-1}$, which is similar to the median velocity for my final catalog of BPMG members (Section 2.3). If a star’s velocity matches the median velocity and its proper motion and parallax measurements are accurate, it will have a proper motion offset of zero. However, as in any association, the members of BPMG exhibit a spread in velocities. A given deviation from the median velocity will correspond to larger offsets at smaller distances. As a result, since the members of BPMG span a large range of distances (a factor of ~ 10), the spread in their offsets can vary significantly with distance. To remove this effect, I have included a factor of “distance/50 pc” in the proper motion offsets. Since my selection of BPMG candidates is based on clustering of the proper motion offsets, it does not depend on the value of the constant in that factor.

To perform my census of BPMG, I began by compiling proposed members from previous studies (e.g., Bell et al. 2015; Shkolnik et al. 2017; Gagné et al. 2018). Within this sample, I identified likely members based on clustering in (1) proper motion offsets calculated from Gaia DR3 data, (2) ages inferred from Gaia CMDs, and (3) U, V , and W velocities as a function of X, Y , and Z Galactic Cartesian positions, respectively. The UVW velocities were available only for stars that have measurements of radial velocities from Gaia DR3 or other sources (Section 2.3). I then searched Gaia DR3 for additional candidate members that resemble the likely members in terms of the proper motion offsets, CMD ages, and UVW velocities (when available). Since stars with disks can appear underluminous in CMDs, I allowed the selection of underluminous stars if they exhibited infrared (IR) excess emission in WISE photometry. I only considered stars with $\sigma_\pi/\pi < 0.1$ and accurate photometry ($\sigma < 0.1 \text{ mag}$) in both G_{BP} and G_{RP} or in both G and G_{RP} . For fainter candidates that

lacked photometry in G_{BP} and thus could be plotted in only a single Gaia CMD, I required that their positions in IR CMDs from 2MASS and WISE were consistent with membership.

Initially, my search for BPMG candidates was performed for a spatial volume directly surrounding the likely members from previous studies. The search volume was then expanded in most directions until few additional candidates were identified. During this process, I found that the BPMG candidates extended into a volume inhabited by a neighboring group called Sco Body that is located in front of the Sco-Cen OB association (Ratzenböck et al. 2023)¹. The two associations have similar kinematics but different ages (Sections 2.3 and 4.3). Based on close inspection of the CMD ages and spatial distribution of young low-mass stars near the interface of BPMG and Sco Body, my BPMG candidates should have little contamination from the latter at $X < 100$ pc, so that was selected as a boundary for my survey. Beyond that boundary, it becomes increasingly difficult to reliably separate members of BPMG and Sco Body. The final volume for my survey was defined by $-80 \text{ pc} < X < 100 \text{ pc}$, $-50 \text{ pc} < Y < 50 \text{ pc}$, and $-70 \text{ pc} < Z < 20 \text{ pc}$.

For the BPMG candidates, I searched for spectroscopic measurements of age diagnostics (e.g., Li) and radial velocities in data archives and previous studies. I pursued new spectroscopy for some candidates to measure spectral types and age diagnostics (Section 2.2). The UVW velocities calculated from radial velocities and Gaia astrometry and the spectroscopic constraints on age were used to further refine the sample of candidates (Sections 2.2 and 2.3). This process produced 180 objects that I have adopted as members of BPMG. To that sample, I have added three previously proposed members that lack parallax measurements from Gaia DR3 but that have parallax data from other sources, consisting of HD 161460, GJ 3076, and PSO J318.5338–22.8603. I searched for companions to the adopted members that are in Gaia DR3 and that did not satisfy the selection criteria for BPMG membership by retrieving DR3 sources that are within $5''$ of the members and whose available kinematic and photometric data are consistent with companionship, which resulted in the addition of 10 likely companions. These objects were not selected initially because they lacked either parallax measurements or photometry in G_{BP} and G_{RP} . Thus, the final catalog of adopted members contains 193 objects, all of which have entries in Gaia DR3 with the exception of the L dwarf PSO J318.5338–22.8603 (Liu et al. 2013). The catalog does not contain separate entries for the substellar

companions to the following stars since they lack Gaia detections: β Pic (Lagrange et al. 2009, 2010, 2019), PZ Tel (Biller et al. 2010; Mugrauer et al. 2010), 51 Eri (Macintosh et al. 2015), AU Mic (Plavchan et al. 2020; Martioli et al. 2021), and AF Lep (Mesa et al. 2023; Franson et al. 2023; De Rosa et al. 2023).

To illustrate the clustering of the adopted BPMG members in proper motion offsets, I have plotted the latter in Figure 1. The outliers are labeled with their names. They are retained as members because their discrepant motions can be attributed to poor astrometric fits, as indicated by the large values (>1.6) of their renormalized unit weight errors (RUWEs, Lindegren 2018). All of the outliers have close companions or consist of a close pair that is unresolved by Gaia (GJ 3305, Kasper et al. 2007), which makes them susceptible to poor fits. In addition to the adopted members, Figure 1 includes a sample of previous candidates that have been excluded from my catalog, which are discussed in Section 2.4.

In Figure 2, I show the adopted members of BPMG in CMDs consisting of $M_{G_{RP}}$ versus $G_{BP} - G_{RP}$ and $G - G_{RP}$. I have omitted photometry with errors greater than 0.1 mag. Each CMD includes a fit to the single-star sequence of the Pleiades cluster (~ 120 Myr, Stauffer et al. 1998; Dahm 2015). The one star that appears below the sequence in the $G_{BP} - G_{RP}$ CMD is Gaia DR3 6806301370521783552. It is much closer to the lower envelope of the sequence for BPMG (corresponding to single stars) when using photometry from the second data release of Gaia (DR2), so its DR3 photometry is probably erroneous, perhaps because of the presence of a companion at a separation of $1''.45$. As often observed in nearby associations (Luhman 2023b), the CMD in $G - G_{RP}$ for BPMG contains a group of red stars that are much too bright at a given color to be unresolved binaries. Those stars are likely to be marginally resolved binaries in which the G -band fluxes are underestimated (Riello et al. 2021).

2.2. Spectroscopy of Candidates

To measure and refine spectral classifications for candidate members of BPMG, I have obtained spectra for 84 sources and I have analyzed archival spectra for four additional stars. For 58 of these sources, spectroscopy is reported for the first time in this study. The new observations were performed with SpeX (Rayner et al. 2003) at the NASA Infrared Telescope Facility (IRTF), the Goodman spectrograph (Clemens et al. 2004) at the Southern Astrophysical Research Telescope (SOAR), FLAMINGOS-2 at the Gemini South telescope (Eikenberry et al. 2004), and the Cerro Tololo Ohio State Multi-Object Spectro-

¹ Portions of Sco Body have also been identified in other Gaia surveys (e.g., Kerr et al. 2021), as discussed in Ratzenböck et al. (2023).

graph (COSMOS)² at the 4 m Blanco telescope at the Cerro Tololo Inter-American Observatory (CTIO). The archival data were collected with the RC spectrograph at the CTIO 1.5 m telescope through program UR10B-05 (E. Mamajek) and with the Gemini Multi-Object Spectrograph (GMOS; Hook et al. 2004) at the Gemini South telescope through programs GS-2012B-Q-92 (D. Rodriguez) and GS-2012B-Q-70 (J. Gagné). The instruments and observing modes are summarized in Table 1. The instruments and observing dates for individual targets are provided in Table 2.

The spectra from SpeX were reduced with the Spextool package (Cushing et al. 2004), which included a correction for telluric absorption (Vacca et al. 2003). The data from the remaining instruments were reduced with routines within IRAF. Examples of the reduced optical and IR spectra are presented in Figure 3. The reduced spectra are available in an electronic file associated with Figure 3.

For all of the spectroscopic targets, the age diagnostics (e.g., Li, Na, FeH, *H*-band continuum) are consistent with those of other BPMG members that I have adopted. The same is true for the known companions to these sources. As a result, all of the spectroscopic targets are among the adopted members of BPMG in Section 2.3. I measured spectral types from the optical spectra through comparison to field dwarf standards for $<M5$ (Henry et al. 1994; Kirkpatrick et al. 1991, 1997) and averages of dwarf and giant standards for $\geq M5$ (Luhman et al. 1997; Luhman 1999). Classifications of the IR spectra are based on comparisons to standard spectra for young stars and brown dwarfs (Luhman et al. 2017). The resulting spectral types are included in Table 2.

2.3. *UVW Velocities*

For the BPMG candidates from Section 2.1 that have radial velocity measurements, their membership has been further constrained using *UVW* velocities. I have compiled measurements of radial velocities from Gaia DR3 and all other available sources. I have only considered velocities that have errors smaller than 5 km s^{-1} . If a star has multiple velocity measurements, I adopt the velocity with the smallest error. For spectroscopic binaries, I use the system velocities if they have been measured. I have not adopted velocities for the following stars since each has a wide range of values and lacks a measurement of the system velocity: Gaia DR3 6747467431032539008, Gaia DR3 6833291426043854976, RX J0050.2+0837, RX J2137.6+0137, HD 199143, and HD 172555B. I have used the adopted radial velocities in conjunction with proper motions from Gaia DR3 and parallactic distances

based on DR3 parallaxes (Bailer-Jones et al. 2021) to calculate *UVW* velocities (Johnson & Soderblom 1987). The velocity errors were derived in the manner described by Luhman & Esplin (2020) using the python package *pyia* (Price-Whelan 2021).

To illustrate their spatial distribution, I have plotted the adopted members of BPMG that have parallax measurements (i.e., excludes five companions that lack parallaxes) in diagrams of *XYZ* Galactic Cartesian positions in the top row of Figure 4. The members are concentrated in two parallel filaments that are elongated in the *X* direction. In the bottom row of Figure 4, the measurements of *U*, *V*, and *W* are plotted versus *X*, *Y*, and *Z*, respectively, for the 134 stars that have parallax measurements and adopted radial velocities. (One companion lacks parallax data but has a radial velocity measurement). As shown in Figure 4, the adopted members are well clustered in *UVW* versus *XYZ*. I have excluded candidates from Section 2.1 that are discrepant relative to those distributions unless the discrepancies can be explained by poor astrometric fits for companions. The velocity components are correlated with their corresponding spatial dimensions, which indicates the presence of expansion. For the 134 adopted members that have measured *UVW* velocities, the median velocity is $U, V, W = -9.3, -15.6, -9.0 \text{ km s}^{-1}$.

To compare BPMG to neighboring young associations (10–20 Myr), I have plotted *XYZ* and *UVW* for members of BPMG, TW Hya (TWA, Luhman 2023b), 32 Ori (Luhman 2022c), and Sco Body (Section 3) in Figure 5. These diagrams only include stars that have radial velocity measurements. In addition, members that have discrepant velocities because of binarity have been omitted. BPMG and 32 Ori are spatially adjacent but are offset in *U* and *V*. BPMG and Sco Body are adjacent in *X* and *Y*, are offset in *Z*, and have overlapping *UVW* velocities that are consistent with a single pattern of expansion, although their ages differ (Section 4.3). Previous studies have proposed that BPMG, TWA, and Sco Body are related to the Sco-Cen OB association (Mamajek & Feigelson 2001; Mamajek et al. 2002; Ortega et al. 2004; Ratzenböck et al. 2023).

In Table 3, I present a catalog of the 193 sources that I have adopted as members of BPMG, which contains source names from Gaia DR3 and previous studies; equatorial coordinates, proper motion, parallax, RUWE, and photometry from Gaia DR3; measurements of spectral types and the type adopted in this work; adopted measurement of the equivalent width of lithium; distance estimate based on the Gaia DR3 parallax (Bailer-Jones et al. 2021); the adopted radial velocity measurement; the *UVW* velocities calculated in this section; the designations and angular separations of the closest sources within $3''$ from 2MASS and WISE; flags indicating whether the Gaia source is the closest match in DR3 for the 2MASS and WISE sources; photometry from 2MASS and WISE (only for the Gaia source that is

² COSMOS is based on an instrument described by Martini et al. (2011).

closest to the 2MASS/WISE source); and flags indicating whether excesses are detected in three WISE bands and a disk classification (Section 5).

Among the 193 adopted members of BPMG, nine lack spectral classifications and 58 lack accurate radial velocity measurements. The former include seven close companions ($\lesssim 2''$) to classified stars and the latter include the six stars mentioned earlier that have large spreads in their available velocities and seven companions to stars that do have radial velocity data. Both spectral classifications and radial velocities are unavailable for six sources (five close companions). Measurements of spectroscopic age diagnostics and radial velocities for these sources would help to better constrain their membership.

2.4. Comparison to Previous Studies

Many of the previously proposed members of BPMG are included in my catalog, which contains 22/24 from Zuckerman et al. (2001b), 30/34 from Zuckerman & Song (2004a), 38/41 from Torres et al. (2006), 24/30 from Mamajek & Bell (2014), 70/89 from Bell et al. (2015), 48/56 from Gagné et al. (2018), 93/113 from Lee & Song (2019), 24/25 (core) and 39/51 (extended) from Couture et al. (2023), and 69/86 from Lee et al. (2024). These numbers omit companions that are not detected by Gaia. Among the previous candidates that have been excluded from my catalog, I discuss those that (1) have been classified as members by several studies (HR 6070, HR 6749, HR 6750, HIP 12545, HD 14082A/B), (2) are notable for having a late spectral type (2MASS J06085283-2753583, Kirkpatrick et al. 2008; Rice et al. 2010; Faherty et al. 2012), a substellar companion (2MASS 02495639-0557352, Dupuy et al. 2018; Chinchilla et al. 2021), or an edge-on disk (BD+45 598, Hinkley et al. 2021), or (3) have been classified as members by two of the more recent membership studies of BPMG (Gagné et al. 2018; Lee et al. 2024), which corresponds to a total of 24 sources. I have compiled their Gaia data, radial velocities, and UVW velocities in Table 4 and I have plotted their proper motion offsets in Figure 1 and UVW velocities in Figure 4 for comparison to the adopted members. To enable the identification of individual sources in those diagrams, they are plotted with numerals from 1 through 24, which are listed in Table 4. For most velocities, the errors are smaller than the sizes of the numerals in Figure 4.

Relative to the adopted members of BPMG, the A star HR 6070 (1) is an outlier in proper motion offsets (Figure 1) and in U and W (Figure 4). The A stars HR 6749 and HR 6750 (2 and 3) form a $1''.8$ binary system. Both components are modest outliers in proper motion offsets and the former is a modest outlier in U (the latter lacks a radial velocity measurement). The two stars are overluminous relative to the single-star sequence for BPMG in Gaia CMDs (Couture et al. 2023), so membership in BPMG would require that each

is an unresolved binary if the Gaia photometry is reliable. The K star HIP 12545 (4) is an outlier in proper motion offsets, V , and W . HD 14082A and B (5 and 6) are F/G stars in a $14''$ binary system. Their UVW velocities are consistent with membership in BPMG and the primary is near the single-star sequence of BPMG in Gaia CMDs (which is close to the zero age main sequence at that spectral type), but the secondary appears below BPMG’s sequence and coincides with the sequence of Tuc-Hor (~ 40 Myr, Section 3). The Li data for these stars are consistent with BPMG as well as older ages (Mentuch et al. 2008; Jeffries et al. 2023). The Gaia photometry for HD 14082B agrees well between DR2 and DR3, so there is no indication that its photometry is erroneous. It also appears underluminous relative to BPMG in other CMDs like M_{K_s} versus $G_{RP} - K_s$. The late-type object 2MASS J06085283-2753583 (7) is a modest outlier in V and W . 2MASS J02495436-0558015 (8) is an outlier in proper motion offsets and V . BD+45 598 (9) is near the edge of the distribution of proper motion offsets of adopted members and is an outlier in U and V . All of these stars have low values of RUWE that suggest good astrometric fits.

Beyond the aforementioned stars, two proposed members from Gagné et al. (2018) are omitted from my catalog for BPMG. Gaia DR3 2478001486169801216 (10) is an outlier in proper motion offsets, V , and W and is located below the single-star sequence for BPMG. The UVW velocity of Gaia DR3 6400160947954197888 (11) is consistent with membership using DR3 data, but it would be rejected with DR2. For both data releases, the star has a large value of RUWE that indicates a poor astrometric fit and it is slightly below the sequence for BPMG.

The 13 remaining stars in Table 4 were assigned membership by Lee et al. (2024) but are absent from my catalog. Stars 12 through 18 are outliers in their space velocities, as shown in Figure 4. V1311 Ori Aa+Ab (19) is a close binary (Janson et al. 2012) that is unresolved by Gaia. Tokovinin (2022) has proposed that it is a member of a multiple system with four other stars, two of which form a second pair that is unresolved by Gaia (Ba+Bb). The two close pairs have poor fits from Gaia based on their RUWEs, leading to significant differences in proper motions among DR2, DR3, and previous astrometric surveys. Given the uncertainties in those motions and the available parallax and radial velocity measurements (Tokovinin 2022), the six stars could be comoving to the degree expected for a multiple system. In addition, their space velocities are consistent with membership in BPMG. However, a nondetection of lithium in an unresolved spectrum of the B and C components, which are separated by $5''.3$, and strong lithium in the D component are not consistent with the same age (Bell et al. 2017; Jeffries et al. 2023). In addition, the D component appears slightly below the sequence for BPMG. Given the uncertainties in the astrometry for A and B and

these inconsistencies, I have omitted all of the components from my catalog.

Gaia DR3 5412403269717562240 (20) is a modest outlier in U . It is spatially and kinematically closer to TWA than BPMG and was adopted as a member of TWA in [Luhman \(2023b\)](#). The UVW velocity of Gaia DR3 66245408072670336 (21) supports membership but it is located slightly below the BPMG sequence and the nondetection of lithium in data from the ninth data release of the Large Sky Area Multi-Object Fiber Spectroscopic Telescope survey ($\lesssim 0.03 \text{ \AA}$, [Cui et al. 2012](#); [Zhao et al. 2012](#)) seems inconsistent with adopted members of BPMG (Section 4.3). CD-27 11535 (22) is a close binary ([Elliott et al. 2015](#)) that is unresolved by Gaia. It has a parallax measurement from DR2 but not DR3. The available radial velocities span more than 10 km s^{-1} . If a value near the middle of that range is adopted, the space velocity is consistent with membership. The binary appears 1.2 mag above the single-star sequence for BPMG, which would require more than two unresolved components for membership. HD 169405 (23) is a K giant ([Houk 1978](#)), which is incompatible with membership in a young association. Gaia DR3 244734765608363136 (24) is an outlier in proper motion offsets and appears slightly below the sequence for BPMG. Since it has a large range of measured radial velocities and no measurement of the system velocity, I have not calculated its UVW velocity.

One of the stars excluded from the catalog for BPMG, Gaia DR3 175329120598595200 (16), was previously classified as a member of 32 Ori ([Luhman 2022c](#)). Four additional stars also have kinematics and CMD positions that indicate membership in 32 Ori, consisting of 2MASS J02495639-0557352 (8), BD+45 598 (9), Gaia DR3 73034991155555456 (13), and Gaia DR3 5177677603263978880 (15). These stars are located outside of the survey volume for 32 Ori in [Luhman \(2022c\)](#). They are plotted as blue squares in Figure 5, where they represent an extension of the previously identified members of 32 Ori to higher values of X , overlapping spatially with members of BPMG. I adopt these four stars as members of 32 Ori.

In addition to proposed members of BPMG, [Lee et al. \(2024\)](#) presented a sample of rejected candidates, which include five sources that are adopted as members in this work: SCR J0017-6645, GJ3331B, GJ2006A, Gaia DR3 6760846563417053056, and Gaia DR3 6652273015676968832³. The kinematics of GJ3331B are discrepant (Figures 1 and 4), but that is attributable to the presence of a close companion (GJ3331C). The UVW velocities for SCR J0017-6645, GJ2006A, and Gaia DR3 6760846563417053056 support membership. The remaining source, Gaia DR3 6652273015676968832,

lacks a radial velocity measurement. [Gagné & Faherty \(2018\)](#) identified it as a candidate L-type member of BPMG using data from Gaia DR2. I find that it continues to be a promising candidate with Gaia DR3 and I have spectroscopically confirmed that it is a young L dwarf (Section 2.2). It is below the sequence of BPMG members in M_{GRP} versus $G - G_{\text{RP}}$ (below the bottom of the CMD in Figure 2), but its positions in other CMDs that use IR photometry from 2MASS and WISE are consistent with membership (see the CMDs in Section 3). This L dwarf is the second coolest object in my catalog for BPMG.

3. NEW CATALOGS FOR OTHER ASSOCIATIONS

To facilitate the interpretation of the disk population in BPMG (Section 5), I have used Gaia data to produce new catalogs for associations and clusters that bracket the age of BPMG (20–50 Myr) and that have the best available constraints on disk fractions for low-mass stars at those ages given their proximity, numbers of members, and mid-IR imaging, which consist of Sco Body, Carina, Columba, χ^1 For (also known as Alessi 13), Tuc-Hor, IC 2602, IC 2391, and NGC 2547. The adopted members of NGC 2547 are compiled in Table 5. My catalogs for the other associations are included with BPMG in Table 3. In the disk analysis, I also will make use of Gaia-derived membership catalogs for additional associations near that age range ([Luhman 2022a,c, 2023a](#)).

3.1. Sco Body

I have not attempted to identify new members of Sco Body and have only revised the catalog from [Ratzenböck et al. \(2023\)](#) to reduce contamination by nonmembers. That catalog contained 373 sources from Gaia DR3. Five of those stars are among my adopted members of BPMG. Among the remaining 368 stars, I have excluded those that have proper motion offsets or UVW velocities that are inconsistent with membership in Sco Body, CMD positions that are below the sequence for the association (unless mid-IR excess emission is present), or $\sigma_{\pi}/\pi > 0.1$. Since multiple bands of Gaia photometry are needed for an age assessment in CMDs, I have discarded stars from [Ratzenböck et al. \(2023\)](#) that have only a single band of Gaia photometry unless they are probable companions to viable candidates. Through these steps, I have retained 299 of the 373 candidate members of Sco Body. In Figure 2, I have included Gaia CMDs for the adopted members of Sco Body. Based on these CMDs, Sco Body is slightly younger than BPMG (Section 4.3). Gaia DR3 6027365242759490688 is underluminous in the $G_{\text{BP}} - G_{\text{RP}}$ CMD for Sco Body. It exhibits mid-IR excess emission that indicates the presence of a disk ([Luhman 2022b](#)), so its anomalous photometry may be caused by accretion-related emission in G_{BP} or an edge-on disk.

³ [Lee et al. \(2024\)](#) did assign membership to companions of two of these stars, GJ3331A and GJ2006B.

3.2. *Carina, Columba, χ^1 For, Tuc-Hor, IC 2602, IC 2391, and NGC 2547*

I have performed searches for members of several additional associations with methods similar to those that I have applied to BPMG. As with the latter, I have characterized the clustering of members in proper motion offsets, spatial positions, and CMDs using previously proposed members of Carina, Columba (Platais et al. 1998; Torres et al. 2008; Zuckerman et al. 2011; Bell et al. 2015; Gagné et al. 2018; Wood et al. 2023), χ^1 For (Dias et al. 2002; Yen et al. 2018; Cantat-Gaudin et al. 2018; Zuckerman et al. 2019; Galli et al. 2021), Tuc-Hor (Torres et al. 2000; Zuckerman & Webb 2000; Zuckerman et al. 2001a; Kraus et al. 2014; Bell et al. 2015; Gagné et al. 2018), IC 2602, IC 2391 (Randich et al. 2001; Barrado y Navascués et al. 2004; Dobbie et al. 2010; Jackson et al. 2020; Nisak et al. 2022), and NGC 2547 (Naylor et al. 2002; Jeffries et al. 2004; Jackson et al. 2020). Large-scale surveys for young populations in the Milky Way also have identified portions of these associations (Cantat-Gaudin et al. 2018; Kounkel & Covey 2019). I then searched for additional candidate members with Gaia DR3 and further refined their membership using space velocities (for stars that have measured radial velocities) and the available spectroscopy. I analyzed new and archival spectra of 49 candidate members of Tuc-Hor, Carina, IC 2602, and IC 2391. The archival data were taken with GMOS at Gemini South through programs GS-2012B-Q-92, GS-2013B-Q-83 (D. Rodriguez), GS-2012B-Q-70, GS-2013A-Q-66, and GS-2014A-Q-55 (J. Gagné), with the RC spectrograph at the CTIO 1.5 m telescope through program STSI 08b-03, and with the Goodman spectrograph at SOAR. The spectroscopic observations are included in Tables 1–3. Pala et al. (2020) obtained optical spectra for one of the members of χ^1 For, Gaia DR3 5093945085525624448. I have measured a spectral type of M0: from those data.

In Carina, Columba, χ^1 For, Tuc-Hor, and IC 2602, I expanded the survey volumes until few additional candidates were found, as done with BPMG. In my analysis of IC 2391, candidate members are present out to large distances from the cluster in all directions in the XY plane, forming an extended population that has been referred to as a “corona” (Kounkel & Covey 2019; Gagné et al. 2021; Meingast et al. 2021). I have truncated my catalog at a radius of 30 pc, which includes part of the extended population. For NGC 2547, I searched for members that are within a radius of 0.7° from the cluster center and that fall within 24 μm images from the Spitzer Space Telescope (Werner et al. 2004), which are used for the disk census in that cluster (Section 5).

Candidate members of Tuc-Hor from previous studies span distances of 30–80 pc while the IC 2602 cluster has a distance near 150 pc, so the populations have appeared to be well separated. However, they share similar

space velocities and ages, leading Gagné et al. (2021) to propose that they are physically connected. Indeed, I find that Tuc-Hor and IC 2602 do form a single population that is spatially and kinematically continuous. Meingast et al. (2021) identified an extended population of stars associated with IC 2602, many of which are recovered in my census. For the purposes of the catalogs in Table 3, members of Tuc-Hor/IC 2602 that are within 16 pc from the center of IC 2602 are assigned to that cluster while the remaining stars are assigned to Tuc-Hor. That radius approximates the boundary of IC 2602’s density enhancement relative to the entire population.

Gagné et al. (2021) noted that Columba, Carina, and other more distant populations (Platais et al. 1998; Kounkel & Covey 2019) are spatially adjacent and appear to have similar ages and kinematics, indicating that they may be physically connected. In my analysis, I do find that those groups form a single large population that is spatially and kinematically continuous. There is enough of a spatial gap between Columba and the other stars that I continue to list Columba as a separate group. The remaining stars are assigned to a second association, which I have named Carina-Extended (Car-Ext) since its closest fringe corresponds to Carina. The more distant cluster that forms the densest concentration in Car-Ext is known as “a Carinae” (Platais et al. 1998) and Platais 8. The star AB Pic is located at the interface of Columba and Car-Ext (which have similar velocities near that position), so it could be assigned to either one. I have placed it in the catalog for Columba.

Outside of the χ^1 For cluster as defined in previous studies (Zuckerman et al. 2019; Galli et al. 2021), I have identified a sparse, extended distribution of members. Those outer members include the stars i Eri and HD 37852, which have earlier spectral types (B6 and B8) than the star χ^1 For (A1). Nevertheless, I refer to this entire population as the χ^1 For association for continuity with previous work.

The Tuc-Hor/IC 2602 and Car-Ext/Columba complexes overlap spatially but have sufficiently distinct kinematics that they are readily separated with Gaia astrometry. They also have different ages, as discussed in Section 4.3.

For the associations discussed in this section, the numbers of adopted members are as follows: 845 in Car-Ext, 51 in Columba, 287 in χ^1 For, 815 in Tuc-Hor, 516 in IC 2602, 486 in IC 2391, and 300 in NGC 2547. Gaia CMDs for these samples are presented in Figures 6–8. Several stars in the CMDs are underluminous, appearing below the sequences for their associations. Most of them have IR excesses (which is why they were not rejected), so their anomalous photometry may be related to the presence of disks, as mentioned for a similar star in Sco Body (Section 3.1). One underluminous star, Gaia DR3 5176144780975151104 (2MASS J02155892-0929121 C), lacks an IR excess. It is a 3.4 companion with a spectral type of M7 (Bowler et al. 2015). It is much bluer in

$G_{BP} - G_{RP}$ than expected for its spectral type, indicating that the G_{BP} photometry is probably erroneous.

BPMG and Tuc-Hor extend to the closest distances among the populations surveyed in this work, so their samples reach the lowest masses. For those associations, I have plotted two additional CMDs in Figure 9 that use IR photometry from 2MASS and WISE, consisting of M_{K_s} versus $G_{RP} - K_s$ and M_{W2} versus $W1 - W2$. The sequences have well-defined lower envelopes with the exception of the WISE CMD for Tuc-Hor, where some of the faintest and most distant members are subject to larger photometric errors and blending with other stars.

In Figures 10–13, I have plotted XYZ and UVW for the adopted members of Car-Ext, Columba, χ^1 For, Tuc-Hor, IC 2602, and IC 2391. The first three associations are spatially adjacent and follow the same correlations of UVW as a function XYZ . The CMDs and Li data for their low-mass stars are consistent with the same age (Section 4.3). Similarly, the spatial and kinematic data for Tuc-Hor and IC 2602 and their CMD sequences (Section 4.3) demonstrate that they represent a single population. As mentioned earlier, most of the previously proposed members of Tuc-Hor had distances within 80 pc, or $Y > -60$ pc in Figure 12. The available measurements of spectral types and radial velocities are concentrated among those closer members of Tuc-Hor and within IC 2602.

3.3. Argus

An age of 40–50 Myr has been reported for the Argus association (Torres et al. 2008; Zuckerman 2019), so I have considered it for inclusion in this work. Bell et al. (2015) found that available membership samples for Argus had significant contamination from nonmembers, leading them to question the existence of the association. Zuckerman (2019) used data from Gaia DR2 to refine the membership for Argus and concluded that the association does exist.

The catalog from Zuckerman (2019) contains 40 proposed members, 39 of which have parallax data from Gaia DR3. Radial velocity measurements are available for 37 of those 39 stars. I have used the most accurate radial velocities for those 37 stars (Gaia DR3, Wilson 1953; Pourbaix et al. 2004; Riedel et al. 2011; Malo et al. 2014a; Soubiran et al. 2018; Buder et al. 2021; Zúñiga-Fernández et al. 2021) and the astrometry from Gaia DR3 to calculate UVW velocities, which are plotted in Figure 14. The errors are omitted when they are smaller than the symbols. Since previous studies of Argus have noted a possible relationship with IC 2391, I have included in Figure 14 the adopted members of IC 2391 that have small velocity errors (< 0.8 km s $^{-1}$). The Argus members do not show the tight clustering in velocities that is found in IC 2391 and the other associations surveyed in this work. To examine the ages of the Argus stars, I have plotted them in one of the CMDs for IC 2391 in Figure 7. Most of the Argus stars are ear-

lier than K and appear near the main sequence, so the CMD provides poor constraints on their coevality. Ten of the stars are redder than the main sequence turn-on for IC 2391 ($G_{BP} - G_{RP} > 1$), and they do not exhibit a well-defined sequence. Approximately eight of the Argus stars have kinematics and CMD positions that are consistent with IC 2391, all of which are located beyond the 30 pc truncation radius for my IC 2391 catalog. I conclude that those stars may be members of the extended population associated with IC 2391 while the remaining Argus candidates from Zuckerman (2019) are field stars that are unrelated to IC 2391 or each other.

3.4. Old M Stars with IR Excesses

A growing number of low-mass stars with ages of >20 Myr have been found to have mid-IR excesses that indicate the presence of disks (White & Hillenbrand 2005; Hartmann et al. 2005; Gorlova et al. 2007; Balog et al. 2009; Boucher et al. 2016; Silverberg et al. 2016, 2020; Murphy et al. 2018; Zuckerman et al. 2019; Lee et al. 2020; Gaidos et al. 2022; Liu et al. 2022; Luhman 2023a). Some of those stars have been previously assigned membership to nearby associations, one of which is 2MASS J15460752–6258042. Lee et al. (2020) classified it as a member of the Argus association based on its space velocity. Lee et al. (2020) quoted an age of 55 Myr for Argus while Zuckerman (2019) estimated an age of 40–50 Myr. As noted by Lee et al. (2020), the star’s Li absorption is too strong for those ages given its spectral type (M5). Instead, its Li measurement falls near the upper envelope of values for BPMG (Section 4.3). The star is near the single-star sequence for BPMG in the $G - G_{RP}$ CMD and appears slightly below BPMG in $G_{BP} - G_{RP}$ (Figure 2). Given the presence of strong hydrogen emission lines (Lee et al. 2020), the older implied age in the latter CMD may be caused by accretion-related emission in G_{BP} . In that case, both the Li data and CMDs would indicate that the star is roughly coeval with BPMG, and therefore is not as old as reported in Lee et al. (2020). The kinematics do not match those of any of the associations considered in this work.

StH α 34 is a spectroscopic binary in which the components have similar spectral types (M3) and are surrounded by a circumbinary disk (White & Hillenbrand 2005; Hartmann et al. 2005). The system was treated as a member of the Taurus star-forming region in some early studies, but the absence of Li absorption indicated an age older than expected for Taurus members. Gaia data have confirmed that its space velocity is inconsistent with membership in Taurus (Luhman 2018, 2023a). As with 2MASS J15460752–6258042, I have included StH α 34 in the CMDs for BPMG in Figure 2 and in a diagram of Li data for BPMG (Section 4.3). In the CMDs, the unresolved photometry for the system has been reduced by a factor of two. Based on those data, the age of StH α 34 is similar to that of BPMG.

The disk-bearing M stars WISEA J080822.18–644357.3 and 2MASS J06320799–6810419 have been previously classified as members of Carina (Silverberg et al. 2016; Gaidos et al. 2022), and they appear in my census of Car-Ext as well. Silverberg et al. (2020) assigned two additional systems of this kind, WISEA 044634.16–262756.1 and WISEA 094900.65–713803.1, to Columba and Carina, respectively. In my analysis, the former is identified as a member of χ^1 For, which is adjacent to Columba. WISEA 094900.65–713803.1 is a 1".5 binary system in which only one of the components has a proper motion offset that is consistent with Car-Ext membership. The component that is inconsistent with membership appears to have a better astrometric fit based on its lower value of RUWE (1.0 versus 2.6), so the system is not included in my catalog for Car-Ext.

4. PROPERTIES OF STELLAR POPULATIONS

4.1. Initial Mass Functions

As done in my previous work, I can characterize the IMFs in the associations that I have surveyed in terms of their histograms of spectral types. In Figure 15, I have plotted such histograms for the adopted members of BPMG, Car-Ext/Columba, χ^1 For, Tuc-Hor, IC 2602, and IC 2391. For stars that lack spectroscopy, I have estimated spectral types from Gaia and 2MASS photometry in conjunction with the typical intrinsic colors of young stars (Luhman 2022a). Five members of BPMG and Tuc-Hor are too cool ($>L1$) to appear within the range of types shown in Figure 15. Gaia DR3 has a high level of completeness at $G \lesssim 19$ –20 for most of the sky (Boubert & Everall 2020; Fabricius et al. 2021). In each histogram, I have marked the spectral type that corresponds to $G = 19$ for the most distant members of the association. All of the associations have similar distributions of spectral types, each reaching a maximum near M5 ($\sim 0.15 M_\odot$), which resembles other nearby associations and star-forming regions (e.g., Luhman 2022a).

4.2. X-ray Emission

The ratio of X-ray to bolometric luminosity is high for newborn stars and decays on a timescale that varies with stellar mass (Feigelson & Montmerle 1999; Güdel 2004; Johnstone et al. 2021; Getman et al. 2022). As a result, X-ray emission can serve as a signature of youth in surveys for members of young populations (Preibisch & Zinnecker 2001; Preibisch 2003; Getman et al. 2002, 2017; Feigelson & Lawson 2004; Stelzer et al. 2004; Güdel et al. 2007; Feigelson et al. 2013). By imaging the entire sky with good sensitivity and angular resolution, the extended Roentgen Survey with an Imaging Telescope Array (eROSITA) on board the Spectrum-Roentgen-Gamma mission (Predehl et al. 2021) is potentially valuable for assessing the youth of candidate members of nearby associations. eROSITA's first all-sky survey (eRASS1) has provided data for the half of the sky between Galactic longitudes of 179°9442

and 359°9442 (Merloni et al. 2024). Within eRASS1, the single-band catalog (0.2–2.3 keV) offers the best sensitivity, so I have identified the single-band sources that are the closest matches to the adopted members of BPMG selected from Gaia in Section 2.1. The Gaia positions were calculated for an epoch of 2020 and the matching threshold was roughly twice the positional error from eRASS1 (POS_ERR). For close pairs of Gaia sources, only the component closest to the eRASS1 source was matched. The eRASS1 coverage encompasses 110 of the 193 adopted members of BPMG. Among those 110 members, 66 are matched to sources from eRASS1, 13 are companions to matched members, and 31 lack counterparts in eRASS1. For the latter members, I have retrieved the 3σ upper limits for count rates that have been estimated at their celestial coordinates (Tubín-Arenas et al. 2024). I have performed the same matching process to eRASS1 for proposed members of other young associations discussed in this study, consisting of TWA (Luhman 2023b), 32 Ori (Luhman 2022c), 93 Tau (Luhman 2023a), Sco Body, Car-Ext, Columba, χ^1 For, Tuc-Hor, IC 2602, and IC 2391 (Table 3).

X-ray data for populations of young stars are often analyzed in terms of L_X/L_{bol} as a function of optical color or spectral type. As done in Luhman (2022a) for eRASS1 data in Sco-Cen, I have calculated an observational parameter for the BPMG members that is analogous to L_X/L_{bol} and that describes the ratio of X-ray and G_{RP} -band fluxes, consisting of $[\log(\text{count rate}) + 0.4 G_{\text{RP}}]$. In Figure 16, I have plotted that parameter versus $G_{\text{BP}} - G_{\text{RP}}$ for members of BPMG and the other young associations for which I have compiled eRASS1 data. In each association, the eRASS1 detections are well clustered and contain no faint outliers that would represent old nonmembers. None of the upper limits on count rates are significantly below the loci of detections, indicating that the nondetections are consistent with the young ages of the associations. There is little variation among the sequences in Figure 16, which is a reflection of the fact that L_X/L_{bol} for low-mass stars ($\lesssim 1 M_\odot$, $G_{\text{BP}} - G_{\text{RP}} \gtrsim 1$) remains near the saturation level across the age range of these associations (e.g., Güdel 2004; Getman et al. 2022).

In the catalogs in Table 3, I have included designations, position uncertainties, angular separations from Gaia counterparts, and count rates of the matching sources from eRASS1. The 3σ upper limits are provided for nondetections in eRASS1. A given eRASS1 source is listed only for the closest matching Gaia source. eRASS1 count rates and upper limits are absent in Table 3 for Gaia-resolved companions that were not the closest match to the X-ray source and for members that are located in the half of the sky that was not covered by eRASS1.

4.3. Ages

Ages of young associations can be estimated from their internal kinematics, Li depletion boundaries (LDBs), and positions in CMDs (Soderblom et al. 2014). Several studies have derived kinematic ages for BPMG (Ortega et al. 2002, 2004; Mamajek & Bell 2014; Crundall et al. 2019; Miret-Roig et al. 2020; Couture et al. 2023), and such analyses should benefit from the larger size and improved reliability of my catalog. However, I focus on the use of Li and CMDs since they are more readily applied to the associations in this study. For associations that have sufficient Li data, I adopt the ages produced by the empirical model for Li depletion from Jeffries et al. (2023), which is called Empirical AGes from Lithium Equivalent widthS (EAGLES)⁴. For the remaining associations, I derive ages from their sequences of low-mass stars in Gaia CMDs in a way that is calibrated to the LDB ages.

The input for EAGLES consists of effective temperatures and Li equivalent widths for a sample of stars with temperatures between 3000–6500 K. To estimate temperatures for stars in my catalogs in a manner that is consistent with EAGLES, I have derived a relation between $G_{BP} - G_{RP}$ and temperature from the young stars in Jeffries et al. (2023) that were used to develop EAGLES. The Gaia colors were corrected for reddening using the extinctions from Jackson et al. (2022) and the appropriate reddening coefficients⁵. My adopted relation is defined by lines connecting the following points: $(\log T, G_{BP} - G_{RP}) = (3.81, 0.61), (3.71, 1.03), (3.67, 1.25), (3.59, 1.91), (3.55, 2.41), (3.50, 2.92), (3.477, 3.3)$.

I have applied EAGLES to the associations in this study that have sufficient Li measurements. The kinematics of Car-Ext, Columba, and χ^1 For indicate that they have a physical relationship, and their sequences of low-mass stars in the Gaia CMDs are consistent with coevality. The same is true for Tuc-Hor and IC 2602. Therefore, I have derived a LDB age from the combined Li data for Car-Ext, Columba, and χ^1 For, and I have done the same for Tuc-Hor and IC 2602. I have excluded Li data for stars that have IR excesses from disks (Section 5) since $G_{BP} - G_{RP}$ can be affected by accretion-related emission. In Figure 17, I have plotted Li equivalent widths versus $G_{BP} - G_{RP}$ for members of BPMG and other associations. The membership samples for 32 Ori and 93 Tau are from Luhman (2022c) and Luhman (2023a) and their Li data are from previous studies and unpublished spectra (K. Luhman, in preparation). The best-fitting ages from EAGLES are $21.0^{+1.0}_{-0.7}$ (32 Ori), $24.7^{+0.9}_{-0.6}$ (BPMG), 29.3 ± 1 (93 Tau), $33.7^{+2.0}_{-1.9}$ (Car-Ext/Columba/ χ^1 For), $40.0^{+1.9}_{-1.4}$ (Tuc-Hor/IC 2602), and $51.0^{+5.6}_{-3.9}$ Myr (IC 2391). The Li equivalent widths predicted by EAGLES for those ages are indicated by the

curves in Figure 17. In addition, I have applied EAGLES to my adopted members of NGC 2547 using Li data from Jeffries et al. (2023), arriving at an age of 34.9 ± 1.2 Myr. The LDB age for IC 2391 has a large uncertainty because of the small number of Li measurements at $G_{BP} - G_{RP} = 1.4$ –2 (K4–M1). In addition, the two stars with the lowest Li at $G_{BP} - G_{RP} = 1$ –2 (one of which is a low outlier for its color) have a large effect on the age. If they are excluded, the LDB age is 48.7 Myr. Li measurements for additional K and early M stars are needed for a reliable LDB age in IC 2391.

Previous studies have estimated LDB ages for BPMG and some of the other associations in my analysis (e.g., Mentuch et al. 2008; Yee & Jensen 2010; Binks & Jeffries 2014; Mamajek & Bell 2014; Shkolnik et al. 2017; Galindo-Guil et al. 2022). Comparison of my LDB ages to those estimates is complicated by the fact the LDB age for a given association depends on the sample of adopted members, the choice of evolutionary models, and the details of how the models and data are compared. Nevertheless, my LDB ages tend to be similar to earlier estimates. I note that the samples of members can differ substantially among studies. For instance, 60 of the stars adopted as BPMG members by Galindo-Guil et al. (2022) are absent from my catalog.

The high-precision photometry and astrometry from Gaia have reduced contamination from nonmembers in catalogs of young associations and have provided accurate measurements of absolute magnitudes for members, both of which have resulted in tight sequences of low-mass stars in CMDs that can be used to estimate relative ages among associations. As done in Luhman (2023a), I plot in Figure 18 histograms of offsets in $M_{G_{RP}}$ ($\Delta M_{G_{RP}}$) from the median CMD sequence for UCL/LCC for low-mass stars ($G_{BP} - G_{RP} = 1.4$ –2.8) in TWA, Sco Body, BPMG, 93 Tau, Car-Ext, χ^1 For, NGC 2547, Tuc-Hor, IC 2602, and IC 2391. Some of the results from these data are as follows: (1) Sco Body is coeval with UCL/LCC and is younger than BPMG; (2) Car-Ext and χ^1 For are coeval; (3) Tuc-Hor and IC 2602 are coeval; and (4) Car-Ext/ χ^1 For are slightly younger than Tuc-Hor/IC 2602.

In Figure 19, I have plotted the median values of $\Delta M_{G_{RP}}$ versus the LDB ages for 32 Ori, BPMG, 93 Tau, Car-Ext/Columba/ χ^1 For, NGC 2547, Tuc-Hor/IC 2602, and IC 2391. In addition, I have included TWA using its expansion age (Luhman 2023b). For the temperatures and ages in question, theoretical evolutionary models predict that isochrones should fade at a rate approximated by $\Delta M_{\text{bol}}/\Delta \log \text{age} = 1.5$ (Baraffe et al. 2015; Choi et al. 2016; Dotter 2016; Feiden 2016), so I have marked a line in Figure 19 with that slope and an arbitrary intercept. The LDB ages exhibit a steeper slope of ~ 2 . Meanwhile, TWA and the four populations at 30–40 Myr are consistent with the slope predicted by evolutionary models. It is unclear whether the de-

⁴ <https://github.com/robdjeff/eagles>

⁵ <https://www.cosmos.esa.int/web/gaia/edr3-extinction-law>

partures from linearity between the LDB ages and the median ΔM_{GRP} accurately reflect the luminosity evolution or whether they originate from an error in the LDB model. Combining the LDB age for Tuc-Hor/IC 2602, the 0.1 mag offset in M_{GRP} between Tuc-Hor/IC 2602 and IC 2391, and a slope of 1.5, the resulting age for IC 2391 is 47 Myr, which is adopted for the disk analysis (Section 5). Based on the LDB age of 32 Ori and the value of ΔM_{GRP} of Sco Body relative to 32 Ori, I adopt an age of 20 Myr for Sco Body.

5. PROPERTIES OF DISK POPULATIONS

5.1. Measurement of Infrared Excesses

I have used mid-IR data from WISE to search for excess emission from disks among the adopted members of BPMG and the other populations from Section 3. If two Gaia sources from my catalogs have the same WISE source as their closest match, the WISE designation is assigned to both of them in Table 3, but WISE data and disk measurements are listed only for the member that is closest to the WISE source. The same approach is taken for matching to sources from 2MASS. I have visually inspected the AllWISE Atlas images and unWISE images (Lang 2014; Meisner et al. 2019) to check for detections that are false or unreliable, which are flagged in Table 3. For a few stars, the detections in W3 or W4 are shifted noticeably relative to the positions in W1 and W2, and thus are likely arising from a disk-bearing companion or a red background source. If a companion is not detected by Gaia, the latter scenario is more likely, and the shifted long-wavelength detection is flagged as false.

NGC 2547 is more distant than the other populations considered in my disk analysis (383 pc), but most of it was observed with Spitzer (Young et al. 2004; Gorlova et al. 2007; Forbrich et al. 2008), which provided better angular resolution and sensitivity than WISE. The Spitzer images were obtained at 3.6, 4.5, 5.8, and 8.0 μm ([3.6], [4.5], [5.8], [8.0]) with the Infrared Array Camera (IRAC; Fazio et al. 2004) and at 24 μm ([24]) with the Multiband Imaging Photometer for Spitzer (MIPS; Rieke et al. 2004). I have utilized the catalog of IRAC sources from Gorlova et al. (2007) and a new catalog of sources that I have derived from the MIPS images. The IRAC and MIPS data for the members of NGC 2547 are included in Table 5.

As done in my previous surveys of young associations (e.g., Luhman 2022b), I have used W1–W2, W1–W3, and W1–W4 to detect excess emission from disks. Those colors are plotted versus spectral type in Figures 20–27 for Sco Body, BPMG, 93 Tau, Car-Ext/Columba, χ^1 For, Tuc-Hor, IC 2602, and IC 2391, which are in order of age. For stars that lack spectroscopy, spectral types are estimated from photometry. The excess measurements for 93 Tau were presented in Luhman (2023a) and are included in this work for comparison. Although Tuc-Hor and IC 2602 form a single population, their data are shown separately to illus-

trate how the limiting spectral type depends on distance. Spitzer and WISE colors for members of NGC 2547 are shown in Figure 28.

In each mid-IR color in Figures 20–28, stellar photospheres appear as a blue sequence and stars with disk excesses have a wider range of redder colors. Significant color excesses are circled in those diagrams. Flags indicating the presence or absence of excesses in W2, W3, and W4 are included in Table 3. A flag for [24] excesses in NGC 2547 is provided in Table 5. An apparent color excess in a given band is flagged only if all detections at longer wavelengths also show excesses. In other words, a few stars seem to have excesses at a shorter wavelength but lack excess emission in detections at longer wavelengths, so those bands are not flagged for excesses. A few stars in Figures 20–28 are significantly bluer or redder than the photospheric sequence and are not circled as excesses (for the red colors). Most of those stars are blended with other stars, so those deviations from photospheric colors probably reflect erroneous photometry.

The sizes of mid-IR excesses can be used to estimate the evolutionary stages of disks from among the following options: full disk, transitional disk, evolved disk, evolved transitional disk, and debris disk (Kenyon & Bromley 2005; Rieke et al. 2005; Hernández et al. 2007; Luhman et al. 2010; Espaillat et al. 2012). The first four classes apply to primordial disks while debris disks usually contain little or no gas and consist primarily of second-generation dust that is produced by collisions among planetesimals. Stars that lack any detected excess emission are designated as class III (Lada & Wilking 1984; Lada 1987). The mid-IR colors of primordial and debris disks do overlap, so they do not provide definitive classifications. The latter can be refined by measuring spectral energy distributions at higher resolution and at longer wavelengths and by measuring tracers of gas. For the stars that exhibit IR excesses, I initially classified their disks based on the sizes of the excesses in K_s –W3 and K_s –W4 (Luhman & Mamajek 2012; Esplin et al. 2014, 2018). Those classifications were then revised based on other available data. All B/A/F/G stars with excesses are classified as debris systems unless they show evidence of accretion from previous measurements (AK Sco, Jensen & Mathieu 1997). For the M-type stars that have IR excesses in BPMG and the older populations, I list their disks as unclassified given the uncertainty in the nature of disks around low-mass stars at those ages (Section 5.11). Stars that lack mid-IR excesses but show disk emission at far-IR or millimeter wavelengths in previous studies are labeled as debris disks.

5.2. Sco Body

Nineteen members of Sco Body exhibit excesses in the WISE data (Figure 20). Evidence of disks has been previously reported for 15 of those stars (Cruz-Saenz et al. 2014; Liu et al. 2014; Cotten & Song

2016; van den Ancker et al. 2021; Luhman 2022b), which includes the well-studied binary system AK Sco (Jensen & Mathieu 1997). Among the previously known disks, WISEAJ 164656.06–324254.3 is the counterpart for a 3''9 binary system in which the primary dominates in W1 and W2 and the disk-bearing secondary dominates in W4. One of the four stars with newly identified excesses, Gaia DR3 5976613675832060288, has only a tentative detection of an excess in a single band (W3). A second of those four stars, Gaia DR3 5962199593783949952, has a tentative excess in W2, lacks detections in W3 and W4, and has excesses at [4.5], [5.8], and [8.0] in archival IRAC data (Benjamin et al. 2003; Churchwell et al. 2009).

5.3. BPMG

The WISE data detect IR excesses for 11 members of BPMG (Figure 21). One of those systems is the K star V4046 Sgr, which has a well-known primordial disk (de la Reza et al. 1986; Jensen & Mathieu 1997; Rosenfeld et al. 2013). The late-M member Gaia 6752579812206787968 (WISEA J193555.98–284635.0) is known to have an excess in W2 (Liu et al. 2016), and I find that it has an excess in W3 as well. With a distance of 57 pc, it is one of the closest known brown dwarfs with a circumstellar disk. The remaining nine stars with IR excesses have early spectral types (A/F/G) and have been found to have debris disks in previous studies (Smith & Terrile 1984; Aumann 1985; Coté 1987; Patten & Wilson 1991; Mannings & Barlow 1998; Zuckerman & Song 2004b; Chen et al. 2008; Rebull et al. 2008; McDonald et al. 2012; Cotten & Song 2016).

Ten members of BPMG lack mid-IR excess emission but have been classified as debris systems in previous work based on observations at longer wavelengths, which consist of 51 Eri, GJ 182, AF Lep, AG Tri, AU Mic, AT Mic, GJ2006A, HD160305, CPD–72 2713, and GSC 07396-00759 (Spangler et al. 2001; Kalas et al. 2004; Liu et al. 2004; Zuckerman & Song 2004b; Chen et al. 2005; Carpenter et al. 2008; Rebull et al. 2008; Plavchan et al. 2009; Riviere-Marichalar et al. 2014; Moór et al. 2016; Sissa et al. 2018; Moór et al. 2020; Tanner et al. 2020; Adam et al. 2021; Cronin-Coltsmann et al. 2022, 2023). For most of the stars, disk emission has been spatially resolved or detected at high significance at multiple wavelengths. Plavchan et al. (2009) reported an excess in [24] MIPS images for AT Mic, but an excess is not present in the [24] photometry measured by Chen et al. (2005) or in the W4 photometry (Figure 21). Excess emission has been detected from AT Mic in a single millimeter band with a significance of 8σ (Cronin-Coltsmann et al. 2023). Patel et al. (2014) identified an excess in W4 for 51 Eri while none was found in [24] MIPS images by Rebull et al. (2008) nor in my analysis of the W4 data. Photometry of 51 Eri at 70 and 100 μm from

the Herschel Space Observatory (Pilbratt et al. 2010) has detected small excesses with a significance of $\sim 4 \sigma$ (Riviere-Marichalar et al. 2014). GJ 182 has single 4σ detection of excess emission at 850 μm (Liu et al. 2004). Given the lower significance of their excess measurements, 51 Eri and GJ 182 are assigned disk classes of “debris?” in Table 3.

The M star Gaia DR3 4067828843907821824 appears to have excess emission in W4, but [24] images from MIPS reveal the presence of extended emission, which likely contaminates the W4 measurement (Gutermuth et al. 2015). A color excess is not present in W1–[24].

5.4. 93 Tau

As found in Luhman (2023a), seven members of 93 Tau have excesses in WISE bands (Figure 22). Five B/A/G stars and one M star have W4 excesses. The M star also has excess emission in W2 and W3. An additional M star exhibits a small excess in W3 and a nondetection in W4.

5.5. Carina-Extended and Columba

Forty members of Car-Ext and Columba have excess emission in the WISE data (Figure 23), 12 of which have had excesses reported in previous work (Mannings & Barlow 1998; Spangler et al. 2001; Rieke et al. 2005; Rhee et al. 2007; Zuckerman et al. 2011; McDonald et al. 2012, 2017; Zuckerman & Song 2012; Cotten & Song 2016; Silverberg et al. 2016; Sgro & Song 2021; Gaidos et al. 2022). Excesses are present in W4 for 13 B/A/F/G stars, five of which also have small W3 excesses. The remaining 27 stars with excesses have M types based on spectroscopy or photometry, which include three stars that were known to have excess emission: WISEA J080822.18–644357.3 (Silverberg et al. 2016; Murphy et al. 2018), WISEA J065648.22–582511.4 (Sgro & Song 2021), and WISEA J063207.99–681041.6 (Gaidos et al. 2022). Ten of the M stars with excesses are underluminous in the Gaia CMDs (Figure 6). Two M stars appear to have W3 excesses in Figure 23 but are not flagged for excesses because their W3 detections have very low signal-to-noise ratios (S/Ns). Two of the new M-type WISE sources with excesses, WISEA J095041.19–714659.9 and WISEA J084828.32–594114.1, are resolved as 2'' binaries by Gaia. In each system, the excess emission appears to originate from the secondary based on inspection of the WISE images. Since the primaries dominate the unresolved W1 photometry for each system, the excesses implied by W1–W3 and W1–W4 for those secondaries are underestimated.

5.6. χ^1 For

Nineteen members of χ^1 For have IR excess emission in the WISE data (Figure 24), 15 of which

have been previously identified as showing evidence of disks (Zuckerman & Song 2004b; Moór et al. 2006; Rhee et al. 2007; McDonald et al. 2012; Rodriguez et al. 2013; Wu et al. 2013; Cotten & Song 2016; Zuckerman et al. 2019; Silverberg et al. 2020; Galli et al. 2021). Seven B/A/F stars have excesses in W4, one of which also has a tentative excess in W3. Twelve M stars exhibit excess emission in W3, some of which also have excesses in W2 or W4. The four new disks have M types based on spectroscopy or photometry, two of which are underluminous in the Gaia CMDs (Figure 6). The latter two stars have UV detections from the Galaxy Evolution Explorer (Bianchi et al. 2017) and one of them, Gaia DR3 5093945085525624448, has intense emission lines from hydrogen and other species in an optical spectrum from Pala et al. (2020) and in archival optical and IR data from the X-shooter spectrograph (Vernet et al. 2011) at the Very Large Telescope, which were obtained through program 109.234F (I. Pelisoli). Zuckerman et al. (2019) reported IR excesses in WISE bands for seven additional members, but they lack excesses in my analysis.

The F star HD 23380 has photospheric emission in the WISE bands but has an excess in 70 μ m data from Herschel (Zuckerman et al. 2019).

5.7. Tuc-Hor

Seventeen members of Tuc-Hor have excess emission in WISE photometry (Figure 25). Evidence of disks has been previously reported for seven of those stars (Oudmaijer et al. 1992; Smith et al. 2006; Zuckerman et al. 2011; Donaldson et al. 2012; Patel et al. 2014; Boucher et al. 2016; Cotten & Song 2016; Silverberg et al. 2016; Higashio et al. 2022). Eleven A/F/G stars have small excesses in W4 and two K stars have small excesses in W3 and nondetections in W4. Three M stars have excesses, which are new detections of disks. One of the M stars, Gaia DR3 5291374733442587520, is underluminous in the Gaia CMDs. The L dwarf 2MASS J02265658–5327032 has a small and tentative excess in W3 and a marginal detection in W4 ($S/N \sim 3$), but a previous detection of Pa β emission supports the presence of an accretion disk (Boucher et al. 2016).

Seven members of Tuc-Hor lack excess emission in WISE bands but exhibit it in 70 μ m data from Spitzer and Herschel (Zuckerman et al. 2011; Donaldson et al. 2012).

5.8. IC 2602

Excesses are detected by WISE for 17 members of IC 2602 (Figure 26), 10 of which have had evidence of disks in previous studies (Rieke et al. 2005; Su et al. 2006; McDonald et al. 2012; Rizzuto et al. 2012). Twelve B/A/F stars have small excesses in W4, six of which also have small W3 excesses. The F star HD 91042 has a small excess in W3 and an unreliable detection in W4

due to extended emission. Four M stars have excesses in W3, some of which also have excesses in W2 or W4. All of these M stars are among the new detections of disks. One of the M stars, Gaia DR3 5237543979881486720, appears below the sequence for IC 2602 in the Gaia CMDs (Figure 7).

5.9. IC 2391

Two members of IC 2391 have excess emission in the WISE bands (Figure 27). The A star HD 72323 has a small excess in W4, which has been reported in previous work (Cotten & Song 2016). The M star Gaia DR3 5318492744638910848 has large excesses in both W3 and W4. In addition, it appears within the IRAC and MIPS images from Siegler et al. (2007). I find that excesses are present in the [8.0] and [24] bands from those observations. The excess emission for this star is newly identified in this work.

The Spitzer images from Siegler et al. (2007) encompass a small fraction of the members of IC 2391 near the cluster center. That study reported [24] excesses for seven of the stars in my catalog. In my analysis of the W1–[24] colors using [24] measurements from the Spitzer Enhanced Imaging Products Source List, I find excesses for two of those stars, which have spectral types of A7 and F3. Both lack significant excesses in W4, which has lower S/N than [24]. For the seven stars, I have assigned the W4 excess flags in Table 3 based on my results from [24] and I have used [24] in place of W4 in Figure 27.

5.10. NGC 2547

Previous studies have used photometry from Spitzer to search for IR excesses among members of NGC 2547 (Young et al. 2004; Gorlova et al. 2007; Forbrich et al. 2008). Those studies have identified several early-type members with excesses in [24] data from MIPS. I have not measured [24] photometry for three of those stars (HD 68451, HD 68496 HD 68396) because their emission is extended (Forbrich et al. 2008), so they are absent from the W1–[24] diagram in Figure 28. The remaining early-type members form a broad locus in W1–[24] in which I cannot reliably distinguish between stellar photospheres and stars with small excesses. Therefore, I do not report a measurement for the [24] excess fraction for those spectral types in NGC 2547 (Section 5.11). Large [24] excesses are present among three M stars, consisting of 2MASS J08093547–4913033 (ID7 in Gorlova et al. (2007)), 2MASS J08090344–4859210, and 2MASS J08085407–4921046. The excess for the first star was identified in all three of the previous Spitzer studies. The disk emission from that star was studied in more detail through mid-IR spectroscopy with Spitzer (Teixeira et al. 2009b). Gorlova et al. (2007) noted the [24] excess for 2MASS J08090344–4859210, who discussed the uncertainty in its membership in NGC 2547. I find that the astrometry from Gaia

support membership. The third M star, 2MASS J08085407–4921046, was found to have a [24] excess in Forbrich et al. (2008). The S/N for its [24] detection is low (~ 5).

The G star 2MASS J08090250–4858172 (ID8 from Gorlova et al. (2007)) has a large excess in [24] and excess emission at shorter wavelengths (Gorlova et al. 2007). Photometric monitoring with Spitzer has revealed significant variability in the emission from the disk (Meng et al. 2012; Su et al. 2019). Previous studies have treated the star as a member of NGC 2547, but I find that the proper motion and parallax from Gaia DR3 and the radial velocity (Sacco et al. 2015) are inconsistent with membership. The value of RUWE from Gaia DR3 is low, so there is no indication that the discrepancy in the Gaia astrometry is caused by a poor astrometric fit.

5.11. Excess Fractions

It has been difficult to measure accurate excess fractions for low-mass stars ($0.1\text{--}0.5 M_{\odot}$) at ages of >20 Myr because the associations that are close enough for their low-mass stars to be detected by WISE have had only small samples of reliable members, as in the case of BPMG. Data from Gaia have now made it possible to significantly expand those membership catalogs and improve their reliability, enabling better constraints on the excess fractions for low-mass stars at older ages.

Disk surveys in clusters and associations typically report excess fractions for individual IR bands or disk fractions based on excesses across multiple bands. In this work, I calculate excess fractions for W3 and W4. [24] data from Spitzer are included with W4 when available (Upper Sco, BPMG). Excess/disk fractions are often measured separately for primordial and debris disks, particularly at early spectral types where the disks are more likely to have adequate data (e.g., gas tracers) for discrimination between the two disk types. I do not attempt such discrimination in my excess fractions given the uncertainty in the nature of the M star disks in this study. I calculate excess fractions for the following three ranges of spectral types: B/A/F, G/K, and M0–M6.

With the exception of unresolved companions, all of the adopted members of the associations in this study are detected in W1 and W2, but the WISE data are increasingly incomplete at longer wavelengths, later spectral types, smaller excesses, and larger distances. To be meaningful, the excess fractions should be calculated in a way that accounts for the incompleteness. Ideally, one would consider only spectral type ranges in which nearly all members of a given association are detected for the band in question, but I have adopted more relaxed constraints to allow the calculation of excess fractions for more bands and spectral types. Namely, if a star is not detected in a given band and the typical magnitude limit indicates that any excess is smaller than ~ 1 mag, the star is counted as not having an excess.

I have adopted limits of W3=11.5 and W4=8.0, which correspond to S/N=5 in the AllWISE Source Catalog (Cutri et al. 2013b). To calculate an excess fraction, I require that at least 75% of the members in a given spectral type range are detected in the WISE band or have the aforementioned limits on excesses. That percentage was $>95\%$ for most of the excess fractions. Members that are not detected by WISE and that lack useful limits are excluded from the excess fractions. The W3 and W4 excess fractions for BPMG and other associations at 10–50 Myr are presented in Table 6. In addition to the associations surveyed in this work, I have included TWA (Luhman 2023b), 32 Ori (Luhman 2022c), Upper Sco, UCL/LCC (Luhman 2022b), and 93 Tau (Luhman 2023a). The statistical errors in the excess fractions are taken from Gehrels (1986).

The ages in Table 6 consist of the LDB values from Section 4.3 when available. I have adopted 10, 11, and 20 Myr for TWA, Upper Sco and UCL/LCC, respectively (Luhman & Esplin 2020; Luhman 2023b), and 20 Myr for Sco Body (Section 4.3).

I do not report excess fractions for NGC 2547 at earlier types for reasons mentioned in Section 5.10. Too few M-type members are detected in W3 and [24] for calculating excess fractions. The detection of three M stars with [24] excesses when the sensitivity to M stars is poor suggests that their excess fraction could be high enough to be consistent with those in the closer associations at similar ages like Car-Ext.

Many studies have examined excess fractions as a function of age, both for primordial disks and debris disks, in an attempt to study disk evolution, particularly at earlier spectral types (Haisch et al. 2001; Rieke et al. 2005; Hernández et al. 2007; Siegler et al. 2007; Meyer et al. 2008; Balog et al. 2009; Mamajek 2009; Gáspár et al. 2009, 2013; Cloutier et al. 2014; Ribas et al. 2015; Meng et al. 2017; Richert et al. 2018; Chen et al. 2020). In Figure 29, I have plotted excess fractions from Table 6 versus the ages of the associations. For clarity, I have included only the fractions that have the smallest errors at a given age, which means omitting TWA, 32 Ori, and Sco Body in favor of Upper Sco and UCL/LCC in most of the diagrams in Figure 29. For W4 at M0–M6, only TWA and Tuc-Hor are close enough for a constraint on the excess fraction. As a reminder, stars that lack excesses in the WISE bands can have excesses at longer wavelengths, as mentioned for BPMG in Section 5.3 (e.g., AU Mic).

Since some disks have excess emission in W4 but not W3, the former is more sensitive to disks when it is available. Among B/A/F stars, the W4 excess fraction has a marginally significant maximum in BPMG, is roughly constant for the other associations at 10–40 Myr, and is lower at the older age of IC 2391. Most of the disks for these early-type stars have been previously classified as debris disks. At G/K types, a substantial number of the disks in Upper Sco are likely to be primordial

(Luhman 2022b) while debris disks should dominate for the older associations. Among the G/K stars at >10 Myr, a peak with marginal significance is once again found for BPMG. For the M stars, the analysis of excess fractions versus age is restricted to W3. In that band, the excess fraction for M stars exhibits a steady decline from Upper Sco to UCL/LCC to BPMG. The latter does not have any M0–M6 members with W3 excesses, and the resulting upper limit on their abundance is quite small. However, the W3 fraction increases at older ages, reaching a peak in Car-Ext/Columba/ χ^1 For, and drops to a lower level in the oldest two associations. This variation in an excess fraction for M stars at 25–50 Myr has been observed for the first time in this study. In their comparison of earlier membership samples for χ^1 For and Tuc-Hor (which they believed were coeval), Zuckerman et al. (2019) did note that χ^1 For appeared to have a significantly higher disk fraction, providing a hint of the peak now detected in Car-Ext/Columba/ χ^1 For. Meanwhile, BPMG is distinct from the other associations in that it contains both the highest excess fraction for early-type stars and the lowest fraction for M stars.

The W3 excess fractions for M stars are suggestive of two populations of disks, decaying primordial disks at 10–20 Myr and a second class of disks arising at older ages, possibly debris disks. In this scenario, the peak for M stars at 34 Myr could be a delayed version of the peak among B/A/F stars at 25 Myr in BPMG. That delay might be related to the longer lifetimes observed for primordial disks of low-mass stars (Carpenter et al. 2006; Luhman 2022b). However, several of the M stars with IR excesses are underluminous in CMDs, indicating that they have blue excess emission from accretion or scattered light from edge-on disks, both of which would seem to require primordial disks rather than debris disks. In addition, some of these stars have detections of UV emission and strong hydrogen emission lines (Section 5.6), which are not observed in debris disks (Wyatt 2008; Matthews et al. 2014; Hughes et al. 2018). WISEA J080822.18–644357 has one of the few disks among older M stars that has been studied in detail. Hydrogen emission lines indicate the presence of accretion (Murphy et al. 2018) but millimeter observations of CO and dust emission are more suggestive of a debris disk (Flaherty et al. 2019).

Given the relatively large number of M star disks that are now available at ages of >20 Myr, it is possible to perform systematic studies of their nature. However, most of these systems have few data available beyond Gaia and WISE. Studies of the disks would benefit from spectral classifications of the stars, measurements of radial velocities for membership confirmation, observations of gas and accretion tracers, and millimeter continuum measurements for estimating dust temperatures and masses. Observations at high angular resolution would also help to constrain the disk radii and better

assess whether background objects are responsible for mid-IR excesses detected by WISE.

6. CONCLUSIONS

I have sought to improve the reliability and completeness of membership samples in BPMG and other nearby associations with ages of 20–50 Myr using photometry, astrometry, and radial velocities from Gaia DR3 and data from other sources, including new and archival spectra. I have used the new catalogs to study these associations in terms of their IMFs, X-ray emission, ages, and circumstellar disks. The results are summarized as follows:

1. The Carina association as defined in previous studies is spatially and kinematically continuous with more distant populations, such as the “a Carinae” cluster (Platais 8). I have treated these stars as a single association, which I have named Carina-Extended (Car-Ext). Columba, χ^1 For, and Car-Ext are spatially adjacent and have similar kinematics and ages, indicating that they are physically related. Similarly, I find that Tuc-Hor and IC 2602 form a coeval population that is spatially and kinematically continuous. These results are consistent with hypotheses from Gagné et al. (2021).
2. In the catalogs presented in this work, the numbers of adopted members are 193 in BPMG, 299 in Sco Body, 845 in Car-Ext, 51 in Columba, 287 in χ^1 For, 815 in Tuc-Hor, 516 in IC 2602, 486 in IC 2391, and 300 in NGC 2547. Most of these catalogs are significantly larger than previous samples of likely members (a factor of ~ 2 –4 for BPMG).
3. The distances of the BPMG members range from 10 to 105 pc and have a median value of 51 pc. The catalog includes a few objects that have non-Gaia parallaxes, such as the L dwarf PSO J318.5338–22.8603 (Liu et al. 2013), and several probable companions that lack parallax measurements. One of the adopted members that has new spectroscopy is Gaia DR3 6652273015676968832, which is classified as an early L dwarf, making it the second coolest object in my catalog for BPMG. *UVW* velocities have been calculated for 134 adopted members, which show evidence of expansion in *X* and *Y*. Among the 193 BPMG members, nine lack spectral classifications (seven are close companions) and 58 lack accurate radial velocity measurements. Their membership could be better constrained with measurements of spectral signatures of youth and radial velocities.
4. I classify four previous BPMG candidates as members of 32 Ori, which include BD+45 598 and 2MASS J02495639–0557352. The former has an edge-on disk (Hinkley et al. 2021) and the latter

- has a substellar companion (Dupuy et al. 2018) with strong H α emission (Chinchilla et al. 2021).
5. The proposed members of Argus from Zuckerman (2019) do not exhibit the tight clustering of *UVW* velocities expected for a young association. Also, the low-mass stars in that sample do not form a well-defined sequence in Gaia CMDs. Roughly 20% of those stars have kinematics and CMD positions that are consistent with membership in the extended population associated with IC 2391 while the remaining candidates appear to be unrelated field stars.
 6. I have constructed histograms of spectral types based on spectroscopy and photometry for BPMG and the other associations in this study. For each association, the distribution reaches a maximum near M5 ($\sim 0.15 M_{\odot}$), which resembles data for other nearby associations and star-forming regions.
 7. For each association, I have compiled the available X-ray counterparts from eROSITA’s eRASS1 catalog. As found in previous X-ray studies of young stars, the ratio of X-ray and optical fluxes exhibits a well-defined distribution as a function of optical color that is similar among the associations. Within the half of the sky covered by eRASS1, none of the adopted members of the associations have X-ray detections or limits that would indicate that they are too old to be members.
 8. I have used the EAGLES model for Li depletion (Jeffries et al. 2023) to estimate LDB ages for associations surveyed in this study and others that are included in the disk analysis (32 Ori, 93 Tau). The resulting ages are $21.0^{+1.0}_{-0.7}$ (32 Ori), $24.7^{+0.9}_{-0.6}$ (BPMG), 29.3 ± 1 (93 Tau), $33.7^{+2.0}_{-1.9}$ (Car-Ext/Columba/ χ^1 For), 34.9 ± 1.2 (NGC 2547), $40.0^{+1.9}_{-1.4}$ (Tuc-Hor/IC 2602), and $51.0^{+5.6}_{-3.9}$ Myr (IC 2391). The LDB age for IC 2391 is poorly constrained, and its CMDs relative to those of Tuc-Hor/IC 2602 suggests an age ~ 47 Myr. A similar comparison to the CMDs of 32 Ori indicates an age of ~ 20 for Sco Body.
 9. I have used mid-IR photometry from WISE to check for excess emission from circumstellar disks among the members of the associations. Excesses are detected in the WISE photometry for 125 sources, 71 of which have had evidence of disks in previous studies. Most notably, this work has dramatically increased the number of known M stars at ages of 30–50 Myr that exhibit IR excesses. For instance, 39 stars of this kind are present in Car-Ext/Columba/ χ^1 For. In addition, I have performed similar analysis of Spitzer data in NGC 2547, where I have recovered previously reported excess emission for three M stars (Young et al. 2004; Gorlova et al. 2007; Forbrich et al. 2008).
 10. Because of their sizes and reliability, the new membership samples have enabled significantly improved measurements of IR excess fractions for the associations in question, which is particularly important for constraining the presence of disks among older M stars. I have calculated excess fractions in W3 and W4 for each association in three ranges of spectral types (B/A/F, G/K, M0–M6), as allowed by the sensitivity of the WISE data. I have included excess fractions measured from previous disk surveys in other nearby associations with ages of 10–30 Myr, consisting of TWA, 32 Ori, Upper Sco, UCL/LCC, and 93 Tau (Luhman 2022b,c, 2023a,b). I have examined the excess fractions as a function of age. Among B through K stars, the W4 excess fraction has a marginally significant maximum in BPMG. Most of those disks have been previously classified as debris disks. For the M stars, W4 excess fractions can be calculated in only a few associations, but accurate fractions are available in W3. The W3 excess fraction for M stars exhibits a steady decline from Upper Sco to UCL/LCC to BPMG, where the latter has a stringent upper limit (<0.015). The W3 fraction then increases at older ages, reaching a peak in Car-Ext/Columba/ χ^1 For ($0.041^{+0.009}_{-0.007}$), and drops to a lower level in the oldest two associations. This peak has not been previously detected. Its origin and the nature of the M star disks at >20 Myr (primordial vs. debris) are unclear.

I thank Robin Jeffries for advice regarding the use of his lithium depletion model and I thank Konstantin Getman for helpful discussions. This work used data from the European Space Agency mission Gaia (<https://www.cosmos.esa.int/gaia>), processed by the Gaia Data Processing and Analysis Consortium (DPAC, <https://www.cosmos.esa.int/web/gaia/dpac/consortium>). Funding for the DPAC has been provided by national institutions, in particular the institutions participating in the Gaia Multilateral Agreement. The IRTF is operated by the University of Hawaii under contract 80HQTR19D0030 with NASA. The data at SOAR and CTIO were obtained through programs 2020B-0049, 2022A-595242, and 2024A-657954 at NOIRLab. CTIO and NOIRLab are operated by the Association of Universities for Research in Astronomy under a cooperative agreement with the NSF. SOAR is a joint project of the Ministério da Ciência, Tecnologia e Inovações do Brasil, the US National Science Foundation's NOIRLab, the University of North Carolina at Chapel Hill, and Michigan State University. The Gemini data were obtained through programs GS-2012B-Q-70, GS-2012B-Q-92, GS-2013A-Q-66, GS-2013B-Q-83, GS-2014A-Q-55, and GS-2024A-FT-109. Gemini Observatory is a program of NSF's NOIRLab, which is managed by the Association of Universities for Research in Astronomy (AURA) under a cooperative agreement with the National Science Foundation on behalf of the Gemini Observatory partnership: the National Science Foundation (United States), National Research Council (Canada), Agencia Nacional de Investigación y Desarrollo (Chile), Ministerio de Ciencia, Tecnología e Innovación (Argentina), Ministério da Ciência, Tecnologia, Inovações e Comunicações (Brazil), and Korea Astronomy and Space Science Institute (Republic of Korea). 2MASS is a joint project of the University of Massachusetts and IPAC at Caltech, funded by NASA and the NSF. WISE is a joint project of the University of California, Los Angeles, and the JPL/Caltech, funded by NASA. The Spitzer Space Telescope was operated by JPL/Caltech under contract with NASA. This work used data from the NASA/IPAC Infrared Science Archive, operated by Caltech under contract with NASA, and the VizieR catalog access tool and the SIMBAD database, both operated at CDS, Strasbourg, France. SRG is a joint Russian-German science mission supported by the Russian Space Agency (Roskosmos), in the interests of the Russian Academy of Sciences represented by its Space Research Institute (IKI), and the Deutsches Zentrum für Luft- und Raumfahrt (DLR). The SRG spacecraft was built by Lavochkin Association (NPOL) and its subcontractors, and is operated by NPOL with support from the Max Planck Institute for Extraterrestrial Physics (MPE). The development and construction of the eROSITA X-ray instrument was led by MPE, with contributions from the Dr. Karl Remeis Observatory Bamberg & ECAP (FAU Erlangen-Nuernberg), the University of Hamburg Observatory, the Leibniz Institute for Astrophysics Potsdam (AIP), and the Institute for Astronomy and Astrophysics of the University of Tübingen, with the support of DLR and the Max Planck Society. The Argelander Institute for Astronomy of the University of Bonn and the Ludwig Maximilians Universität München

REFERENCES

- Abdurro'uf, Accetta, K., Aerts, C., et al. 2022, *ApJS*, 259, 35
- Abt, H. A., & Morrell, N. I. 1995, *ApJS*, 99, 135
- Adam, C., Olofsson, J., van Holstein, R. G., et al. 2021, *A&A*, 653, A88
- Alcalá, J. M., Terranegra, L., Wichmann, R., et al. 1996, *A&AS*, 119, 7
- Allers, K. N., Gallimore, J. F., Liu, M. C., & Dupuy, T. J. 2016, *ApJ*, 819, 133
- Allers, K. N., & Liu, M. C. 2013, *ApJ*, 772, 79
- Artigau, É., Gagné, J., Faherty, J., et al. 2015, *ApJ*, 806, 254
- Aumann, H. H. 1985, *PASP*, 97, 885
- Bailer-Jones, C. A. L., Rybizki, J., Fouesneau, M., Demleitner, M., & Andrae, R. 2021, *AJ*, 161, 147
- Bailer-Jones, C. A. L., Rybizki, J., Fouesneau, M., Mantelet, G., & Andrae, R. 2018, *AJ*, 156, 58
- Bailey, John I., III, White, Russel J., Blake, Cullen H., et al. 2012, *ApJ*, 749, 16
- Balog, Z., Kiss, L. L., Vinkó, J., et al. 2009, *ApJ*, 698, 1989
- Bar, I., Vreeswijk, P., Gal-Yam, A., Ofek, E. O., & Nelemans, G. 2017, *ApJ*, 850, 34
- Baraffe, I., Horneier, D., Allard, F., & Chabrier, G. 2015, *A&A*, 577, 42
- Barrado y Navascués, D., Stauffer, J. R., & Jayawardhana, R. 2004, *ApJ*, 614, 386
- Barrado y Navascués, D., Stauffer, J. R., Song, I., & Caillault, J.-P. 1999, *ApJ*, 520, L123
- Bell, C. P. M., Mamajek, E. E., & Naylor, T. 2015, *MNRAS*, 454, 593
- Bell, C. P. M., Murphy, S. J., & Mamajek, E. E. 2017, *MNRAS*, 468, 1198
- Benjamin, R. A., Churchwell, E., Babler, B. L., et al. 2003, *PASP*, 115, 953
- Bianchi, L., Shiao, B., & Thilker, D. 2017, *ApJS*, 230, 24
- Biller, B. A., Liu, M. C., Wahhaj, Z., et al. 2010, *ApJL*, 720, L82
- Binks, A. S., & Jeffries, R. D. 2014, *MNRAS*, 438, L11
- Binks, A. S., & Jeffries, R. D. 2016, *MNRAS*, 455, 3345
- Binks, A. S., & Jeffries, R. D. 2017, *MNRAS*, 469, 579
- Borisov, S. B., Chilingarian, I. V., Rubtsov, E. V. 2023, *ApJS*, 266, 11
- Boubert, D., & Overall, A. 2020, *MNRAS*, 497, 4246
- Boucher, A., Lafrenière, D., Gagné, J., et al. 2016, *ApJ*, 832, 50
- Boudreault, S., & Bailer-Jones, C. A. L. 2009, *ApJ*, 706, 1484
- Bowler, B. P., Hinkley, S., Ziegler, C., et al. 2019, *ApJ*, 877, 60
- Bowler, B. P., Shkolnik, E. L., Liu, M. C., et al. 2015, *ApJ*, 806, 62
- Brown, E. L., Jeffers, S. V., Marsden, S. C., et al. 2022, *MNRAS*, 514, 4300
- Buder, S., Sharma, S., Kos, J., et al. 2021, *MNRAS*, 506, 150
- Burgasser, A. J., Logsdon, S. E., Gagné, J., et al. 2015, *ApJS*, 220, 18
- Buscombe, W. 1965, *MNRAS*, 129, 411
- Cannon, A. J., & Pickering, E. C. 1993, *yCat*, 3135, 0
- Cantat-Gaudin, T., Jordi, C., Vallenari, A., et al. 2018, *A&A*, 618, A93
- Carpenter, J. M., Bouwman, J., Silverstone, M. D., et al. 2008, *ApJS*, 179, 423
- Carpenter, J. M., Mamajek, E. E., Hillenbrand, L. A., & Meyer, M. R. 2006, *ApJ*, 651, L49
- Chen, C. H., Fitzgerald, M. P., & Smith, P. S. 2008, *ApJ*, 689, 539
- Chen, C. H., Patten, B. M., Werner, M. W., et al. 2005, *ApJ*, 634, 1372
- Chen, C. H., Su, K. Y. L., & Xu, S. 2020, *Nature Astronomy*, 4, 328
- Chinchilla, P., Béjar, V. J. S., Lodieu, N., Zapatero Osorio, M. R., & Gauza, B. 2021, *A&A*, 645, A17
- Choi, J., Dotter, A., Conroy, C., et al. 2016, *ApJ*, 823, 102
- Churchwell, E., Babler, B. L., Meade, M. R., et al. 2009, *PASP*, 121, 213
- Clemens, J. C., Crain, J. A., & Anderson, R. 2004, *Proc. SPIE*, 5492, 331
- Cloutier, R., Currie, T., Rieke, G. H., et al. 2014, *ApJ*, 796, 127
- Corbally, C. J. 1984, *ApJS*, 55, 657
- Coté, J. 1987, *A&A*, 181, 77
- Cotten, T. H., & Song, I. 2016, *ApJS*, 225, 15
- Couture, D., Gagné, J., & Doyon, R. 2023, *ApJ*, 946, 6
- Cowley, A. 1972, *AJ*, 77, 750
- Cowley, A., Cowley, C., Jaschek, M., & Jaschek, C. 1969, *AJ*, 74, 375
- Crifo, F., Phan-Bao, N., Delfosse, X., et al. 2005, *A&A*, 441, 653
- Cronin-Coltsmann, P. F., Kennedy, G. M., Adam, C., et al. 2022, *MNRAS*, 512, 4752
- Cronin-Coltsmann, P. F., Kennedy, G. M., Kral, Q., et al. 2023, *MNRAS*, 526, 5401
- Crundall, T. D., Ireland, M. J., Krumholz, M. R., et al. 2019, *MNRAS*, 489, 3625
- Cruz, K. L., Kirkpatrick, J. D., & Burgasser, A. J. 2009, *AJ*, 137, 3345

- Cruz, K. L., Núñez, A., Burgasser, A. J., et al. 2018, *AJ*, 155, 34
- Cruz, K. L., Reid, I. N., Kirkpatrick, J. D., et al. 2007, *AJ*, 133, 439
- Cruz, K. L., Reid, I. N., Liebert, J., Kirkpatrick, J. D., & Lowrance, P. J. 2003, *AJ*, 126, 2421
- Cruz-Saenz, de Miera, F., Chavez, M., Bertone, E., & Vega, O. 2014, *MNRAS*, 437, 391
- Cui, X., Zhao, Y., Chu, Y., et al. 2012, *RAA*, 12, 1197
- Cushing, M. C., Vacca, W. D., & Rayner, J. T. 2004, *PASP*, 116, 362
- Cutri, R. M., Wright, E. L., Conrow, T., et al. 2012a, *yCat*, 2311, 0C
- Cutri, R. M., Wright, E. L., Conrow, T., et al. 2012b, Explanatory Supplement to the WISE All-Sky Data Release Products
- Cutri, R. M., Wright, E. L., Conrow, T., et al. 2013a, *yCat*, 2328, 0C
- Cutri, R. M., Wright, E. L., Conrow, T., et al. 2013b, Explanatory Supplement to the AllWISE Data Release Products, 1
- Dahm, S. E. 2015, *ApJ*, 813, 108
- da Silva, L., Torres, C. A. O., de la Reza, R., et al. 2009, *A&A*, 508, 833
- de Bruijne, J. H. J. 2012, *Ap&SS*, 341, 31
- de la Reza, R., Quast, G., Torres, C. A. O., et al. 1986, *ESA Special Publication*, Vol. 263, *New Insights in Astrophysics. Eight Years of UV Astronomy with IUE* ed E. J. Rolfe and R. Wilson, 107
- De Rosa, R. J., Nielsen, E. L., Wahhaj, Z., et al. 2023, *A&A*, 672, A94
- Deshpande, R., Martín, E. L., Montgomery, M. M., et al. 2012, *AJ*, 144, 99
- Dias, W. S., Alessi, B. S., Moitinho, A., et al. 2002, *A&A*, 389, 871
- Dobbie, P. D., Lodieu, N., & Sharp, R. G. 2010, *MNRAS*, 409, 1002
- Donaldson, J. K., Roberge, A., Chen, C. H., et al. 2012, *ApJ*, 753, 147
- Dotter, A. 2016, *ApJS*, 222, 8
- Dupuy, T. J., Liu, M. C., Allers, K. N., et al. 2018, *AJ*, 156, 57
- Eikenberry, S., Albert, L., Forveille, T., et al. 2004, *Proc. SPIE*, 5492, 1196
- Elliott, P., Bayo, A., Melo, C. H. F., et al. 2014, *A&A*, 568, A26
- Elliott, P., Huélamo, N. Bouy, H., et al. 2015, *A&A*, 580, A88
- Espallat, C., Ingleby, L., Hernandez, J., et al. 2012, *ApJ*, 747, 103
- Esplin, T. L., & Luhman, K. L. 2017, *AJ*, 154, 134
- Esplin, T. L., Luhman, K. L., & Mamajek, E. E. 2014, *ApJ*, 784, 126
- Esplin, T. L., Luhman, K. L., Miller, E. B., & Mamajek, E. E. 2018, *AJ*, 156, 75
- Fabircius, C., Luri, X., Arenou, F., et al. 2021, *A&A*, 649, A5
- Faherty, J. K., Burgasser, A. J., Walter, F. M., et al. 2012, *ApJ*, 752, 56
- Faherty, J. K., Riedel, A. R., Cruz, K. L., et al. 2016, *ApJS*, 225, 10
- Fazio, G. G., Hora, J. L., Allen, L. E., et al. 2004, *ApJS*, 154, 10
- Feiden, G. A. 2016, *A&A*, 593, A99
- Feigelson, E. D., & Lawson, W. A. 2004, *ApJ*, 614, 267
- Feigelson, E. D., & Montmerle, T. 1999, *ARA&A*, 37, 363
- Feigelson, E. D., Townsley, L. K., Broos, P. S., et al. 2013, *ApJS*, 209, 26
- Flaherty, K., Hughes, A. M., Mamajek, E. E., & Murphy, S. J. 2019, *ApJ*, 872, 92
- Forbrich, J., Lada, C. J., Muench, A. A., & Teixeira, P. S. 2008, *ApJ*, 687, 1107
- Fouqué, P., Moutou, C., Malo, L., et al. 2018, *MNRAS*, 475, 1960
- Franson, K., Bowler, B. P., Zhou, Y., et al. 2023, *ApJL*, 950, L19
- Gagné, J., & Faherty, J. K. 2018, *ApJ*, 862, 138
- Gagné, J., Faherty, J. K., Cruz, K. L., et al. 2015, *ApJS*, 219, 33
- Gagné, J., Faherty, J. K., Moranta, L., & Popinchalk, M. 2021, *ApJL*, 915, L29
- Gagné, J., Lafrenière, D., Doyon, R., Malo, L., & Artigau, É. 2014, *ApJ*, 783, 121
- Gagné, J., Mamajek, E. E., Malo, L., et al. 2018, *ApJ*, 856, 23
- Gahm, G. F., Ahlin, P., & Lindroos, K. P. 1983, *A&AS*, 51, 143
- Gaia Collaboration, Brown, A. G. A., Vallenari, A., Prusti, T., et al. 2021, *A&A*, 649, A1
- Gaia Collaboration, Prusti, T., de Bruijne, J. H. J., et al. 2016, *A&A*, 595, A1
- Gaia Collaboration, Vallenari, A., Brown, A. G. A., et al. 2023, *A&A*, 674, A1
- Gaidos, E., Mann, A. W., Lépine, S., et al. 2014, *MNRAS*, 443, 2561
- Gaidos, E., Mann, A. W., Rojas-Ayala, B., et al. 2022, *MNRAS*, 514, 1386
- Galindo-Guil, F. J., Barrado, D., Bouy, H., et al. 2022, *A&A*, 664, A70

- Galli, P. A. B., Bouy, H., Olivares, J., et al. 2021, *A&A*, 654, A122
- Galli, P. A. B., Miret-Roig, N., Bouy, H., Olivares, J., & Barrado, D. 2023, *MNRAS*, 520, 6245
- Garrison, R. F., & Gray, R. O. 1994, *AJ*, 107, 1556
- Gáspár, A., Rieke, G. H., & Balog, Z. 2013, *ApJ*, 768, 25
- Gáspár, A., Rieke, G. H., Su, K. Y. L., et al. 2009, *ApJ*, 697, 1578
- Gehrels, N. 1986, *AJ*, 303, 336
- Getman, K. V., Broos, P. S., Kuhn, M. A., et al. 2017, *ApJS*, 229, 28
- Getman, K. V., Feigelson, E. D., Garmire, G. P., et al. 2022, *ApJ*, 935, 43
- Getman, K. V., Feigelson, E. D., Townsley, L., et al. 2002, *ApJ*, 575, 354
- Gizis, J. E., Monet, D. G., Reid, I. N. 2000, *AJ*, 120, 1085
- Gontcharov, G. A. 2006, *AstL*, 32, 759
- Gorlova, N., Balog, Z., Rieke, G. H., et al. 2007, *ApJ*, 670, 516
- Gray, R. O. 1989, *AJ*, 98, 1049
- Gray, R. O., Corbally, C. J., Garrison, R. F., et al. 2006, *AJ*, 132, 161
- Gray, R. O., & Garrison, R. F. 1987, *ApJS*, 65, 581
- Gray, R. O., Riggs, Q. S., Koen, C., et al. 2017, *AJ*, 154, 31
- Güdel, M. 2004, *A&A Rv*, 12, 71
- Güdel, M., Briggs, K. R., Arzner, K., et al. 2007, *A&A*, 468, 353
- Guenther, E. W., Neuhäuser, R., Huélamo, N., Brandner, W., & Alves, J. 2001, *A&A*, 365, 514
- Gutermuth, R. A., & Heyer, M. 2015, *AJ*, 149, 64
- Gutiérrez Albarrán, M. L., Montes, D., Gómez Garrido, M., et al. 2020, *A&A*, 643, A71
- Haisch, K. E., Lada, E. A., & Lada, C. J. 2001, *ApJ*, 553, L153
- Hartmann, L., Calvet, N., Watson, D. M., et al. 2005, *ApJ*, 628, L147
- Hartoog, M. R. 1976, *ApJ*, 205, 807
- Henry, T. J., Kirkpatrick, J. D., & Simons, D. A. 1994, *AJ*, 108, 1437
- Herczeg, G. J., & Hillenbrand, L. A. 2015, *ApJ*, 808, 23
- Hernández, J., Hartmann, L., Megeath, T., et al. 2007, *ApJ*, 662, 1067
- Higashio, S., Kuchner, M. J., Silverberg, S. M., et al. 2022, *ApJ*, 933, 13
- Hiltner, W. A., Garrison, R. F., & Schild, R. E. 1969, *ApJ*, 157, 313
- Hinkley, S., Matthews, E. C., Lefevre, C., et al. 2021, *ApJ*, 912, 115
- Hook, I., Jørgensen, I., Allington-Smith, J. R., et al. 2004, *PASP*, 116, 425
- Houk, N. 1978, *Michigan Catalogue of Two-dimensional Spectral Types for the HD Stars. Vol. 2*, (Ann Arbor: Univ. Mich.)
- Houk, N. 1982, *Michigan Catalogue of Two-dimensional Spectral Types for the HD Stars. Vol. 3*, (Ann Arbor: Univ. Mich.)
- Houk, N., Cowley, A. P. 1975, *Michigan Catalogue of Two-dimensional Spectral Types for the HD Stars. Vol. 1*, (Ann Arbor: Univ. Mich.)
- Houk, N., & Smith-Moore, M. 1988, *Michigan Catalogue of Two-dimensional Spectral Types for the HD Stars. Vol. 4*, (Ann Arbor: Univ. Mich.)
- Houk, N., & Swift, C. 1999, *Michigan Catalogue of Two-dimensional Spectral Types for the HD Stars. Vol. 5*, (Ann Arbor: Univ. Mich.)
- Hourihane, A., François, P., Worley, C. C., et al. 2023, *A&A*, 676, A129
- Hughes, A. M., Duchêne, G., & Matthews, B. C. 2018, *ARA&A*, 56, 541
- Iglesias, D., Bayo, A., Olofsson, J., et al. 2018, *MNRAS*, 480, 488
- Jackson, R. J., Jeffries, R. D., Wright, N. J., et al. 2020, *MNRAS*, 496, 4701
- Jackson, R. J., Jeffries, R. D., Wright, N. J., et al. 2022, *MNRAS*, 509, 1664
- Jackson, J., & Stoy, R. H. 1955, *AnCap*, 18, 0
- Janson, M., Hormuth, F., Bergfors, C., et al. 2012, *ApJ*, 754, 44
- Jeffries, R. D., Jackson, R. J., Wright, N. J., et al. 2023, *MNRAS*, 523, 802
- Jeffries, R. D., Naylor, T., Devey, C. R., & Totten, E. J. 2004, *MNRAS*, 351, 1401
- Jeffries, R. D., & Oliveira, J. M. 2005, *MNRAS*, 358, 13
- Jeffries, R. D., Oliveira, J. M., Barrado y Navascués, D., & Stauffer, J. R. 2003, *MNRAS*, 343, 1271
- Jensen, E. L. N., & Mathieu, R. D. 1997, *AJ*, 114, 301
- Johnson D. R. H., & Soderblom D. R., 1987, *AJ*, 93, 864
- Johnstone, C. P., Bartel, M., & Güdel, M. 2021, *A&A*, 649, A96
- Jönsson, H., Holtzman, J. A., Allende Prieto, C., et al. 2020, *AJ*, 160, 120
- Kaisler, D., Zuckerman, B., Song, I., et al. 2004, *A&A*, 414, 175
- Kalas, P., Liu, M. C., & Matthews, B. C. 2004, *Science*, 303, 1990
- Kerr, R., Rizzuto, A. C., Kraus, A. L., & Offner, S. S. R. 2021, *ApJ*, 917, 23
- Kasper, M., Apai, D., Janson, M., & Brandner, W. 2007, *A&A*, 472, 321
- Keenan P. C., & McNeil R. C. 1989, *ApJS*, 71, 245

- Kenyon, S. J., & Bromley, B. C. 2005, *AJ*, 130, 269
- Kirkpatrick, J. D., Barman, T. S., Burgasser, A. J., et al. 2006, *ApJ*, 639, 1120
- Kirkpatrick, J. D., Cruz, K. L., Barman, T. S., et al. 2008, *ApJ*, 689, 1295
- Kirkpatrick, J. D., Cushing, M. C., Gelino, C. R., et al. 2011, *ApJS*, 197, 19
- Kirkpatrick, J. D., Henry, T. J., & Irwin, M. J. 1997, *AJ*, 113, 1421
- Kirkpatrick, J. D., Henry, T. J., & McCarthy, D. W. 1991, *ApJS*, 77, 417
- Kirkpatrick, J. D., Looper, D. L., Burgasser, A. J., et al. 2010, *ApJS*, 190, 100
- Kiss, L. L., Moór, A., Szalai, T., et al. 2011, *MNRAS*, 411, 117
- Koen, C., Miszalski, B., Väisänen, P., & Koen, T. 2017, *MNRAS*, 465, 4723
- Kounkel, M., & Covey, K. 2019, *AJ*, 158, 122
- Kraus, A. L., Shkolnik, E. L., Allers, K. N., & Liu, M. C. 2014, *AJ*, 147, 146
- Krautter, J., Wichmann, R., Schmitt, J. H. M. M., et al. 1997, *A&AS*, 123, 329
- Lada, C. J. 1987, in *IAU Symp. 115, Star Forming Regions*, ed. M. Peimbert & J. Jugaku (Dordrecht: Reidel), 1
- Lada, C. J., & Wilking, B. A. 1984, *ApJ*, 287, 610
- Lafarga, M., Ribas, I., Lovis, C., et al. 2020, *A&A*, 636, A36
- Lagrange, A.-M., Bonnefoy, M., Chauvin, G., et al. 2010, *Science*, 329, 57
- Lagrange, A.-M., Gratadour, D., Chauvin, G., et al. 2009, *A&A*, 493, L21
- Lagrange, A.-M., Meunier, N., Rubini, P., et al. 2019, *Nature Astronomy*, 3, 1135
- Lang, D. 2014, *AJ*, 147, 108
- Lee, J., & Song, I. 2019, *MNRAS*, 486, 3434
- Lee, J., Song, I., & Murphy, S. 2020, *MNRAS*, 494, 62
- Lee, J., Song, I., & Murphy, S. J. 2022, *MNRAS*, 511, 6179
- Lee, R. A., Gaidos, E., van Saders, J., Feiden, G. A., & Gagné, J. 2024, *MNRAS*, 528, 4760
- Lépine, S., Hilton, E. J., Mann, A. W., et al. 2013, *AJ*, 145, 102
- Lépine, S., & Simon, M. 2009, *AJ*, 137, 3632
- Lindgren, L. 2018, Re-normalising the astrometric chi-square in Gaia DR2, GAIA-C3-TN-LU-LL-124-01, http://www.rssd.esa.int/doc_fetch.php?id=3757412
- Liu, M. C., Dupuy, T. J., & Allers, K. N. 2016, *ApJ*, 833, 96
- Liu, M. C., Magnier, E. A., Deacon, N. R., et al. 2013, *ApJL*, 777, L20
- Liu, M. C., Magnier, E. A., Zhang, Z., et al. 2022, *AJ*, 164, 165
- Liu, M. C., Matthews, B. C., Williams, J. P., & Kalas, P. G. 2004, *ApJ*, 608, 526
- Liu, Q., Wang, T., & Jiang, P. 2014, *AJ*, 148, 3
- Lodieu, N., Scholz, R.-D., McCaughrean, M. J., et al. 2005, *A&A*, 440, 1061
- Lowrance, P. J., Schneider, G., Kirkpatrick, J. D., et al. 2000, *ApJ*, 541, 390
- Luhman, K. L. 1999, *ApJ*, 525, 466
- Luhman, K. L. 2007, *ApJS*, 173, 104
- Luhman, K. L. 2018, *AJ*, 156, 271
- Luhman, K. L. 2022a, *AJ*, 163, 24
- Luhman, K. L. 2022b, *AJ*, 163, 25
- Luhman, K. L. 2022c, *AJ*, 164, 151
- Luhman, K. L. 2023a, *AJ*, 165, 37
- Luhman, K. L. 2023b, *AJ*, 165, 269
- Luhman, K. L., Allen, P. R., Espaillat, C., Hartmann, L., & Calvet, N. 2010, *ApJS*, 186, 111
- Luhman, K. L., & Esplin, T. L. 2020, *AJ*, 160, 44
- Luhman, K. L., Liebert, J., & Rieke, G. H. 1997, *ApJL*, 489, L165
- Luhman, K. L., & Mamajek, E. E. 2012, *ApJ*, 758, 31
- Luhman, K. L., Mamajek, E. E., Shukla, S. J., & Loutrel, N. P. 2017, *AJ*, 153, 46
- MacDonald, J., & Mullan, D. J. 2010, *ApJ*, 723, 1599
- Macintosh, B., Graham, J. R., Barman, T., et al. 2015, *Science*, 350, 64
- Malo, L., Artigau, É., Doyon, R., et al. 2014a, *ApJ*, 788, 81
- Malo, L., Doyon, R., Feiden, G. A., et al. 2014b, *ApJ*, 792, 37
- Malo, L., Doyon, R., Lafrenière, D., et al. 2014, *ApJ*, 762, 88
- Mamajek, E. E. 2009, in *AIP 1158, Exoplanets and Disks: Their Formation and Diversity*, ed. T. Usuda, M. Tamura, & M. Ishii (Melville, NY: AIP), 3
- Mamajek, E. E., & Bell, C. P. M. 2014, *MNRAS*, 445, 2169
- Mamajek, E. E., & Feigelson, E. D. 2001, *ASP Conf. Ser. 244, Young Stars Near Earth: Progress and Prospects*, ed. R. Jayawardhana & T. Greene (San Francisco, CA: ASP), 104
- Mamajek, E. E., Meyer, M. R., & Liebert, J. 2002, *AJ*, 124, 1670
- Mannings, V., & Barlow, M. J. 1998, *ApJ*, 497, 330
- Martín, E. L., & Brandner, W. 1995, *A&A*, 294, 744
- Martín, E. L., Phan-Bao, N., Bessell, M., et al. 2010, *A&A*, 517, A53
- Martini, P., Stoll, R., Derwent, M. A., et al. 2011, *PASP*, 123, 187
- Martioli, E., Hébrard, G., Correia, A. C. M., Laskar, J., & Lecavelier des Etangs, A. 2021, *A&A*, 649, A177

- Matthews, B. C., Krivov, A. V., Wyatt, M. C., Bryden, G., Eiroa, C. 2014, in *Protostars and Planets VI*, ed. H. Beuther et al. (Tucson, AZ: Univ. Arizona Press), 521
- McDonald, I., Zijlstra, A. A., & Boyer, M. L. 2012, *MNRAS*, 427, 343
- McDonald, I., Zijlstra, A. A., & Watson, R. A. 2017, *MNRAS*, 471, 770
- Meingast, S., Alves, J., & Rottensteiner, A. 2021, *A&A*, 645, A84
- Meisner, A. M., Lang, D., Schlafly, E. F., & Schlegel, D. J. 2019, *PASP*, 131, 124504
- Meng, H. Y. A., Rieke, G. H., Su, K. Y. L., et al. 2012, *ApJL*, 751, L17
- Meng, H. Y. A., Rieke, G. H., Su, K. Y. L., & Gáspár, A. 2017, *ApJ*, 836, 34
- Mentuch, E., Brandeker, A., van Kerkwijk, M. H., Jayawardhana, R., & Hauschildt, P. H. 2008, *ApJ*, 689, 1127
- Merloni, A., Lamer, G., Liu, T., et al. 2024, *A&A*, 682, A34
- Mermilliod, J. -C., Mayor, M., & Udry, S. 2009, *A&A*, 498, 949
- Mesa, D., Gratton, R., Kervella, P., et al. 2023, *A&A*, 672, A93
- Meyer, M. R., Carpenter, J. M., Mamajek, E. E., et al. 2008, *ApJ*, 673, L181
- Miret-Roig, N., Galli, P. A. B., Brandner, W., et al. 2020, *A&A*, 642, A179
- Moór, A., Ábrahám, P., Derekas, A., et al. 2006, *ApJ*, 644, 525
- Moór, A., Kóspál, Á., Ábrahám, P., et al. 2016, *ApJ*, 826, 123
- Moór, A., Pawellek, N., Ábrahám, P., et al. 2020, *AJ*, 159, 288
- Moór, A., Szabó, Gy. M., Kiss, L. L., et al. 2013, *MNRAS*, 435, 1376
- Mugrauer, M., Vogt, N., Neuhäuser, R., & Schmidt, T. O. B. 2010, *A&A*, 523, L1
- Murphy, S. J., Mamajek, E. E., & Bell, C. P. M. 2018, *MNRAS*, 476, 3290
- Naylor, T., Totten, E. J., Jeffries, R. D., et al. 2002, *MNRAS*, 335, 291
- Nesterov, V. V., Kuzmin, A. V., Ashimbaeva, N. T., et al. 1995, *A&AS*, 110, 367
- Neuhäuser, R., Guenther, E., Mugrauer, M., Ott, Th., & Eckart, A. 2002, *A&A*, 395, 877
- Newton, E. R., Charbonneau, D., & Irwin, J. 2014, *AJ*, 147, 20
- Nielson, E. L., De Rosa, R. J., Wang, J., et al. 2016, *AJ*, 152, 175
- Nisak, A. H., White, R. J., Yep, A., et al. 2022, *AJ*, 163, 278
- Ortega, V. G., de la Reza, R., Jilinski, E., & Bazzanella, B. 2002, *ApJ*, 575, L75
- Ortega, V. G., de la Reza, R., Jilinski, E., & Bazzanella, B. 2004, *ApJ*, 609, 243
- Oudmaijer, R. D., van der Veen, W. E. C. J., Waters, L. B. F. M., et al. 1992, *A&AS*, 96, 625
- Pala, A. F., Gänsicke, B. T., Breedt, E., et al. 2020, *MNRAS*, 494, 3799
- Pasquini, L., Schmitt, J. H. M. M., Harnden, F. R., Jr., Tozzi, G. P., & Krautter, J. 1989, *A&A*, 218, 187
- Patel, R. I., Metchev, S. A., & Heinze, A. 2014, *ApJS*, 212, 10
- Patten, B. M., & Simon, T. 1996, *ApJS*, 106, 489
- Patten, B. M., & Wilson, L. A. 1991, *AJ*, 102, 323
- Pawellek, N., Wyatt, M., Matrà, L., Kennedy, G., & Yelverton, B. 2021, *MNRAS*, 502, 5390
- Pecaut, M. J., & Mamajek, E. E. 2013, *ApJS*, 208, 9
- Pecaut, M. J., & Mamajek E. E. 2016, *MNRAS*, 461, 794
- Pecaut, M. J., Mamajek E. E., & Bubar E. J. 2012, *ApJ*, 746, 154
- Perry, C. L., & Bond, H. E. 1969, *PASP*, 81, 629
- Perryman, M. A. C., de Boer, K. S., Gilmore, G., et al. 2001, *A&A*, 369, 339
- Phan-Bao, N., & Bessell, M. S. 2006, *A&A*, 446, 515
- Phan-Bao, N., Bessell, M. S., Nguyen-Thanh, D., et al. 2017, *A&A*, 600, A19
- Pilbratt, G. L., Riedinger, J. R., Passvogel, T., et al. 2010, *A&A*, 518, L1
- Platais, I., Kozhurina-Platais, V., & van Leeuwen, F. 1998, *AJ*, 116, 2423
- Plavchan, P., Barclay, T., Gagné, J., et al. 2020, *Nature*, 582, 497
- Plavchan, P., Werner, M. W., Chen, C. H., et al. 2009, *ApJ*, 698, 1068
- Pourbaix, D., Tokovinin, A. A., Batten, A. H. 2004, *A&A*, 424, 727
- Predehl, P., Andritschke, R., Arefiev, V., et al. 2021, *A&A*, 647, A1
- Preibisch, T. 2003, *A&A*, 401, 543
- Preibisch, T., & Zinnecker, H. 2001, *AJ*, 122, 866
- Pribulla, Sabastian, D., Ammler-von Eiff, M., et al. 2014, *MNRAS*, 443, 2815
- Price-Whelan, A. 2021, *adrn/pyia: v1.3*, Zenodo, doi:10.5281/zenodo.5057363
- Quast, G. R., Torres, C. A. O., de La Reza, R., da Silva, L., & Mayor, M. 2000, *IAUS*, 200, 28
- Randich, S., Gilmore, G.I, Magrini, L., et al. 2022, *A&A*, 666, A121
- Randich, S., Pallavicini, R., Meola, G., Stauffer, J. R., & Balachandran, S. C. 2001, *A&A*, 372, 862

- Randich, S., Tognelli, E., Jackson, R., et al. 2018, *A&A*, 612, A99
- Ratzenböck, S., Großschedl, J. E., Möller, T., et al. 2023, *A&A*, 677, A59
- Rayner, J. T., Toomey, D. W., Onaka, P. M., et al. 2003, *PASP*, 115, 362
- Rebull, L. M., Stapelfeldt, K. R., Werner, M. W., et al. 2008, *ApJ*, 681, 1484
- Reid, I. N., Cruz, K. L., & Allen, P. R. 2007, *AJ*, 133, 2825
- Reid, I. N., Cruz, K. L., Kirkpatrick, J. D., et al. 2008, *AJ*, 136, 1290
- Reid, I. N., Hawley, S. L., & Gizis, J. E. 1995, *AJ*, 110, 1838
- Reid, I. N., Kirkpatrick, J. D., Liebert, J., et al. 2002, *AJ*, 124, 519
- Rhee, J. H., Song, I., Zuckerman, B., & McElwain, M. 2007, *ApJ*, 660, 1556
- Riaz, B., Gizis, J. E., & Harvin, J. 2006, *AJ*, 132, 866
- Ribas, Á, Bouy, H., & Merín, B. 2015, *A&A*, 576, A52
- Richert, A. J. W., Getman, K. V., Feigelson, E. D., et al. 2018, *MNRAS*, 477, 5191
- Rice, E. L., Faherty, J. K., & Cruz, K. L. 2010, *ApJL*, 715, L165
- Riedel, A. R., Alam, M. K., Rice, E. L., Cruz, K. L., & Henry, T. J. 2017, *ApJ*, 840, 87
- Riedel, A. R., Finch, C. T., Henry, T. J., et al. 2014, *AJ*, 147, 85
- Riedel, A. R., Murphy S., Henry, T. J., et al. 2011, *AJ*, 142, 104
- Rieke, G. H., Su, K. Y. L., Stansberry, J. A., et al. 2005, *ApJ*, 620, 1010
- Rieke, G. H., Young, E. T., Engelbracht, C. W., et al. 2004, *ApJS*, 154, 25
- Riello, M., De Angeli, F., Evans, D. W., et al. 2021, *A&A*, 649, A3
- Riviere-Marichalar, P. Barrado, D., Montesinos, B., et al. 2014, *A&A*, 565, A68
- Rizzuto, A. C., Ireland, M. J., & Kraus, A. L. 2015, *MNRAS*, 448, 2737
- Rizzuto, A. C., Ireland, M. J., & Zucker, D. B. 2012, *MNRAS*, 421, L97
- Robertson, T. H. 1984, *AJ*, 89, 1229
- Rodriguez, D. R., Zuckerman, B., Kastner, J. H., et al. 2013, *ApJ*, 774, 101
- Rosenfeld, K. A., Andrews, S. M., Wilner, D. J., Kastner, J. H., & McClure, M. K. 2013, *ApJ*, 775, 136
- Sacco, G. G., Jeffries, R. D., Randich, S., et al. 2015, *A&A*, 574, L7
- Schlieder, J. E., Lépine, S., Rice, E., et al. 2012b, *AJ*, 143, 114
- Schlieder, J. E., Lépine, S., & Simon, M. 2012a, *AJ*, 143, 80
- Schlieder, J. E., Lépine, S., & Simon, M. 2012c, *AJ*, 144, 109
- Schlieder, J. E., Lépine, S., & Simon, M. 2010, *AJ*, 140, 119
- Schmidt, S. J., Cruz, K. L., Bongiorno, B. J., Liebert, J., & Reid, I. N. 2007, *AJ*, 133, 2258
- Schneider, A. C., Burgasser, A. J., Bruursema, J., et al. 2023, *ApJL*, 943, L16
- Schneider, A. C., Shkolnik, E. L., Allers, K. N., et al. 2019, *AJ*, 157, 234
- Schneider, G., Silverstone, M. D., Hines, D. C., et al. 2006, *ApJ*, 650, 414
- Schütz, O., Meeus, G., Sterzik, M. F. & Peeters, E. 2009, *A&A*, 507, 261
- Sgro, L. A., & Song, I. 2021, *MNRAS*, 508, 3084
- Shkolnik, E. L., Allers, K. N., Kraus, A. L., Liu, M. C., & Flagg, L. 2017, *AJ*, 154, 69
- Shkolnik, E., Anglada-Escudé, G., Liu, M. C., et al. 2012, *ApJ*, 758, 56
- Shkolnik, E., Liu, M. C., & Reid, I. N. 2009, *ApJ*, 699, 649
- Siegler, N., Muzerolle, J., Young, E. T., et al. 2007, *ApJ*, 654, 580
- Silverberg, S. M., Kuchner, M. J., Wisniewski, J. P., et al. 2016, *ApJL*, 830, L28
- Silverberg, S. M., Wisniewski, J. P., Kuchner, M. J., et al. 2020, *ApJ*, 890, 106
- Sissa, E., Olofsson, J., Vigan, A., et al. 2018, *A&A*, 613, L6
- Skrutskie, M., Cutri, R. M., Stiening, R., et al. 2003, 2MASS All-Sky Point Source Catalog, IPAC, doi:10.26131/IRSA2
- Skrutskie, M., Cutri, R. M., Stiening, R., et al. 2006, *AJ*, 131, 1163
- Smith, B. A., & Terrile, R. J. 1984, *Science*, 226, 1421
- Smith, P. S., Hines, D. C., Low, F. J., et al. 2006, *ApJ*, 644, L125
- Soderblom, D. R., Hillenbrand, L. A., Jeffries, R. D., Mamajek, E. E., & Naylor, T. 2014, *Protostars and Planets VI*. Univ. Arizona Press, Tucson, AZ, 219
- Song, I., Bessell, M. S., & Zuckerman, B. 2002, *ApJ*, 581, L43
- Song, I., Zuckerman, B., & Bessell, M. S. 2003, *ApJ*, 599, 342
- Soubiran, C., Jasniewicz, G., Chemin, L., et al. 2018, *A&A*, 616, A7
- Spangler, C., Sargent, A. I., Silverstone, M. D., Becklin, E. E., & Zuckerman, B. 2001, *ApJ*, 555, 932
- Stahl, A. G., Johns-Krull, C. M., & Flagg, L. 2022, *ApJ*, 941, 101
- Stauffer, J. R., Schultz, G., & Kirkpatrick, J. D. 1998, *ApJ*, 499, L199

- Steinmetz, M., Guiglion, G., McMillan, P. J. 2020, *AJ*, 160, 83
- Stelzer, B., Micela, G., & Neuhäuser, R. 2004, *A&A*, 423, 1029
- Stephenson, C. B. 1986, *AJ*, 91, 144
- Stoeke, J. T., Morris, S. L., Gioia, I. M., et al. 1991, *ApJS*, 76, 813
- Strassmeier, K. G., & Rice, J. B. 2000, *A&A*, 360, 1019
- Su, K. Y. L., Jackson, A. P., Gáspár, A., et al. 2019, *AJ*, 157, 202
- Su, K. Y. L., Rieke, G. H., Stansberry, J. A., et al. 2006, *ApJ*, 653, 675
- Tanner, A., Plavchan, P., Bryden, G., et al. 2020, *PASP*, 132, 084401
- Teixeira, P. S., Lada, C. J., Wood, K., Robitaille, T. P., & Luhman, K. L. 2009b, *ApJ*, 700, 454
- Teixeira, R., Ducourant, C., Chauvin, G., et al. 2009a, *A&A*, 503, 281
- Terrien, R. C., Mahadevan, S., Deshpande, R., & Bender, C. F. 2015, *ApJS*, 220, 16
- The, P. S., & Staller, R. F. A. 1974, *A&A*, 36, 155
- The, P. S., de Winter, D., & Perez, M. R. 1994, *A&AS*, 104, 315
- Tokovinin, A. 2022, *AJ*, 163, 127
- Torres, C. A. O., da Silva, L., Quast, G. R., de la Reza, R., & Jilinski, E. 2000, *AJ*, 120, 1410
- Torres, C. A. O., Quast, G. R., Melo, C. H. F., & Sterzik, M. F. 2008, in *Handbook of Star Forming Regions*, Volume II, ed. B. Reipurth, 757
- Torres, C. A. O., Quast, G. R., da Silva, L., et al. 2006, *A&A*, 460, 695
- Tubín-Arenas, D., Krumpe, M., Lamer, G., et al. 2024, *A&A*, 682, A35
- Vacca, W. D., Cushing, M. C., & Rayner, J. T. 2003, *PASP*, 115, 389
- van den Ancker, M. E., Gentile Fusillo, N. P., Haworth, T. J., et al. 2021, *A&A*, 651, L11
- Vernet, J., Dekker, H., D'Odorico, S., et al. 2011, *A&A*, 536, A105
- Vysotsky, A. N. 1956, *AJ*, 61, 201
- Werner, M. W., Roellig, T. L., Low, F. J., et al. 2004, *ApJS*, 154, 1
- White, R. J., Gabor, J. M., & Hillenbrand, L. A. 2007, *AJ*, 133, 2524
- White, R. J., & Hillenbrand, L. A. 2005, *ApJ*, 621, L65
- Whiteoak, J. B. 1961, *MNRAS*, 123, 245
- Wilson, R. E. 1953, *General Catalogue of Stellar Radial Velocities* (Washington, DC: Carnegie Institution of Washington)
- Wittrock, J. M., Dreizler, S., Reefe, M. A., et al. 2022, *AJ*, 164, 27
- Wittrock, J. M., Plavchan, P. P., Cale, B. L., et al. 2023, *AJ*, 166, 232
- Wood, M. L., Mann, A. W., Barber, M. G., et al. 2023, *AJ*, 166, 247
- Wright, E. L., Eisenhardt, P. R., Mainzer, A. K., et al. 2010, *AJ*, 140, 1868
- Wright, E. L., Eisenhardt, P. R. M., Mainzer, A. K., et al. 2013, *AllWISE Source Catalog*, IPAC, doi:10.26131/IRSA1
- Wu, C.-J., Wu, H., Lam, M.-I., et al. 2013, *ApJS*, 208, 29
- Wyatt, M. C. 2008, *ARA&A*, 46, 339
- Yee, J. C., & Jensen, E. L. N. 2010, *ApJ*, 711, 303
- Yen, S. X., Reffert, S., Schilbach, E., et al. 2018, *A&A*, 615, A12
- Young, E. T., Lada, C. J., Teixeira, P., et al. 2004, *ApJS*, 154, 428
- Zhao, G., Zhao Y. H., Chu Y. Q., Jing Y. P., Deng L. C., 2012, *RAA*, 12, 723
- Zickgraf, F.-J., Alcalá, J. M., Krautter, J., et al. 1998, *A&A*, 339, 457
- Zuckerman, B. 2019, *ApJ*, 870, 27
- Zuckerman, B., Klein, B., & Kastner, J. 2019, *ApJ*, 887, 87
- Zuckerman, B., Rhee, J. H., Song, I., & Bessell, M. S. 2011, *ApJ*, 732, 61
- Zuckerman, B., & Song, I. 2004a, *ARA&A*, 42, 685
- Zuckerman, B., & Song, I. 2004b, *ApJ*, 603, 738
- Zuckerman, B., & Song, I. 2012, *ApJ*, 758, 77
- Zuckerman, B., Song, I., Bessell, M. S., & Webb, R. A. 2001b, *ApJ*, 562, L87
- Zuckerman, B., Song, I., & Webb, R. A. 2001a, *ApJ*, 559, 388
- Zuckerman, B., & Webb, R. A. 2000, *ApJ*, 535, 959
- Zúñiga-Fernández, S., Bayo, A., Elliott, P., et al. 2021, *A&A*, 645, A30

Table 1. Summary of Spectroscopic Observations

Telescope/Instrument	Mode/Aperture	Wavelengths/Resolution	Targets
IRTF/SpeX	prism/0''.8 slit	0.8–2.5 μm /R=150	56
CTIO 4 m/COSMOS	red VPH/1''.2 slit	0.55–0.95 μm /4 \AA	36
CTIO 1.5 m/RC Spec	47 Ib/2'' slit	0.56–0.69 μm /3 \AA	2
CTIO 1.5 m/RC Spec	58 I/2'' slit	0.62–0.88 μm /6 \AA	1
Gemini South/GMOS	R400/0''.5	0.52–0.91 μm /4 \AA	4
Gemini South/GMOS	R400/0''.75	0.6–1 μm /5 \AA	6
Gemini South/GMOS	R400/1''	0.6–1 μm /7 \AA	2
Gemini South/FLAMINGOS-2	JH/HK/0''.72	0.9–2.5 μm /R=700	1
SOAR/Goodman	400/0''.45	0.6–0.9 μm /3 \AA	4
SOAR/Goodman	600/1''	0.63–0.9 μm /4 \AA	40

Table 2. Spectroscopic Data for Adopted Members of BPMG and Other Associations

Column Label	Description
Gaia	Gaia DR3 source name
RAdeg	Gaia DR3 right ascension (ICRS at Epoch 2016.0)
DEdeg	Gaia DR3 declination (ICRS at Epoch 2016.0)
SpType	Spectral type ^a
Instrument	Instrument for spectroscopy
Date	Date of spectroscopy

^aUncertainties are 0.25 and 0.5 subclass for optical and IR spectral types, respectively, unless indicated otherwise.

NOTE— The table is available in its entirety in machine-readable form.

Table 3. Adopted Members of BPMG, Sco Body, Car-Ext, Columba, χ^1 For, Tuc-Hor, IC 2602, and IC 2391

Column Label	Description
GaiaDR3	Gaia DR3 source name
Name	Other source name
RAdeg	Gaia DR3 right ascension (ICRS at Epoch 2016.0) ^a
DEdeg	Gaia DR3 declination (ICRS at Epoch 2016.0) ^a
SpType	Spectral type
r_SpType	Spectral type reference ^b
Adopt	Adopted spectral type
f_EWLi	Flag for EWLi
EWLi	Equivalent width of Li
e_EWLi	Error in EWLi ^c
r_EWLi	Li reference ^c
pmRA	Gaia DR3 proper motion in right ascension ^a
e_pmRA	Error in pmRA
pmDec	Gaia DR3 proper motion in declination ^a
e_pmDec	Error in pmDec
plx	Gaia DR3 parallax ^a
e_plx	Error in plx
rmedgeo	Median of geometric distance posterior (Bailer-Jones et al. 2021) ^a
rlogeo	16th percentile of geometric distance posterior (Bailer-Jones et al. 2021) ^a
rhigeo	84th percentile of geometric distance posterior (Bailer-Jones et al. 2021) ^a
RVel	Radial velocity
e_RVel	Error in RVel
r_RVel	Radial velocity reference ^d
U	U component of space velocity
e_U	Error in U
V	V component of space velocity
e_V	Error in V
W	W component of space velocity
e_W	Error in W
Gmag	Gaia DR3 G magnitude
e_Gmag	Error in Gmag
GBPmag	Gaia DR3 G_{BP} magnitude
e_GBPmag	Error in GBPmag
GRPmag	Gaia DR3 G_{RP} magnitude
e_GRPmag	Error in GRPmag
RUWE	Gaia DR3 renormalized unit weight error
2m	Closest 2MASS source within 3''
2msep	Angular separation between Gaia DR3 (epoch 2000) and 2MASS
2mclosest	Is this Gaia source the closest match for the 2MASS source?
wise	Closest WISE source within 3'' ^e
wiseseq	Angular separation between Gaia DR3 (epoch 2010.5) and WISE
wiseclosest	Is this Gaia source the closest match for the WISE source?
Jmag	2MASS J magnitude
e_Jmag	Error in Jmag
Hmag	2MASS H magnitude
e_Hmag	Error in Hmag
Ksmag	2MASS K_s magnitude
e_Ksmag	Error in Ksmag
W1mag	WISE W1 magnitude
e_W1mag	Error in W1mag

Table 3 continued

Table 3 (*continued*)

Column Label	Description
W2mag	WISE W2 magnitude
e_W2mag	Error in W2mag
f_W2mag	Flag on W2mag ^f
W3mag	WISE W3 magnitude
e_W3mag	Error in W3mag
f_W3mag	Flag on W3mag ^f
W4mag	WISE W4 magnitude
e_W4mag	Error in W4mag
f_W4mag	Flag on W4mag ^f
ExcW2	Excess in W2?
ExcW3	Excess in W3?
ExcW4	Excess in W4?
DiskType	Disk type
erass1	eRASS1 source name
poserr	Position error from eRASS1 1B Catalog
xsep	Angular separation between Gaia DR3 (epoch 2020) and eRASS1
f_rate	Flag for rate
rate	Count rate from eRASS1 1B Catalog
e_rate	Error in rate
association	Association

Table 3 *continued*

Table 3 (*continued*)

Column Label	Description
^a	The astrometry and distance for HD 161460 are from Gaia DR2 and Bailer-Jones et al. (2018). Those parameters are from Liu et al. (2016) for PSO J318.5338-22.8603. The proper motion, parallax, and distance for GJ 3076 are from Riedel et al. (2014).
^b	(1) Houk & Smith-Moore (1988); (2) Cannon & Pickering (1993); (3) Torres et al. (2006); (4) Pecaú & Mamajek (2013); (5) Riaz et al. (2006); (6) Riedel et al. (2017); (7) this work; (8) Kraus et al. (2014); (9) Riedel et al. (2014); (10) The & Staller (1974); (11) Shkolnik et al. (2017); (12) Bowler et al. (2019); (13) Terrien et al. (2015); (14) Gaidos et al. (2014); (15) Reid et al. (1995); (16) Newton et al. (2014); (17) Reid et al. (2007); (18) Shkolnik et al. (2009); (19) Zuckerman & Song (2004a); (20) Vyssotsky (1956); (21) Schlieder et al. (2012b); (22) Gizis et al. (2000); (23) Allers & Liu (2013); (24) Zickgraf et al. (1998); (25) Cowley et al. (1969); (26) Gray (1989); (27) Houk & Swift (1999); (28) Stephenson (1986); (29) Yee & Jensen (2010); (30) Cruz et al. (2003); (31) Kirkpatrick et al. (2008); (32) Deshpande et al. (2012); (33) Lépine et al. (2013); (34) Gray et al. (2006); (35) Schlieder et al. (2012c); (36) Robertson (1984); (37) Henry et al. (1994); (38) Alcalá et al. (1996); (39) Gagné et al. (2015); (40) Schneider et al. (2019); (41) Houk (1978); (42) Song et al. (2003); (43) Houk & Cowley (1975); (44) Krautter et al. (1997); (45) Pasquini et al. (1989); (46) Martín & Brandner (1995); (47) Houk (1982); (48) Stahl et al. (2022); (49) Phan-Bao et al. (2017); (50) Nesterov et al. (1995); (51) Gray & Garrison (1987); (52) Lowrance et al. (2000); (53) Guenther et al. (2001); (54) Reid et al. (2008); (55) Martín et al. (2010); (56) Faherty et al. (2016); (57) Lépine & Simon (2009); (58) Schmidt et al. (2007); (59) Lee et al. (2022); (60) Keenan & McNeil (1989); (61) Pribulla et al. (2014); (62) Neuhäuser et al. (2002); (63) Liu et al. (2013); (64) Shkolnik et al. (2012); (65) Rizzuto et al. (2015); (66) Pecaú & Mamajek (2016); (67) Mamajek et al. (2002); (68) The et al. (1994); (69) Pecaú et al. (2012); (70) Gaidos et al. (2022); (71) Silverberg et al. (2016); (72) Murphy et al. (2018); (73) Hiltner et al. (1969); (74) Crito et al. (2005); (75) Cruz et al. (2007); (76) Cruz et al. (2018); (77) Abt & Morrell (1995); (78) Stocke et al. (1991); (79) Galli et al. (2021); (80) Rodriguez et al. (2013); (81) Jackson & Stoy (1955); (82) Corbally (1984); (83) Silverberg et al. (2020); (84) Koen et al. (2017); (85) Bar et al. (2017); (86) Kirkpatrick et al. (2011); (87) Gray et al. (2017); (88) Cruz et al. (2009); (89) Phan-Bao & Bessell (2006); (90) Kirkpatrick et al. (2006); (91) Bowler et al. (2015); (92) Garrison & Gray (1994); (93) Artigau et al. (2015); (94) Lodieu et al. (2005); (95) Kirkpatrick et al. (2010); (96) Cowley (1972); (97) Luhman (2007); (98) Dobbie et al. (2010); (99) Whiteoak (1961); (100) Boudreault & Bailer-Jones (2009); (101) Barrado y Navascués et al. (2004); (102) Perry & Bond (1969); (103) Patten & Simon (1996); (104) Buscombe (1965); (105) Gahm et al. (1983).
^c	(1) Torres et al. (2006); (2) this work; (3) Malo et al. (2014b); (4) Shkolnik et al. (2017); (5) Kiss et al. (2011); (6) Malo et al. (2013); (7) Binks & Jeffries (2016); (8) Mentuch et al. (2008); (9) Reid et al. (2002); (10) Zickgraf et al. (1998); (11) Bowler et al. (2019); (12) Song et al. (2003); (13) da Silva et al. (2009); (14) Yee & Jensen (2010); (15) Stahl et al. (2022); (16) Alcalá et al. (1996); (17) Moór et al. (2013); (18) White et al. (2007); (19) Kraus et al. (2014); (20) Song et al. (2002); (21) Gaidos et al. (2022); (22) Wood et al. (2023); (23) Murphy et al. (2018); (24) Rodriguez et al. (2013); (25) Phan-Bao et al. (2017); (26) Hourihane et al. (2023); (27) Pecaú & Mamajek (2016); (28) Nisak et al. (2022); (29) Jeffries et al. (2023); (30) Gutiérrez Albarrán et al. (2020); (31) Dobbie et al. (2010); (32) Barrado y Navascués et al. (2004).
^d	(1) Gaia DR3; (2) Miret-Roig et al. (2020); (3) Malo et al. (2014a); (4) Shkolnik et al. (2017); (5) Fouqué et al. (2018); (6) Shkolnik et al. (2012); (7) Macintosh et al. (2015); (8) Faherty et al. (2016); (9) Soubiran et al. (2018); (10) Zúñiga-Fernández et al. (2021); (11) Lafarga et al. (2020); (12) Schneider et al. (2019); (13) Gontcharov (2006); (14) Strassmeier & Rice (2000); (15) Abdurro'uf et al. (2022); (16) Quast et al. (2000); (17) Torres et al. (2006); (18) Stahl et al. (2022); (19) Buder et al. (2021); (20) Burgasser et al. (2015); (21) Allers et al. (2016); (22) Kraus et al. (2014); (23) Gaia DR2; (24) Brown et al. (2022); (25) Gaidos et al. (2022); (26) Murphy et al. (2018); (27) Moór et al. (2013); (28) Iglesias et al. (2018); (29) White et al. (2007); (30) Rodriguez et al. (2013); (31) Galli et al. (2021); (32) Galli et al. (2023); (33) Boucher et al. (2016); (34) Hourihane et al. (2023); (35) Nisak et al. (2022); (36) Mermilliod et al. (2009); (37) Randich et al. (2022); (38) Steinmetz et al. (2020); (39) Randich et al. (2018); (40) Pourbaix et al. (2004); (41) Jackson et al. (2020); (42) Borisov et al. (2023).
^e	Source name from the AllWISE Source Catalog, the AllWISE Reject Catalog, or the WISE All-Sky Source Catalog.
^f	nodet = nondetection; false = detection from WISE appears to be false or unreliable based on visual inspection.
NOTE—	The table is available in its entirety in machine-readable form.

Table 4. Previous Candidates Excluded from BPMG Catalog

Column Label	Description
ID	ID in Figures 1 and 4
GaiaDR3	Gaia DR3 source name
Name	Other source name
RAdeg	Gaia DR3 right ascension (ICRS at Epoch 2016.0) ^a
DEdeg	Gaia DR3 declination (ICRS at Epoch 2016.0) ^a
pmRA	Gaia DR3 proper motion in right ascension ^a
e_pmRA	Error in pmRA
pmDec	Gaia DR3 proper motion in declination ^a
e_pmDec	Error in pmDec
plx	Gaia DR3 parallax ^a
e_plx	Error in plx
rmedgeo	Median of geometric distance posterior (Bailer-Jones et al. 2021) ^a
rlogeo	16th percentile of geometric distance posterior (Bailer-Jones et al. 2021) ^a
rhigeo	84th percentile of geometric distance posterior (Bailer-Jones et al. 2021) ^a
RVel	Radial velocity
e_RVel	Error in RVel
r_RVel	Radial velocity reference ^b
U	U component of space velocity
e_U	Error in U
V	V component of space velocity
e_V	Error in V
W	W component of space velocity
e_W	Error in W
Gmag	Gaia DR3 G magnitude
e_Gmag	Error in G mag
GBPmag	Gaia DR3 G_{BP} magnitude
e_GBPmag	Error in GBP mag
GRPmag	Gaia DR3 G_{RP} magnitude
e_GRPmag	Error in GRP mag
RUWE	Gaia DR3 renormalized unit weight error

^aThe astrometry and distance for CD-27 11535 are from Gaia DR2 and Bailer-Jones et al. (2018).

^b(1) Gaia DR3; (2) Gontcharov (2006); (3) Bailey et al. (2012); (4) Soubiran et al. (2018); (5) Rice et al. (2010); (6) Shkolnik et al. (2017); (7) Fouqué et al. (2018); (8) Schneider et al. (2019); (9) Miret-Roig et al. (2020); (10) Tokovinin (2022); (11) Jönsson et al. (2020); (12) Elliott et al. (2014).

NOTE— The table is available in its entirety in machine-readable form.

Table 5. Adopted Members of NGC 2547

Column Label	Description
GaiaDR3	Gaia DR3 source name
Name	Other source name
RAdeg	Gaia DR3 right ascension (ICRS at Epoch 2016.0)
DEdeg	Gaia DR3 declination (ICRS at Epoch 2016.0)
SpType	Spectral type
r_SpType	Spectral type reference ^a
Adopt	Adopted spectral type
pmRA	Gaia DR3 proper motion in right ascension
e_pmRA	Error in pmRA
pmDec	Gaia DR3 proper motion in declination
e_pmDec	Error in pmDec
plx	Gaia DR3 parallax
e_plx	Error in plx
rmedgeo	Median of geometric distance posterior (Bailer-Jones et al. 2021)
rlogeo	16th percentile of geometric distance posterior (Bailer-Jones et al. 2021)
rhigeo	84th percentile of geometric distance posterior (Bailer-Jones et al. 2021)
RVel	Radial velocity
e_RVel	Error in RVel
r_RVel	Radial velocity reference ^b
Gmag	Gaia DR3 <i>G</i> magnitude
e_Gmag	Error in Gmag
GBPmag	Gaia DR3 <i>G_{BP}</i> magnitude
e_GBPmag	Error in GBPmag
GRPmag	Gaia DR3 <i>G_{RP}</i> magnitude
e_GRPmag	Error in GRPmag
RUWE	Gaia DR3 renormalized unit weight error
wise	AllWISE source name
W1mag	WISE W1 magnitude
e_W1mag	Error in W1mag
W2mag	WISE W2 magnitude
e_W2mag	Error in W2mag
W3mag	WISE W3 magnitude
e_W3mag	Error in W3mag
f_W3mag	Flag on W3mag ^c
W4mag	WISE W4 magnitude
e_W4mag	Error in W4mag
f_W4mag	Flag on W4mag ^c
24mag	Spitzer [24] magnitude
e_24mag	Error in 24mag
Exc24	Excess in [24]?

^a (1) Jeffries et al. (2003); (2) Cannon & Pickering (1993); (3) Hartoog et al. (1976); (4) Houk (1978); (5) Jeffries & Oliveira (2005); (6) Teixeira et al. (2009b).

^b (1) Gaia DR3; (2) Hourihane et al. (2023); (3) Jackson et al. (2020); (4) Gontcharov (2006).

^c nodet = nondetection; false = detection from AllWISE appears to be false or unreliable based on visual inspection.

NOTE— The table is available in its entirety in machine-readable form.

Table 6. Excess Fractions for Associations with Ages of 10–50 Myr

Association	Age ^a (Myr)	W3 Excess Fractions			W4 Excess Fractions		
		B/A/F	G/K	M0–M6	B/A/F	G/K	M0–M6
TWA	10	$1/2 = 0.500^{+1.150}_{-0.413}$	0/1	$10/50 = 0.200^{+0.085}_{-0.062}$	$1/2 = 0.500^{+1.150}_{-0.413}$	0/1	$10/42 = 0.238^{+0.102}_{-0.074}$
U Sco	11	$9/47 = 0.191^{+0.087}_{-0.063}$	$7/60 = 0.117^{+0.063}_{-0.043}$	$184/899 = 0.205^{+0.016}_{-0.015}$	$14/47 = 0.298^{+0.103}_{-0.079}$	$17/56 = 0.304^{+0.093}_{-0.073}$...
UCL/LCC	20	$23/245 = 0.094^{+0.024}_{-0.019}$	$7/278 = 0.025^{+0.014}_{-0.009}$	$234/3024 = 0.077 \pm 0.005$	$80/245 = 0.327^{+0.041}_{-0.036}$	$12/244 = 0.049^{+0.019}_{-0.014}$...
Sco Body	20	$4/19 = 0.211^{+0.166}_{-0.101}$	$1/27 = 0.037^{+0.085}_{-0.031}$	$8/199 = 0.040^{+0.020}_{-0.014}$	$7/19 = 0.368^{+0.198}_{-0.136}$	$1/24 = 0.042^{+0.096}_{-0.034}$...
32 Ori	21	$1/15 = 0.067^{+0.153}_{-0.055}$	0/13 = <0.142	$10/121 = 0.083^{+0.035}_{-0.026}$	$4/16 = 0.250^{+0.198}_{-0.120}$	0/13 = <0.142	...
BPMG	25	$3/15 = 0.200^{+0.195}_{-0.109}$	$1/18 = 0.056^{+0.128}_{-0.046}$	0/126 = <0.015	$8/15 = 0.533^{+0.263}_{-0.185}$	$2/18 = 0.111^{+0.147}_{-0.072}$	0/98 = <0.019
93 Tau	29	0/14 = <0.132	0/26 = <0.071	$2/131 = 0.015^{+0.020}_{-0.010}$	$4/14 = 0.286^{+0.226}_{-0.137}$	$1/26 = 0.038^{+0.088}_{-0.032}$...
Car-Ext/Col/ χ^1 For	34	$6/71 = 0.085^{+0.050}_{-0.034}$	0/132 = <0.014	$31/764 = 0.041^{+0.009}_{-0.007}$	$19/71 = 0.268^{+0.077}_{-0.061}$	$2/106 = 0.019^{+0.025}_{-0.012}$...
Tuc-Hor/IC 2602	40	$7/94 = 0.074^{+0.040}_{-0.027}$	$2/150 = 0.013^{+0.018}_{-0.009}$	$6/835 = 0.007^{+0.004}_{-0.003}$	$23/94 = 0.245^{+0.062}_{-0.051}$	0/111 = <0.017	...
IC 2391	47	0/34 = <0.054	0/59 = <0.031	$1/275 = 0.004^{+0.008}_{-0.003}$	$3/34 = 0.088^{+0.086}_{-0.048}$

^a Sources of ages are described in Section 5.11.

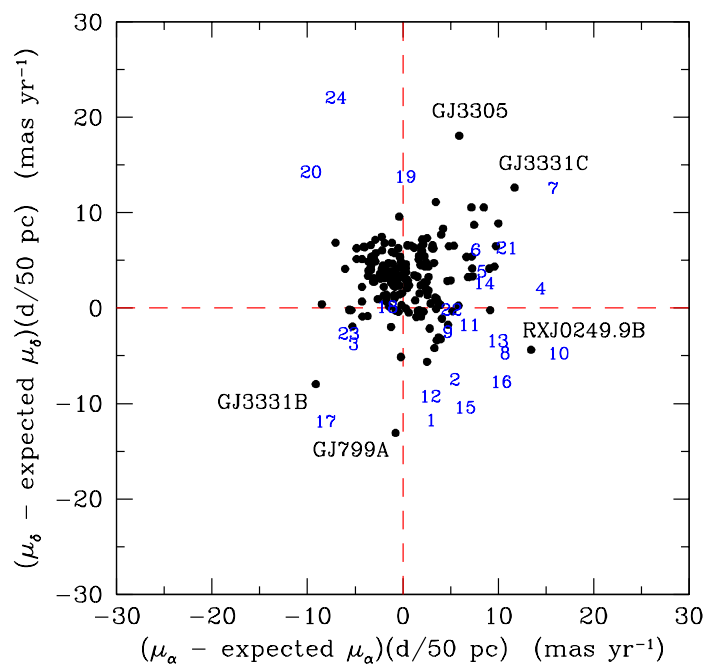


Figure 1. Proper motion offsets based on Gaia DR3 for adopted members of BPMG and a sample of previously identified candidates that are excluded from my catalog (blue numerals). Discrepant measurements for adopted members are labeled with the source names.

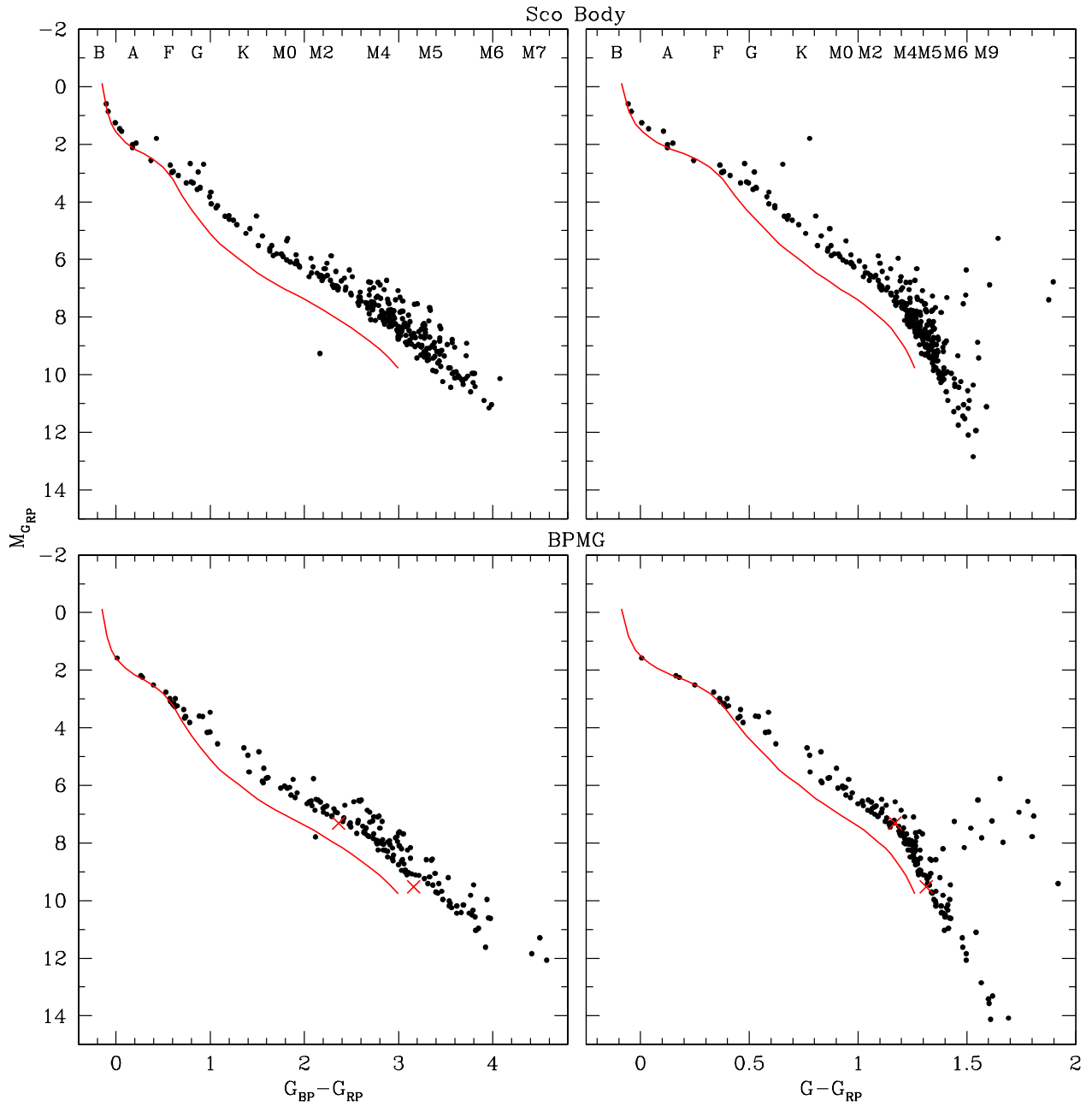


Figure 2. $M_{G_{RP}}$ versus $G_{BP} - G_{RP}$ and $G - G_{RP}$ for adopted members of Sco Body and BPMG. In addition, the disk-bearing stars StH α 34 (White & Hillenbrand 2005; Hartmann et al. 2005) and 2MASS 15460752–6258042 (Lee et al. 2020) are plotted in the diagrams for BPMG (red crosses). Each CMD includes a fit to the single-star sequence of the Pleiades. The spectral types that correspond to the colors of young stars are indicated (Luhman 2022a).

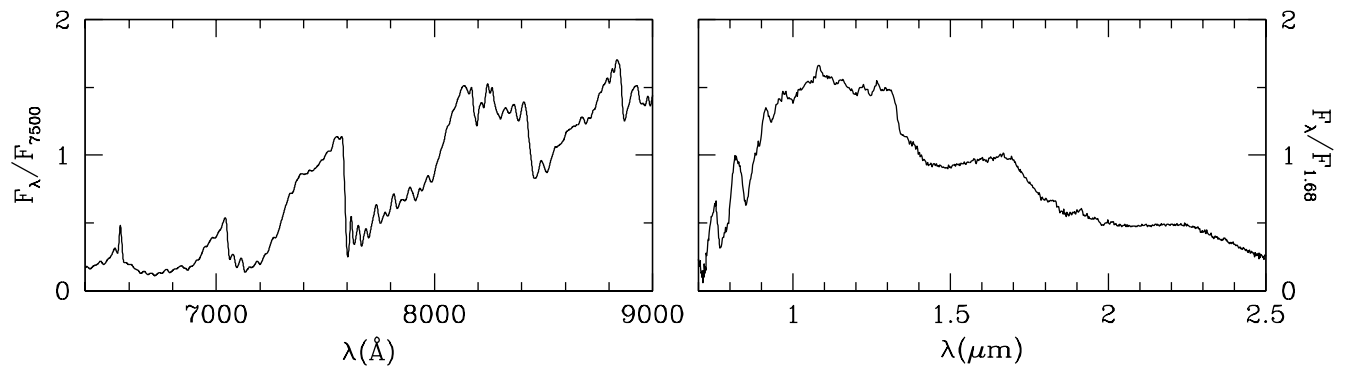


Figure 3. Examples of optical and IR spectra of adopted members of BMPG (Gaia DR3 5809284739228623232 and Gaia DR3 6754492932379552896). Each object has a spectral type of M6. The optical spectrum is displayed at a resolution of 13 \AA .

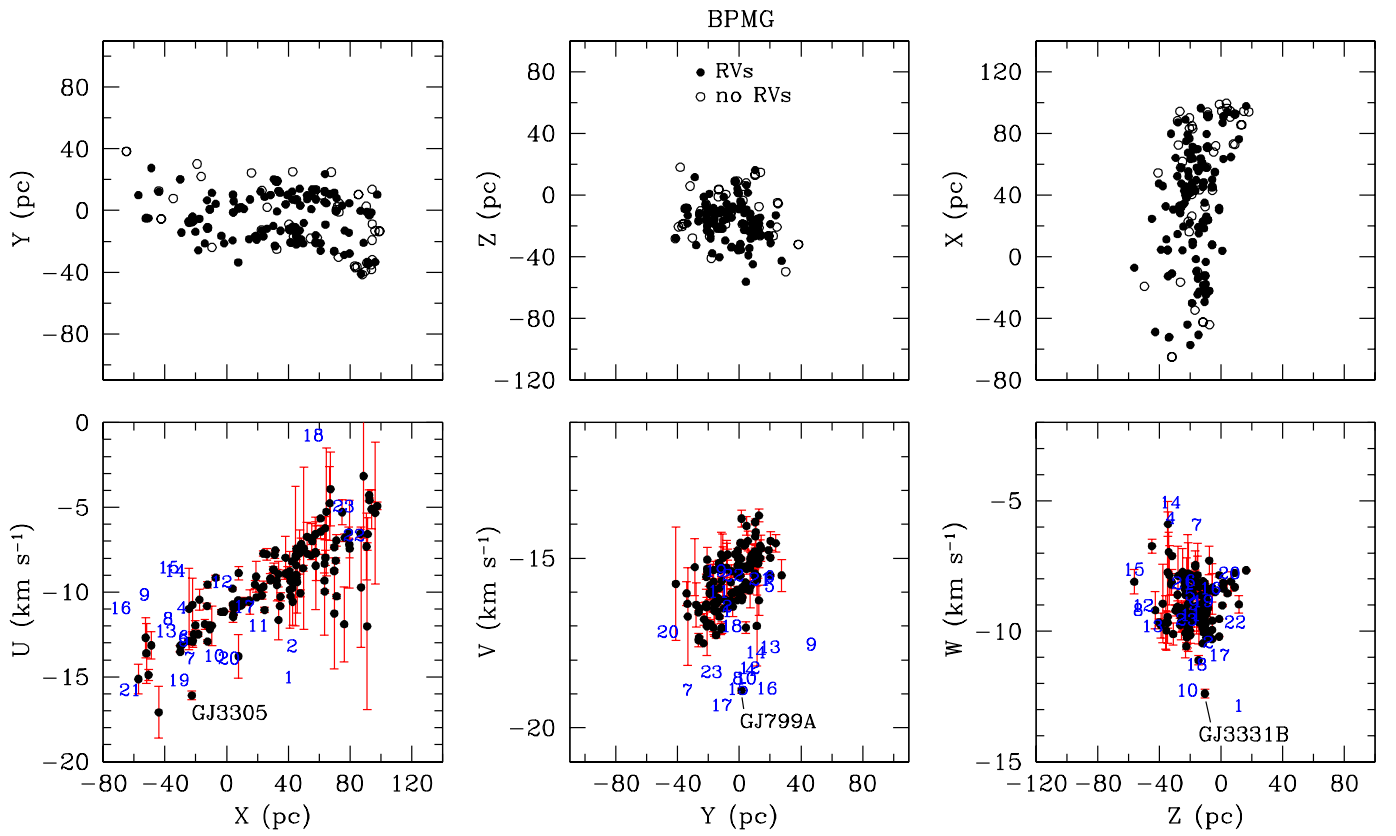


Figure 4. Galactic Cartesian coordinates and UVW velocities for the adopted members of BPMG and a sample of previously identified candidates that are excluded from my catalog (blue numerals; Table 4). Discrepant measurements for BPMG members are labeled with the source names.

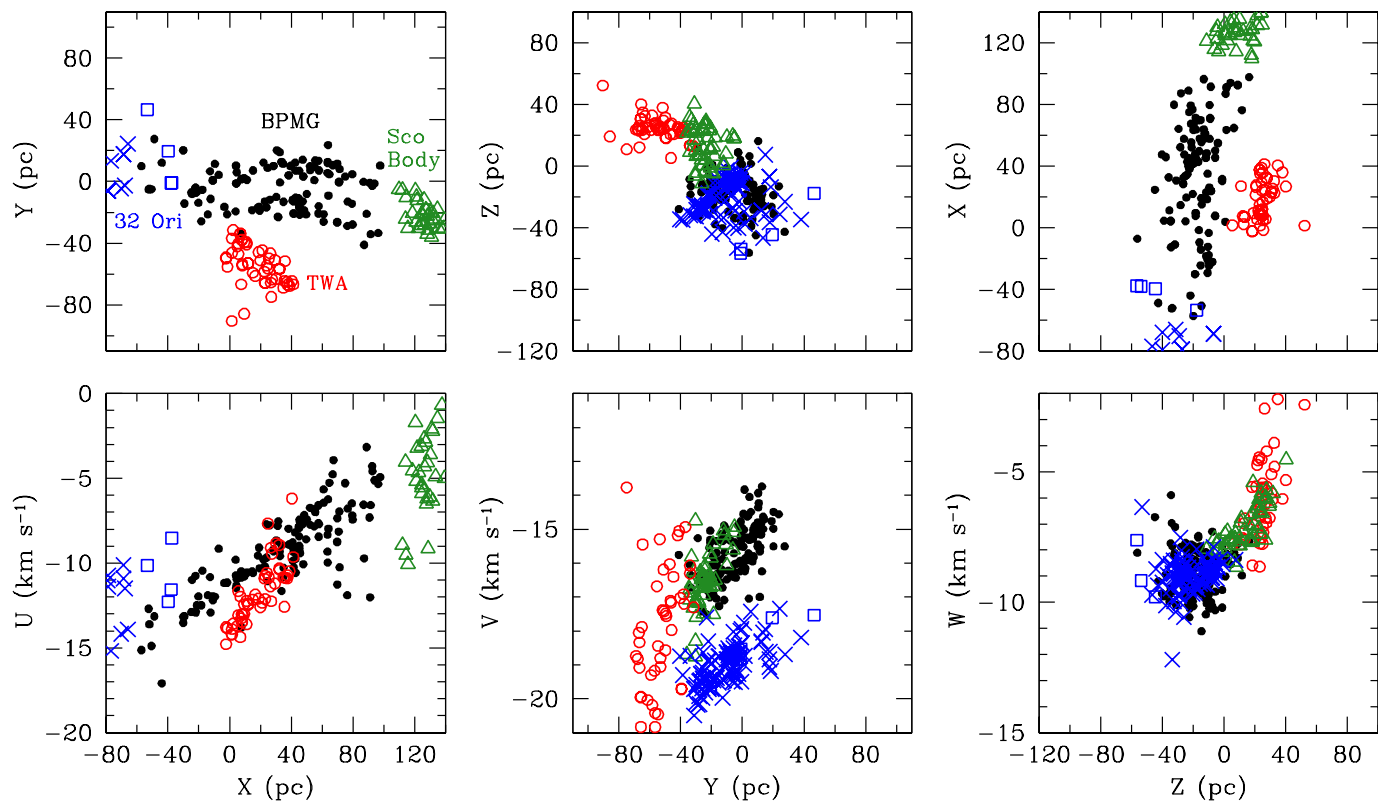


Figure 5. Galactic Cartesian coordinates and UVW velocities for members of BPMG (black points), TWA (red circles), 32 Ori (blue crosses), and Sco Body (green triangles) that have radial velocity measurements. Four newly proposed members of 32 Ori are included (blue squares).

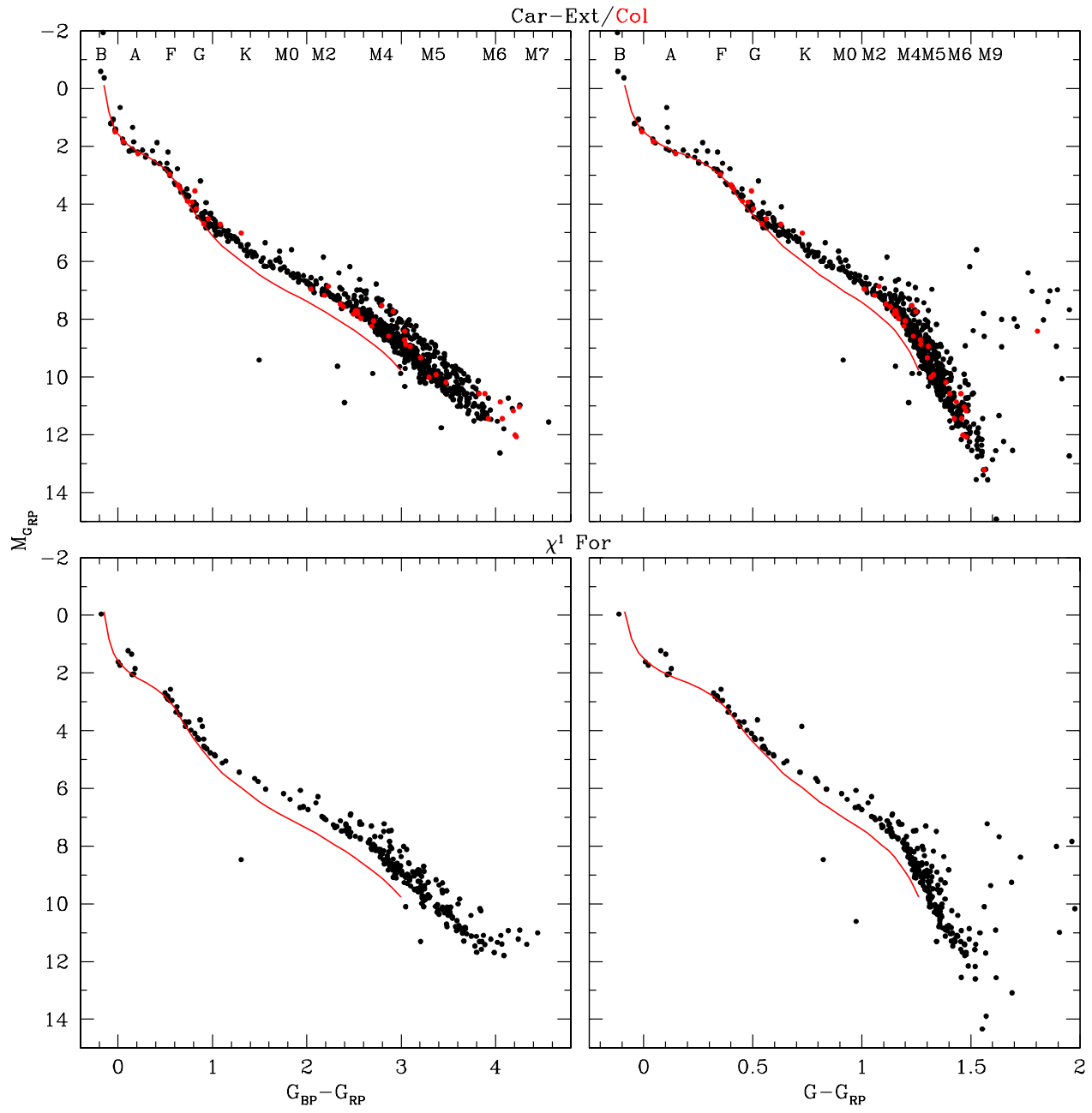


Figure 6. CMDs for adopted members of Car-Ext, Columba, and χ^1 For.

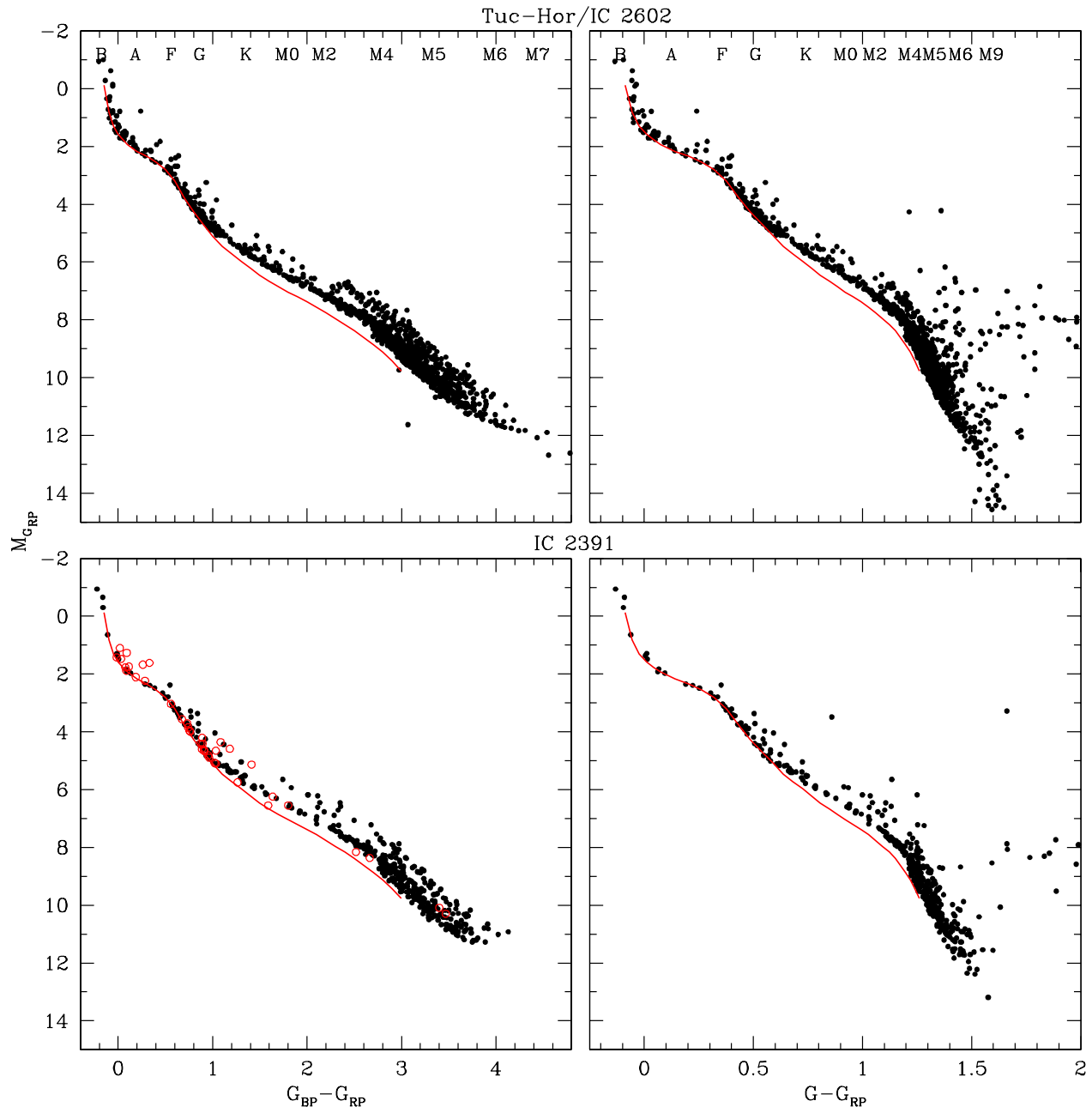


Figure 7. CMDs for adopted members of Tuc-Hor, IC 2602, and IC 2391. The left CMD for IC 2391 includes proposed members of the Argus association from [Zuckerman \(2019\)](#) (red circles).

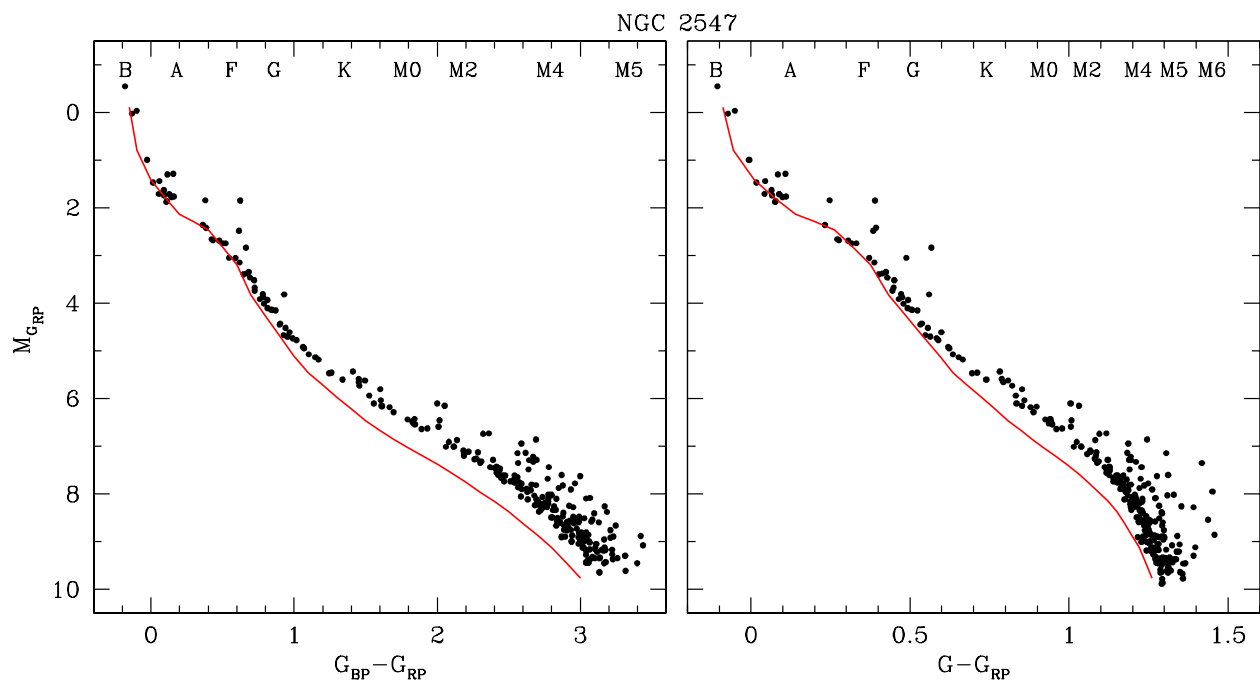


Figure 8. CMDs for adopted members of NGC 2547.

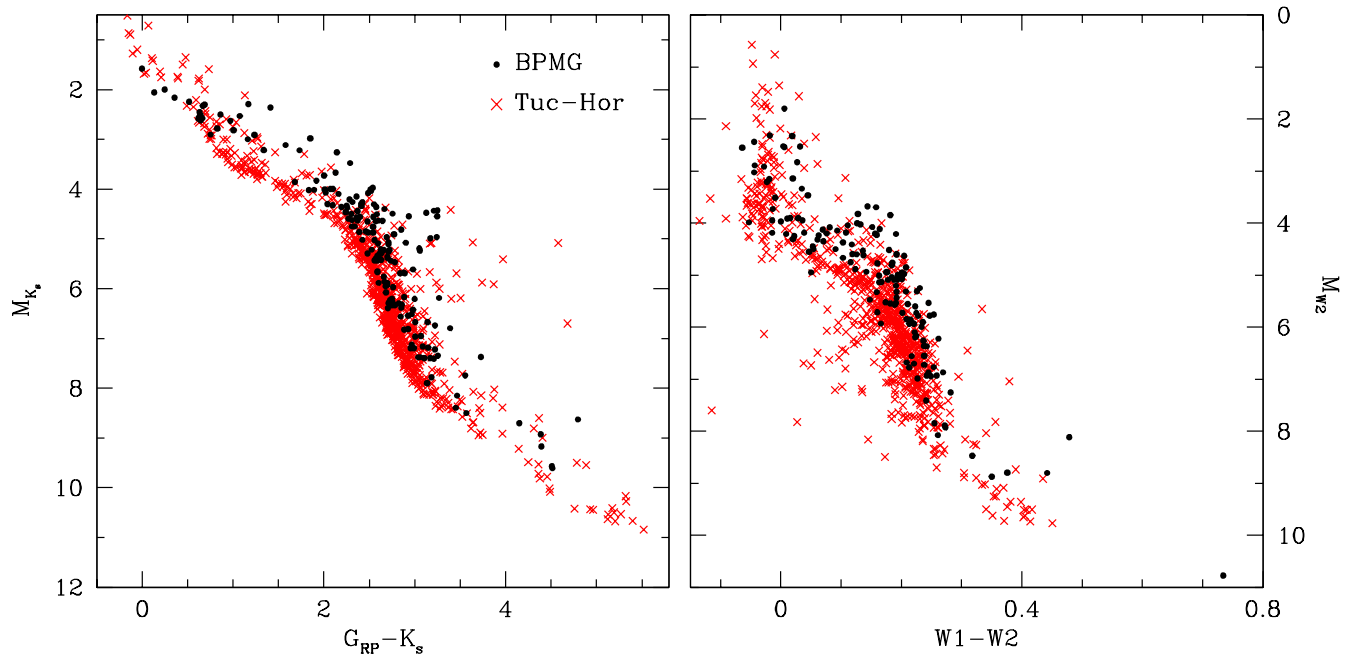


Figure 9. M_{K_s} versus $G_{RP} - K_s$ and M_{W2} versus $W1 - W2$ for adopted members of BPMG and Tuc-Hor. The faintest known member of BPMG in M_{W2} , PSO J318.5338–22.8603 (Liu et al. 2013), is absent from the left diagram since it lacks a detection with Gaia.

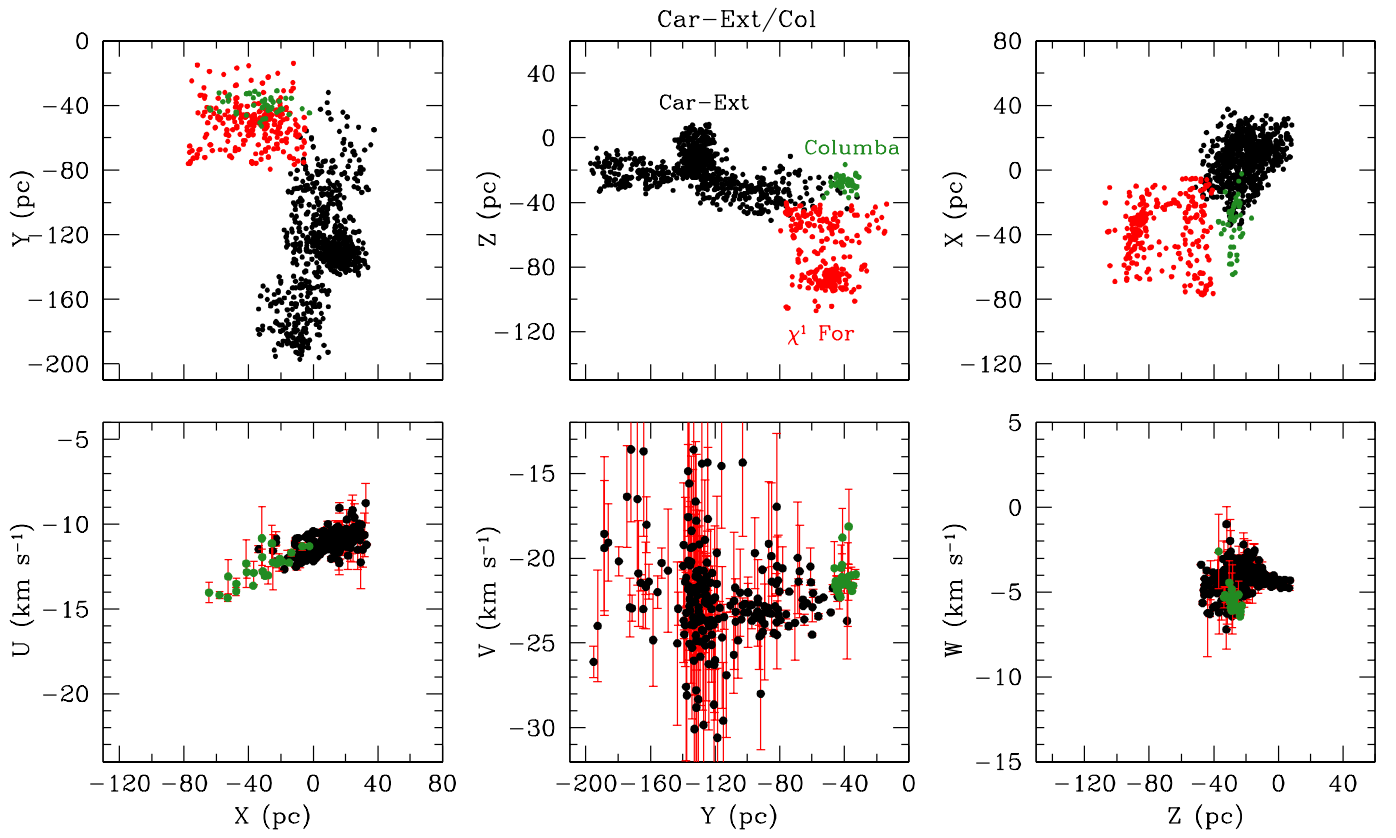


Figure 10. Galactic Cartesian coordinates and UVW velocities for the adopted members of Car-Ext and Columba. The coordinates for members of χ^1 For are included in the top diagrams.

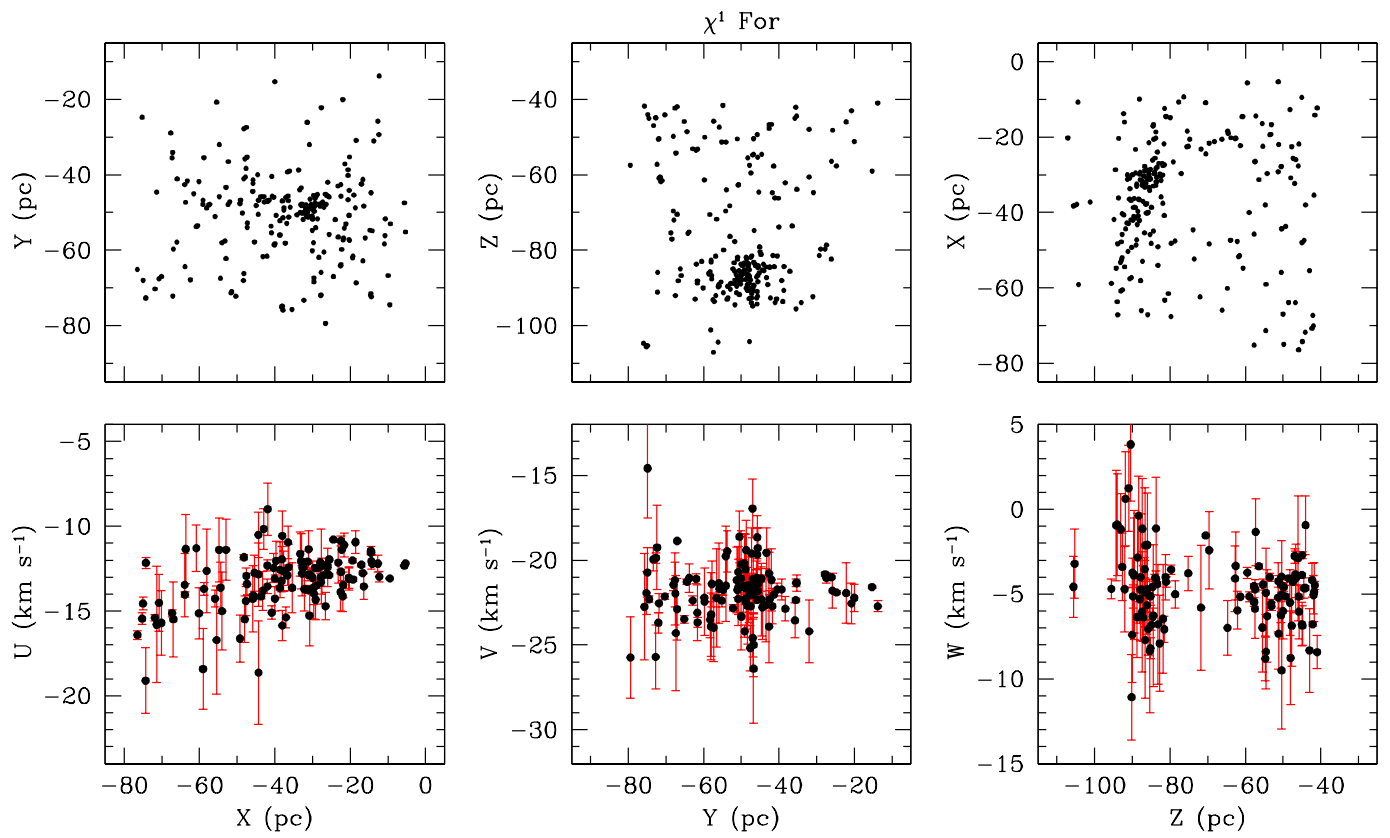


Figure 11. Galactic Cartesian coordinates and UVW velocities for the adopted members of χ^1 For.

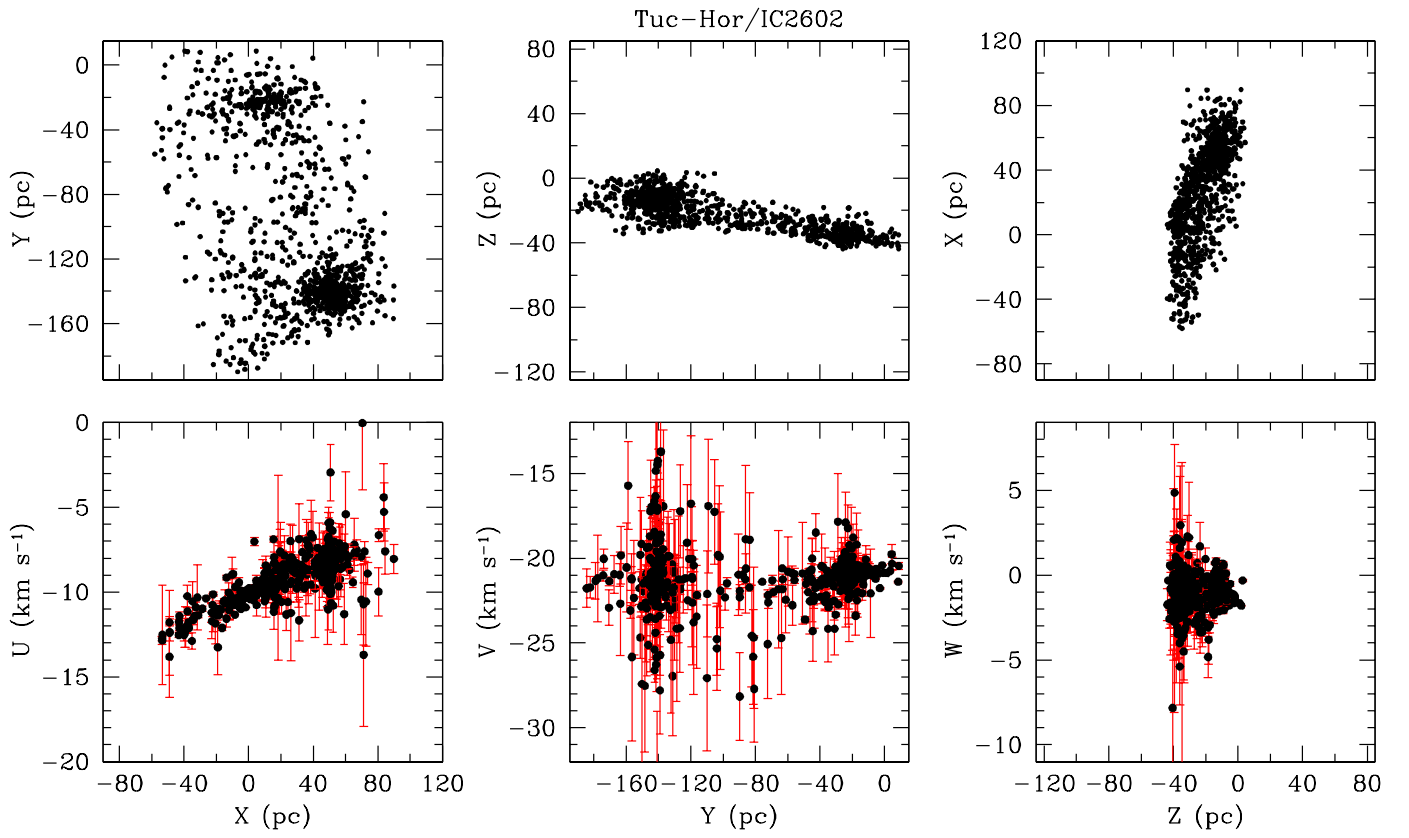


Figure 12. Galactic Cartesian coordinates and UVW velocities for the adopted members of Tuc-Hor and IC 2602.

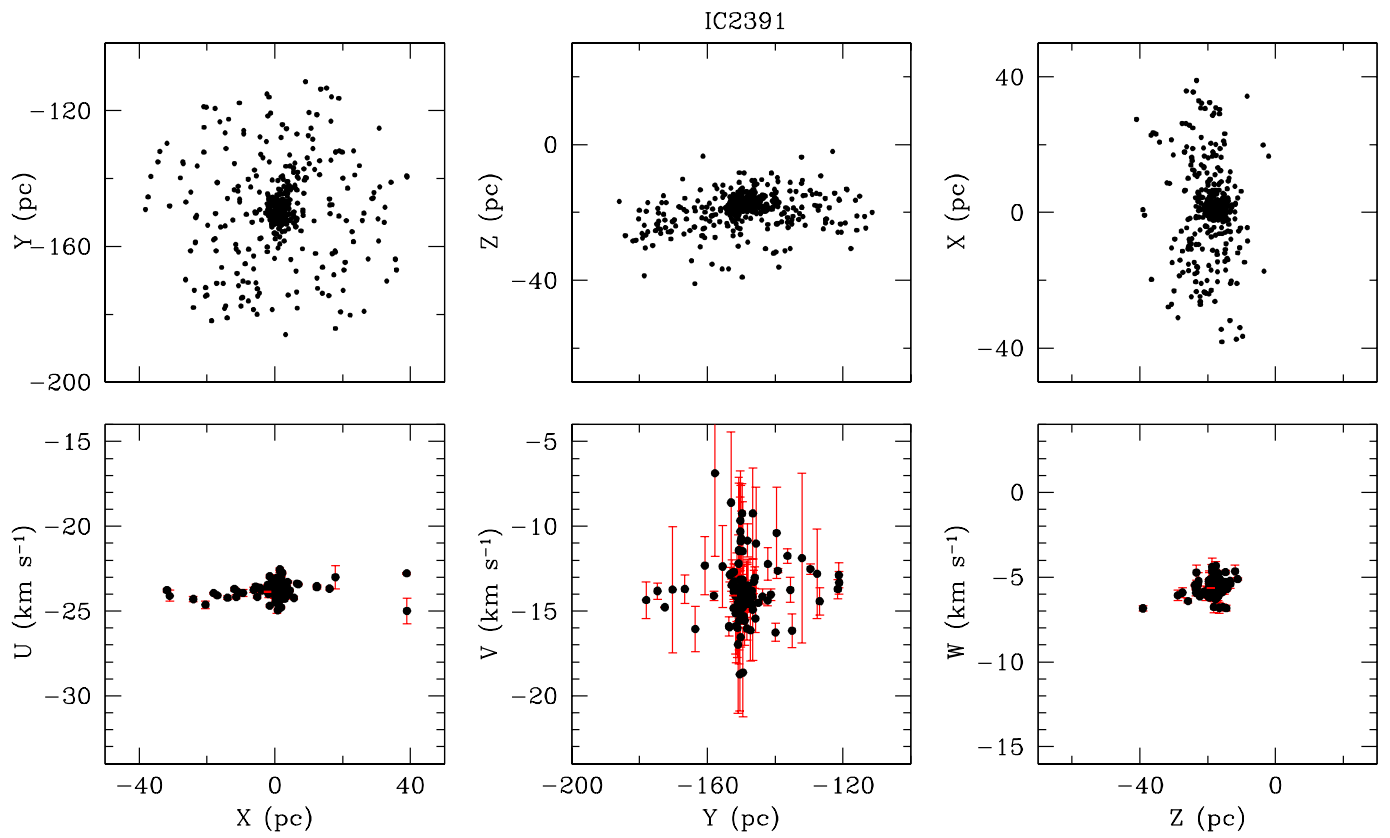


Figure 13. Galactic Cartesian coordinates and UVW velocities for the adopted members of IC 2391.

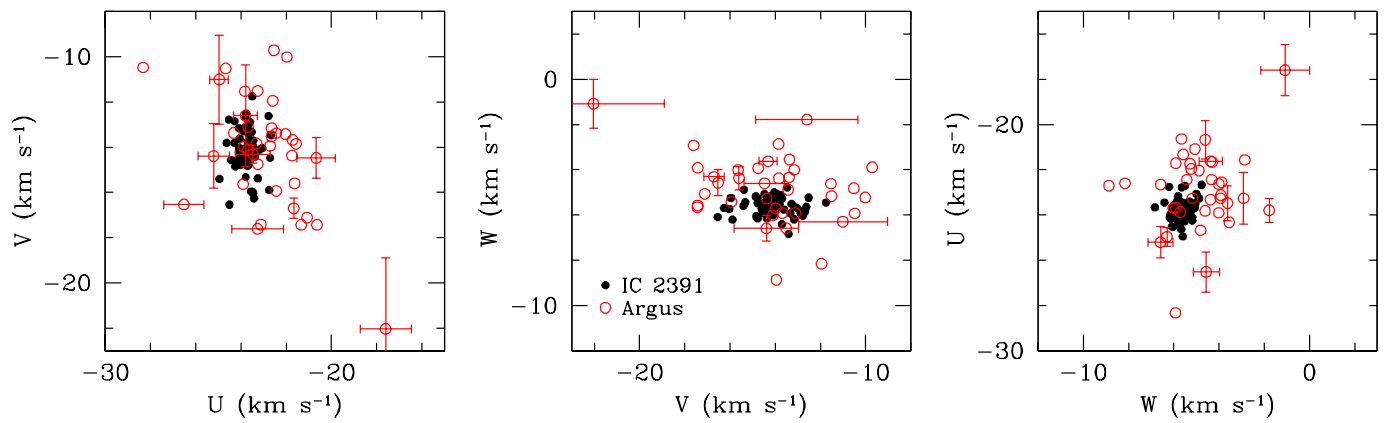


Figure 14. UVW velocities for members of IC 2391 with errors less than 0.8 km s^{-1} and proposed members of the Argus association from Zuckerman (2019).

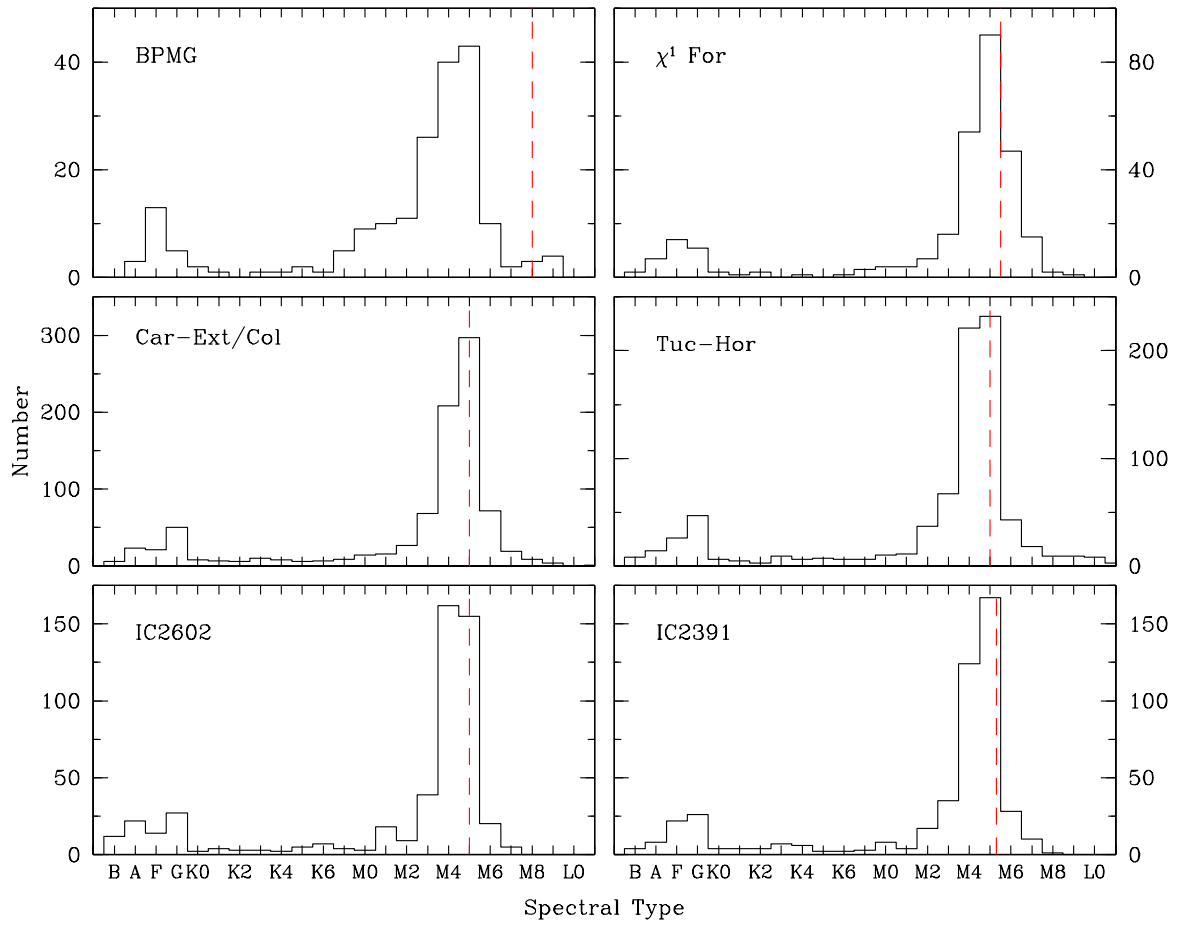


Figure 15. Histograms of spectral types for adopted members of BPMG and other young associations. Completeness limits are indicated (dashed lines).

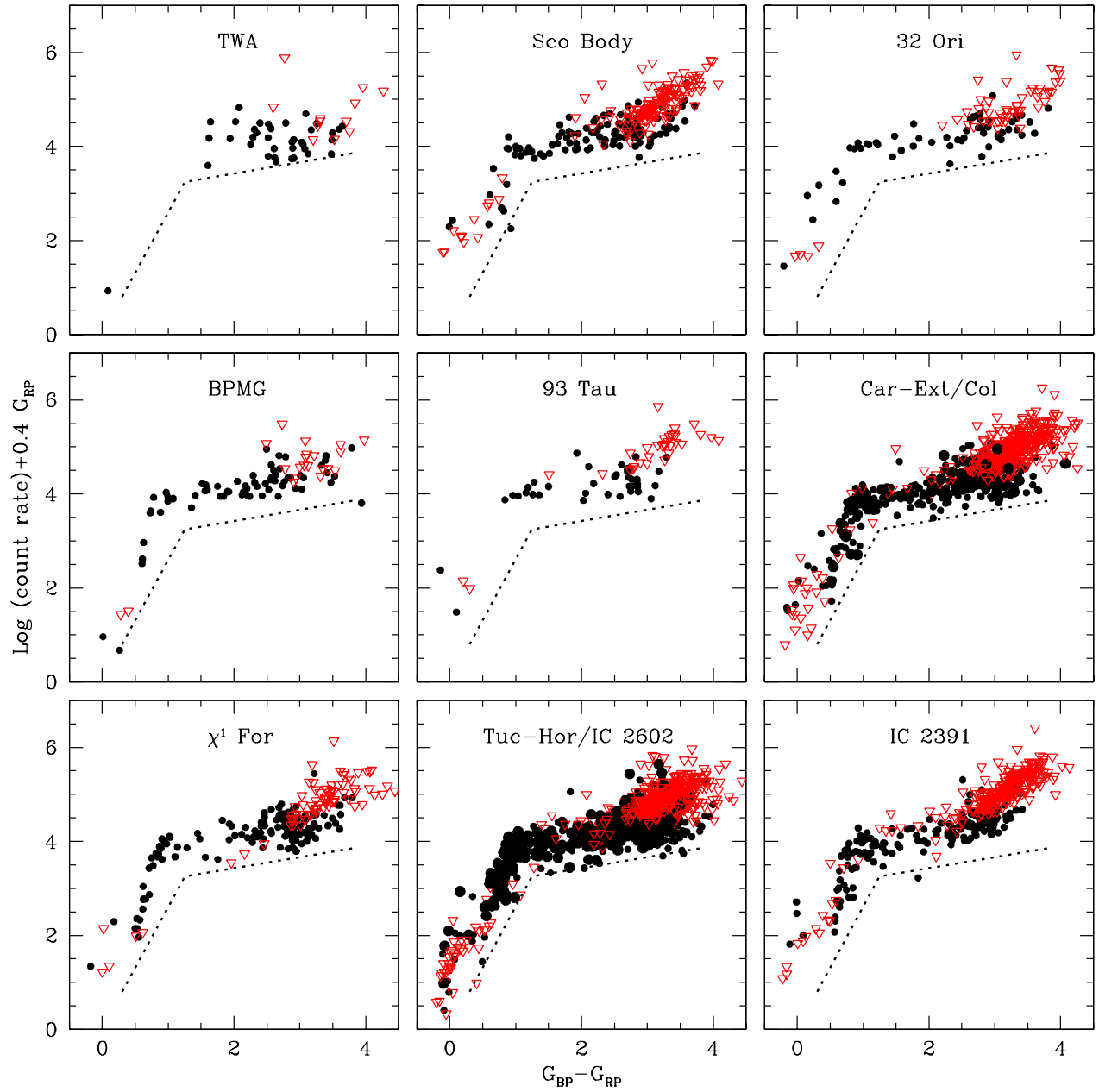


Figure 16. Ratio of X-ray and G_{RP} fluxes versus $G_{BP} - G_{RP}$ for adopted members of BPMG and other young associations based on data from eRASS1 and Gaia DR3. Upper limits for stars that are not detected in eRASS1 are indicated (3σ , red triangles). A boundary that follows the lower envelope of the data in Car-Ext/Columba is included in each diagram to facilitate comparison of the associations (dotted line).

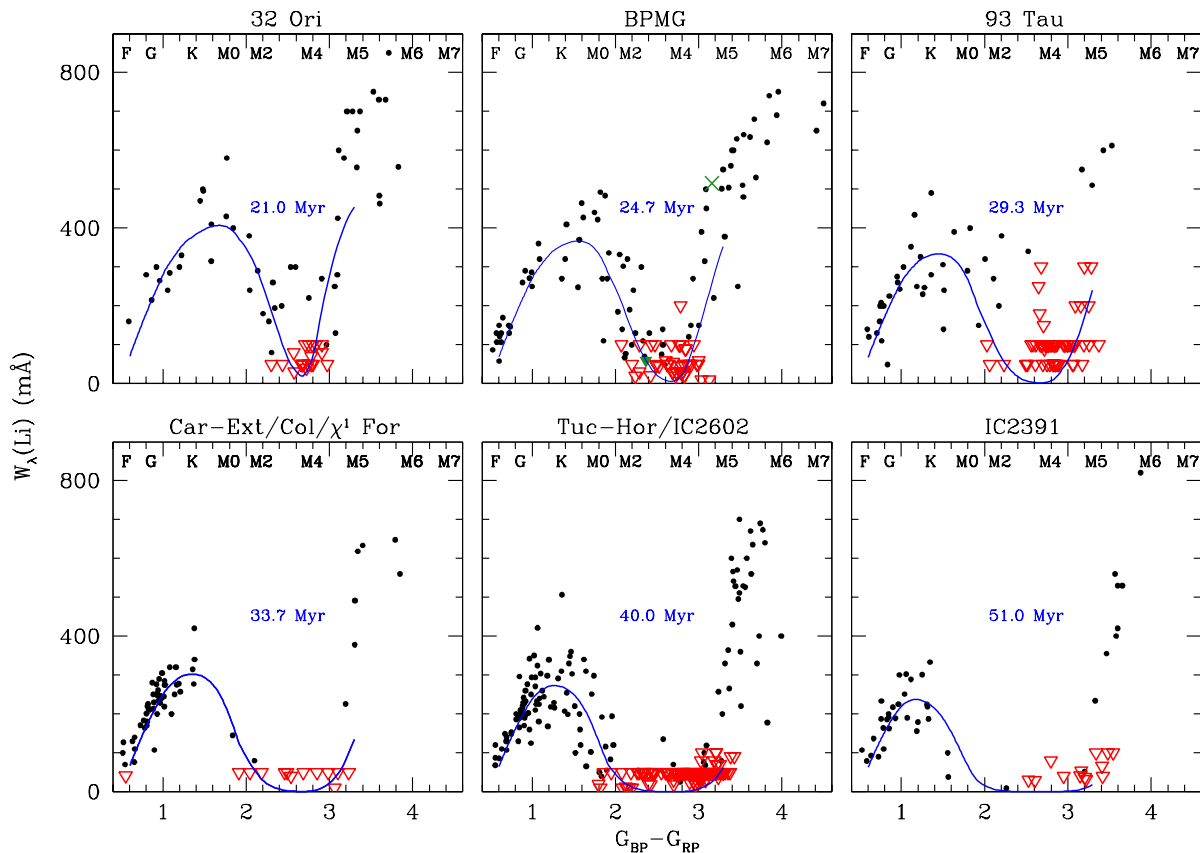


Figure 17. Equivalent widths of Li versus $G_{BP} - G_{RP}$ for adopted members of BPMG and other young associations (black points and red triangles) and the values produced by the EAGLES model for Li depletion (Jeffries et al. 2023) for the best-fitting ages (blue lines). The disk-bearing stars StH α 34 (White & Hillenbrand 2005; Hartmann et al. 2005) and 2MASS 15460752–6258042 (Lee et al. 2020) are plotted in the diagram for BPMG (green triangle and green cross). The spectral types that correspond to the colors of young stars are indicated (Luhman 2022a).

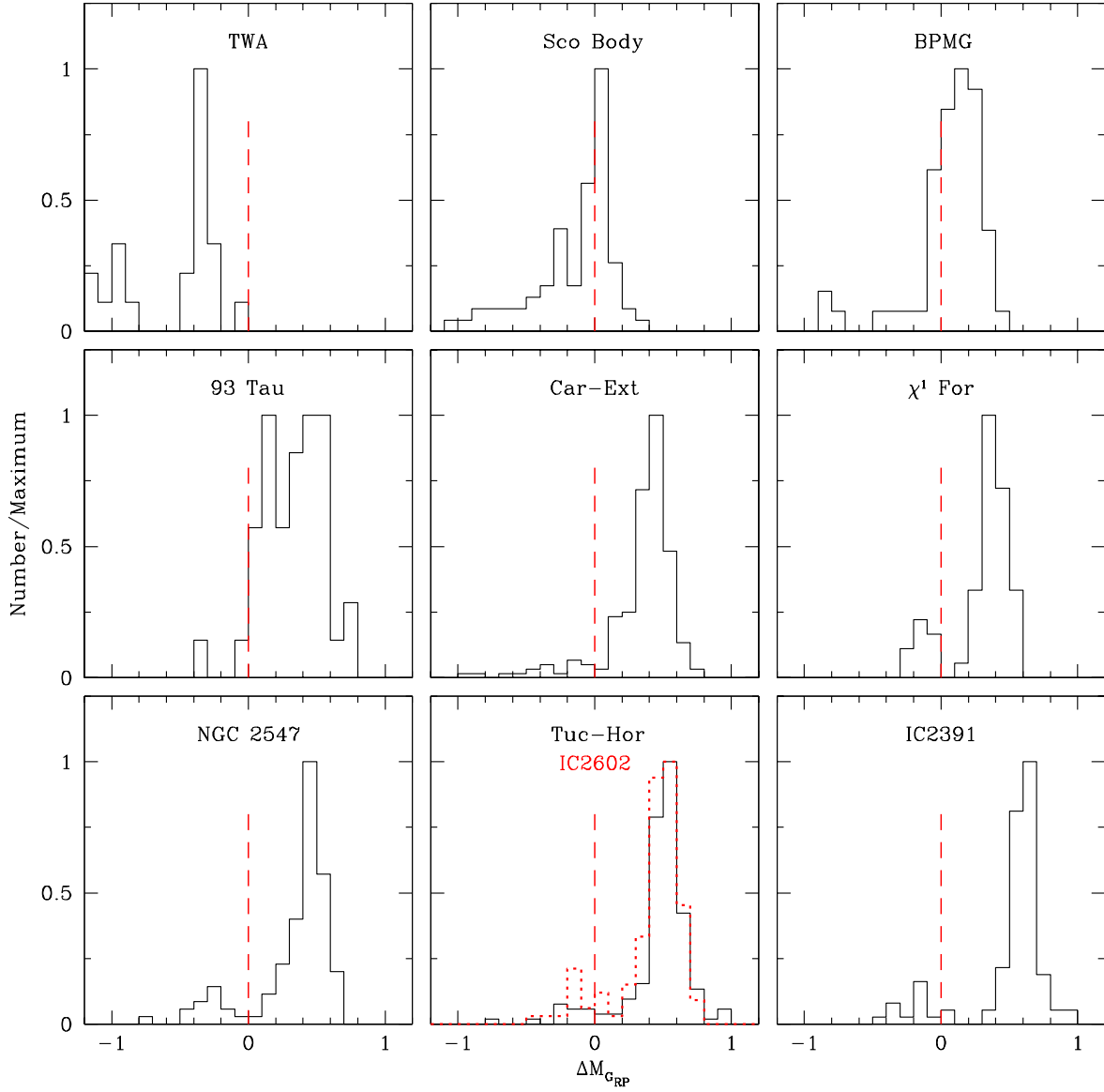


Figure 18. Histograms of offsets in M_{GRP} from the median CMD sequence for UCL/LCC for low-mass stars in BPMG and other young associations (Figures 2 and 6–8, Luhman 2023a,b). Negative values correspond to brighter magnitudes and younger ages.

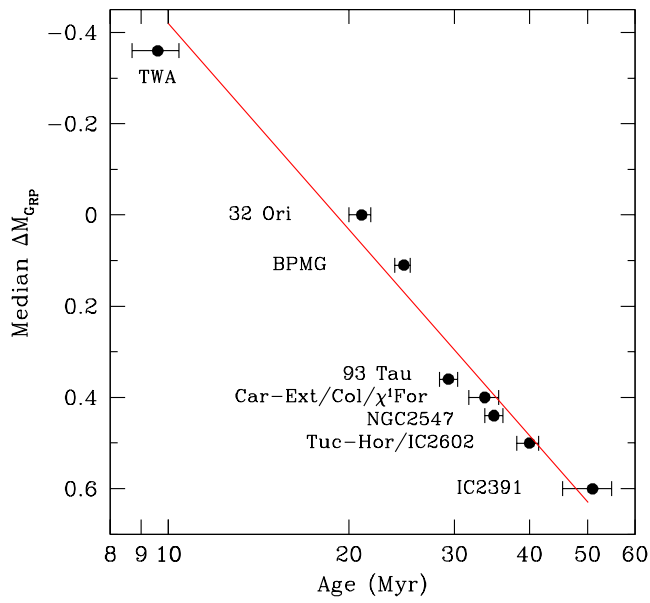


Figure 19. Median offset in M_{GRP} from the median CMD sequence for UCL/LCC (Figure 18) versus age for low-mass stars in BPMG and other young associations. The age for TWA is based on its expansion (Luhman 2023b) while the other ages are from the LDB (Figure 17). A linear relation with a slope of 1.5 and an arbitrary intercept is indicated (red line).

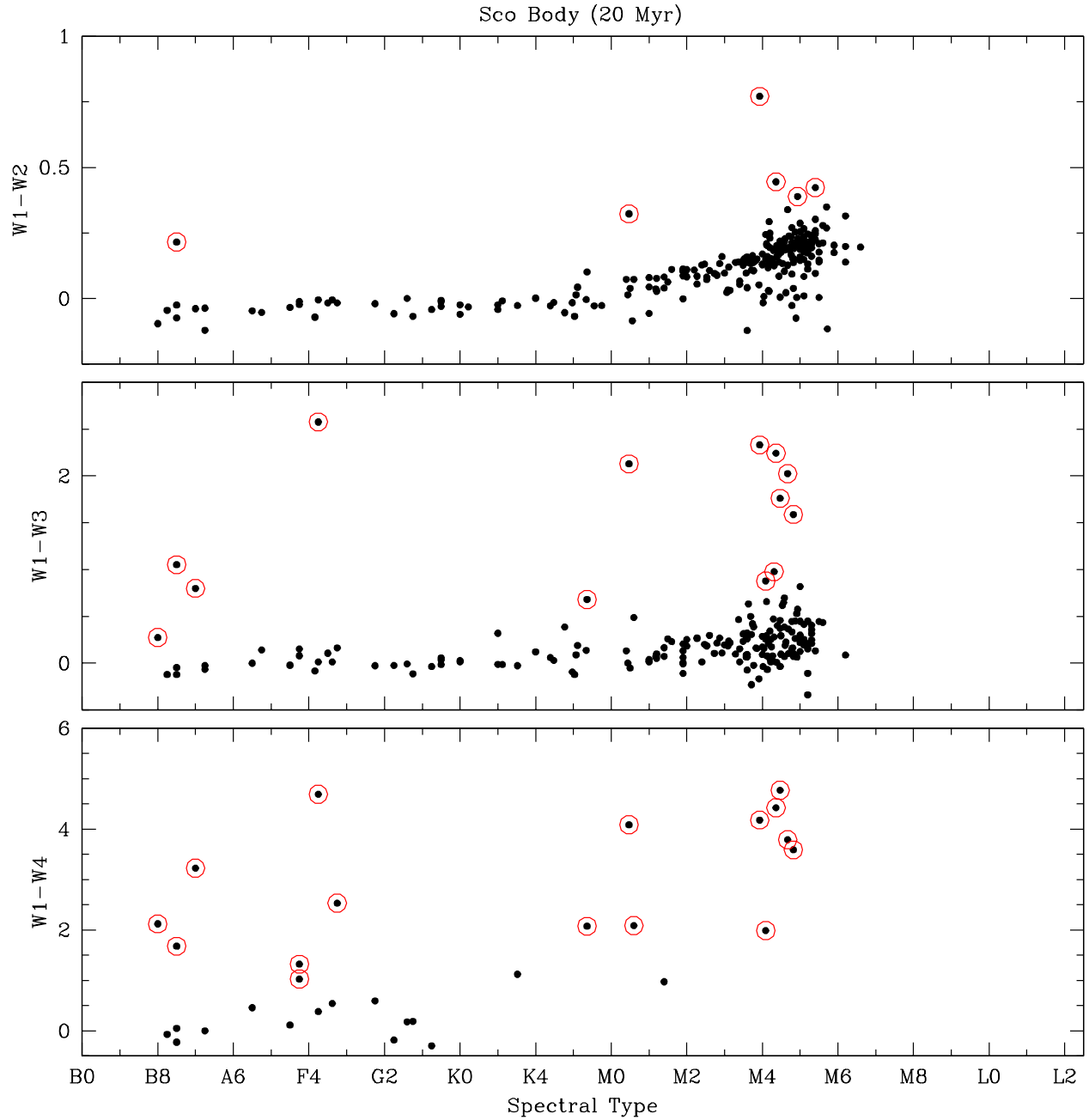


Figure 20. IR colors versus spectral type for adopted members of Sco Body. For stars that lack spectroscopy, spectral types have been estimated from photometry. In each diagram, the sequence of blue colors corresponds to stellar photospheres. Color excesses from disks are indicated (red circles).

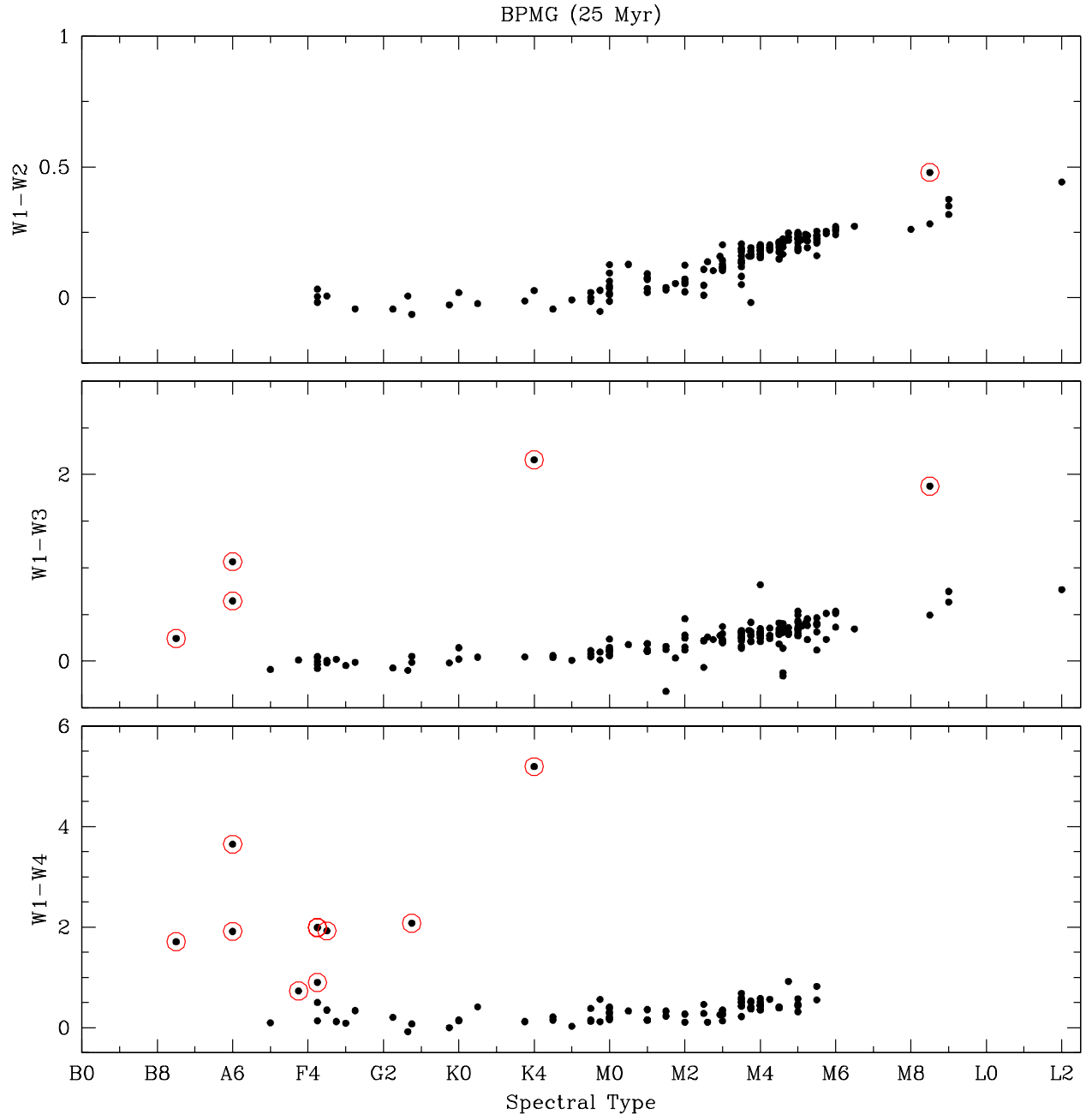


Figure 21. IR colors versus spectral type for adopted members of BPMG.

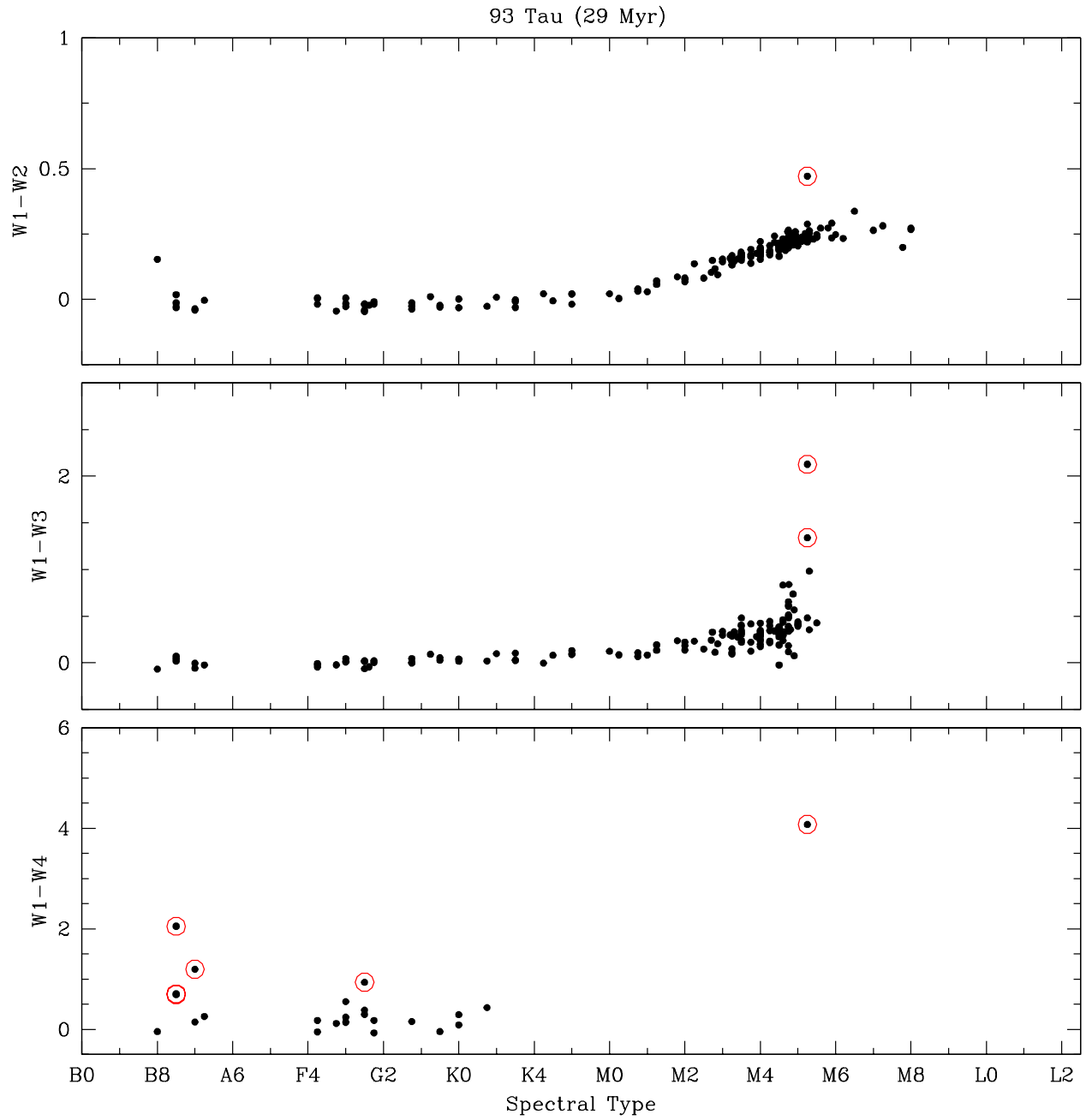


Figure 22. IR colors versus spectral type for adopted members of 93 Tau (Luhman 2023a).

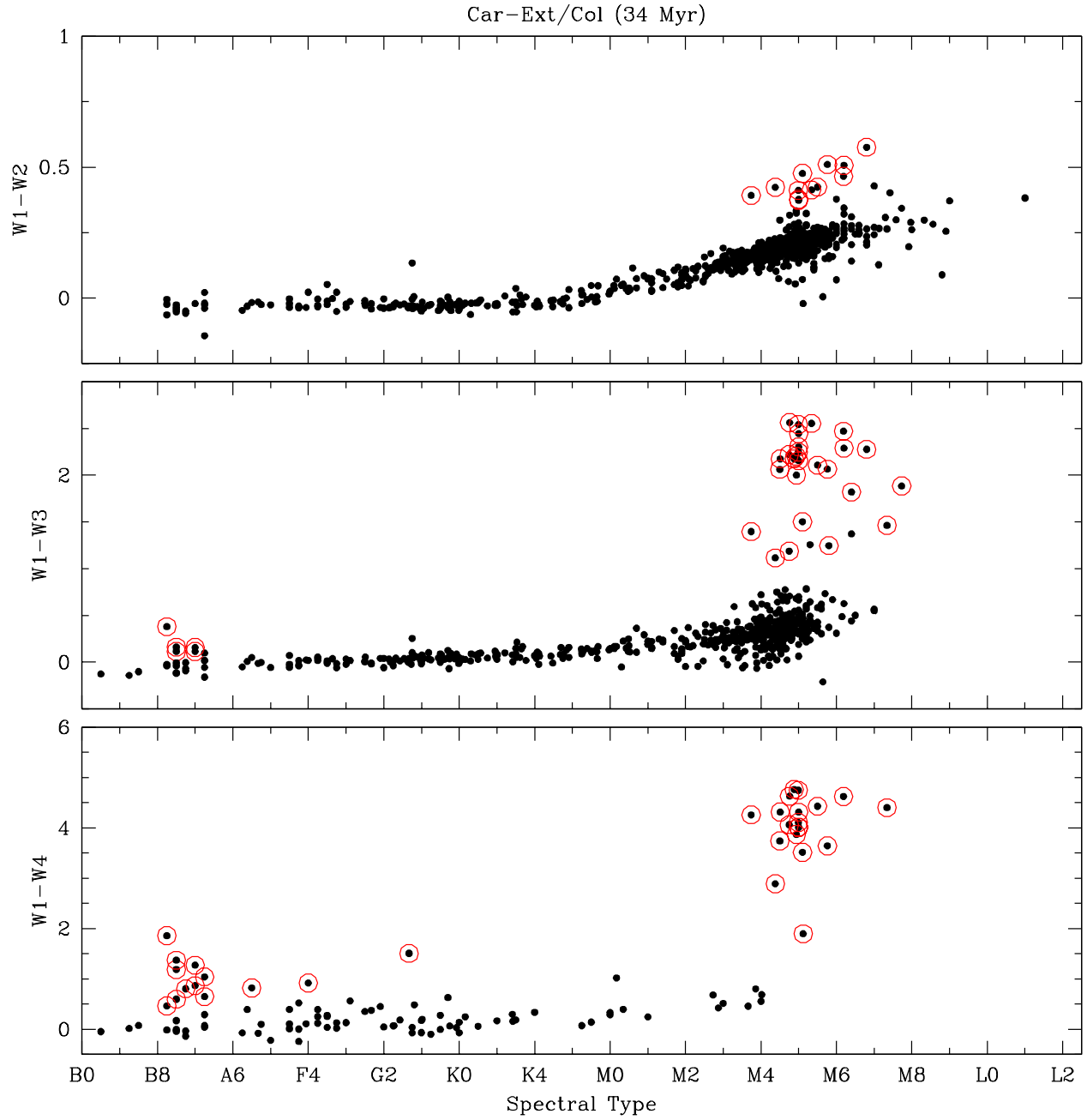


Figure 23. IR colors versus spectral type for adopted members of Car-Ext and Columba.

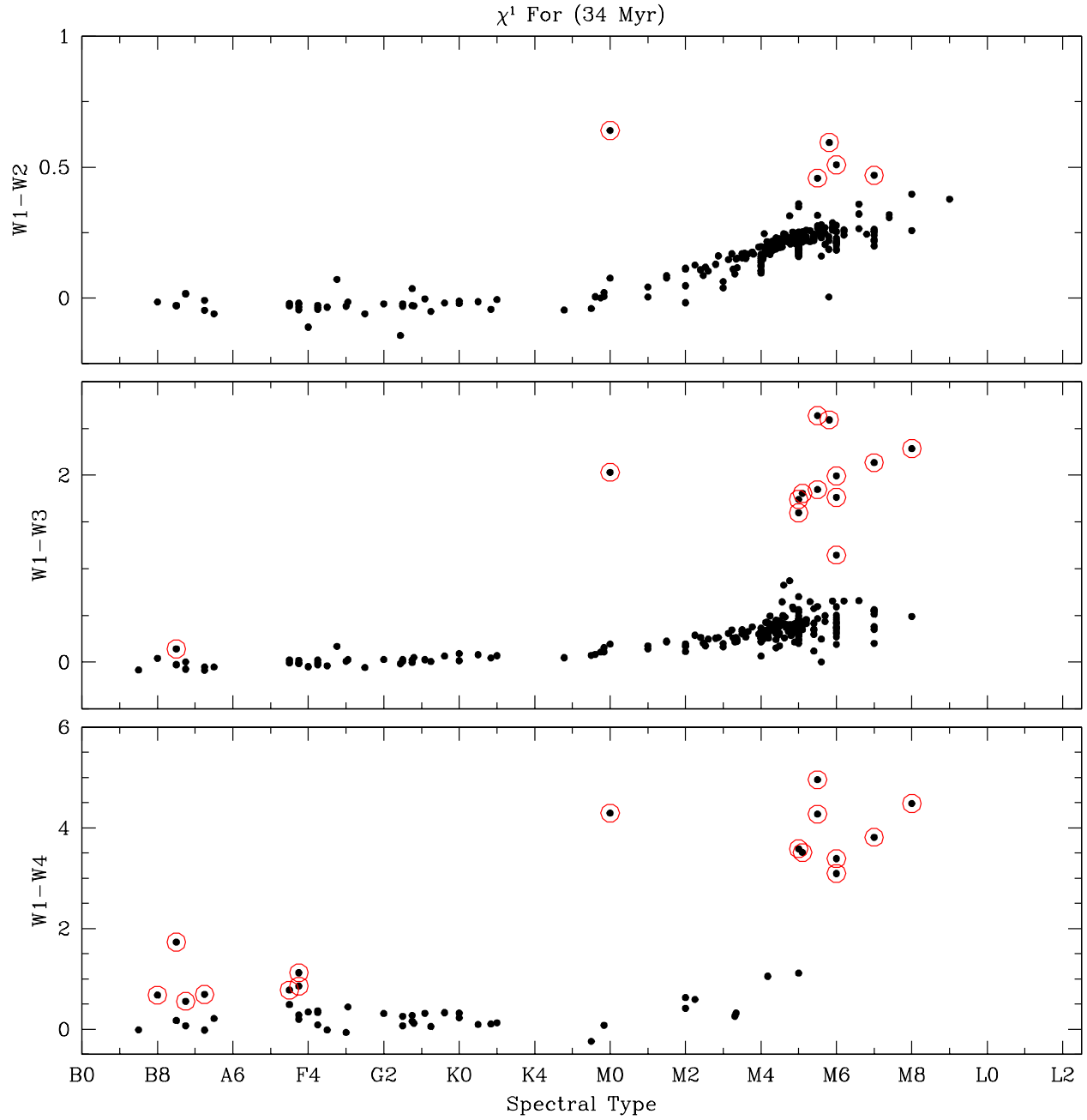


Figure 24. IR colors versus spectral type for adopted members of χ^1 For.

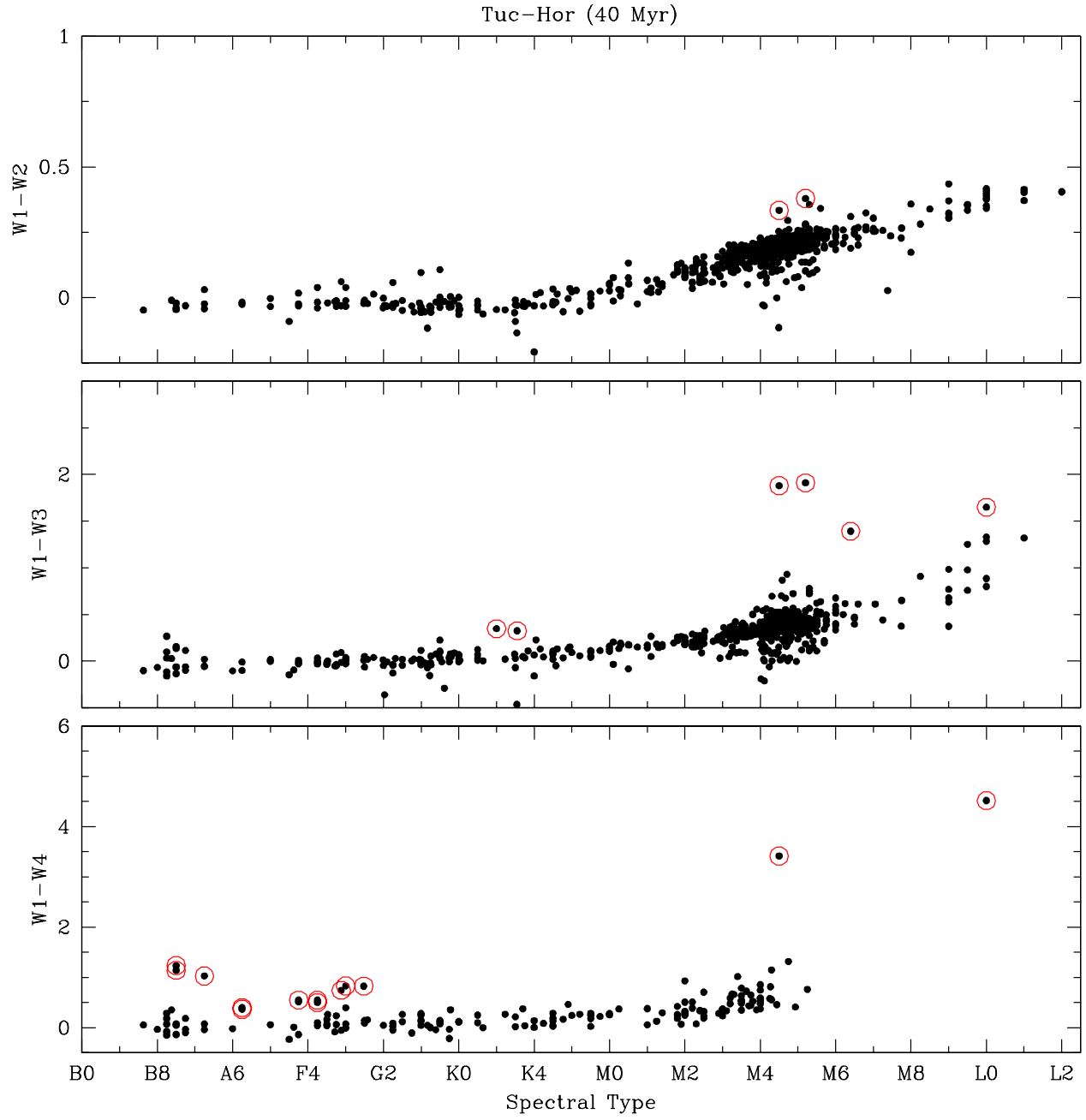


Figure 25. IR colors versus spectral type for adopted members of Tuc-Hor.

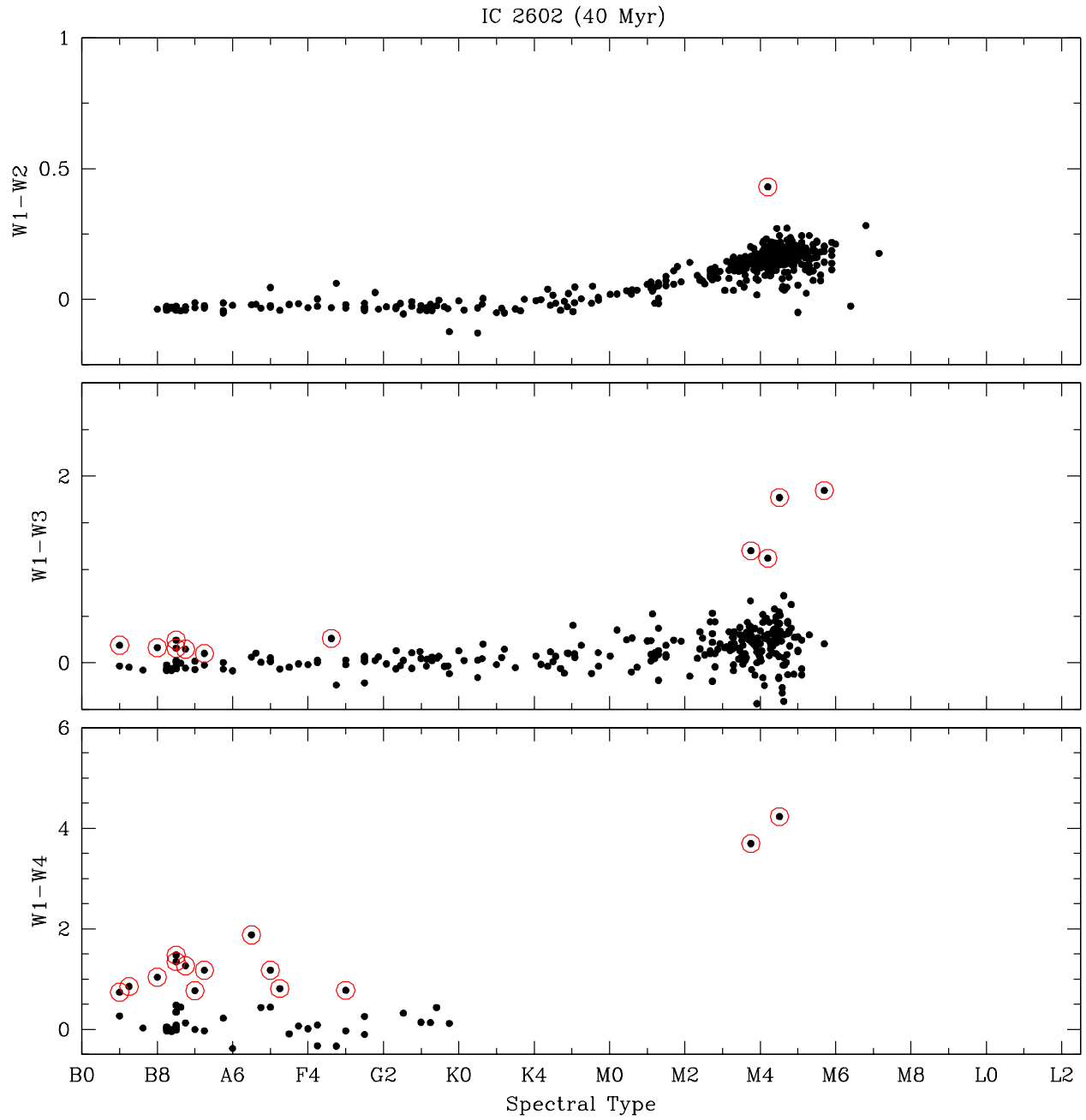


Figure 26. IR colors versus spectral type for adopted members of IC 2602.

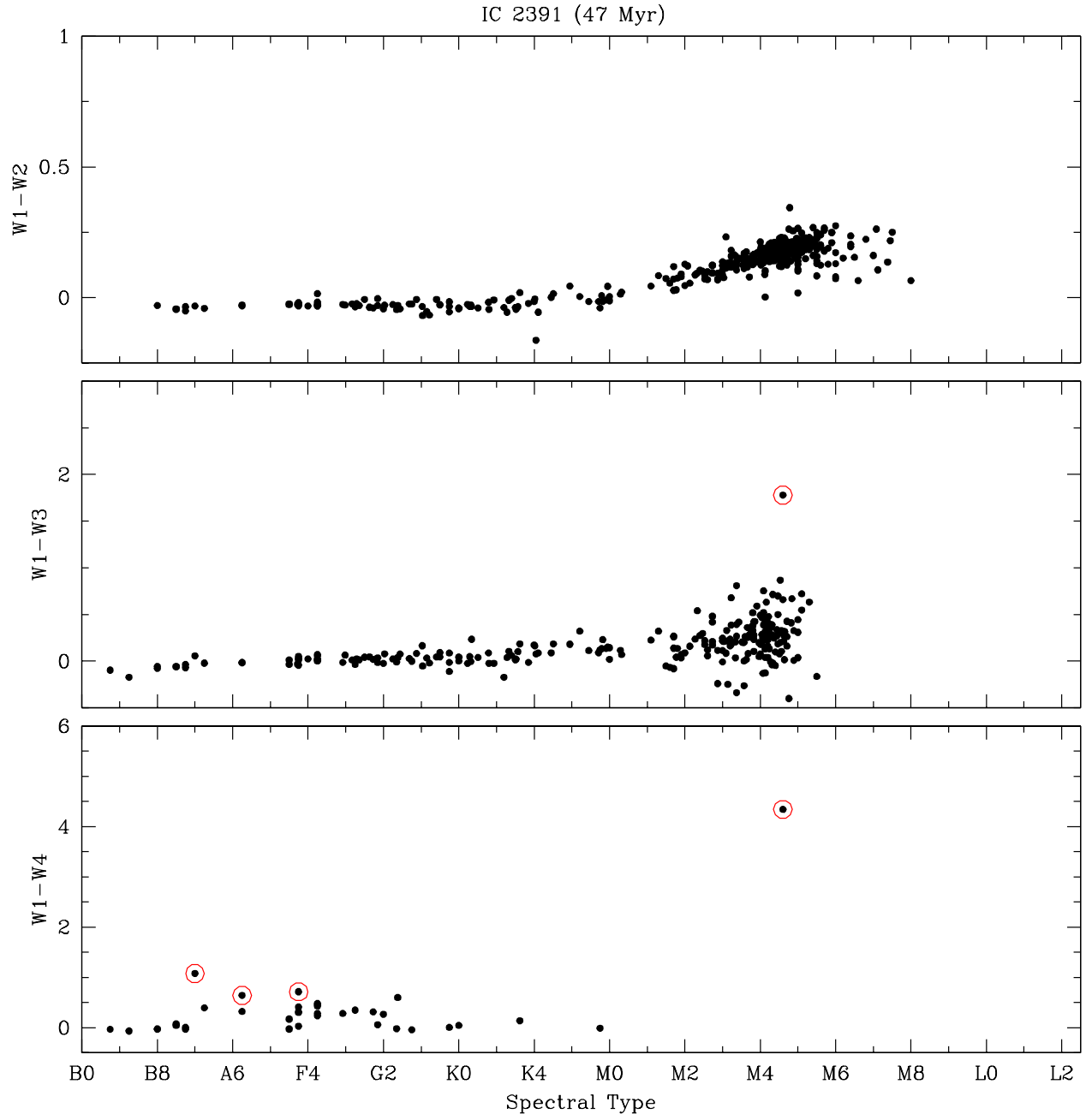


Figure 27. IR colors versus spectral type for adopted members of IC 2391.

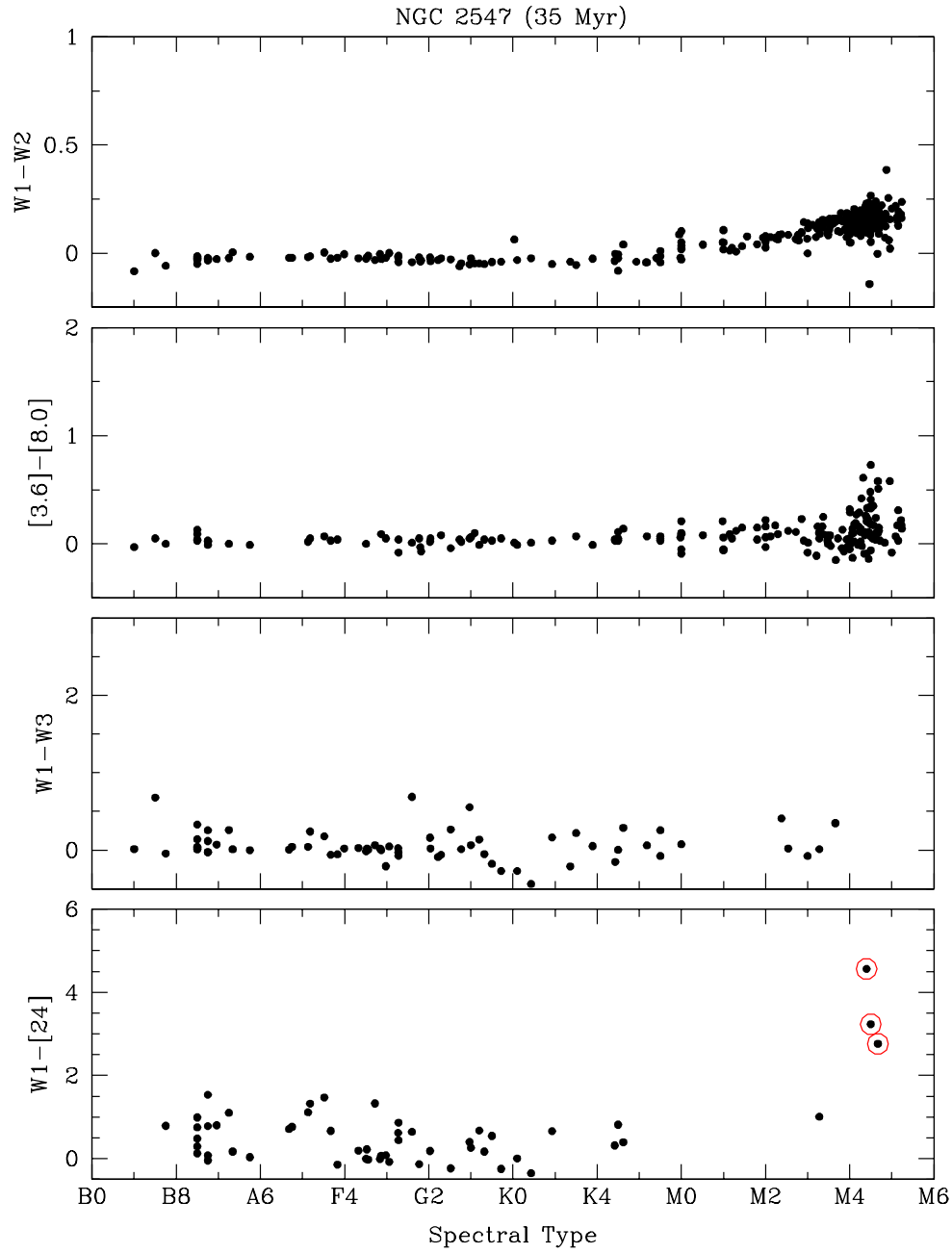


Figure 28. IR colors versus spectral type for adopted members of NGC 2547 (Gorlova et al. 2007; Forbrich et al. 2008, Table 5).

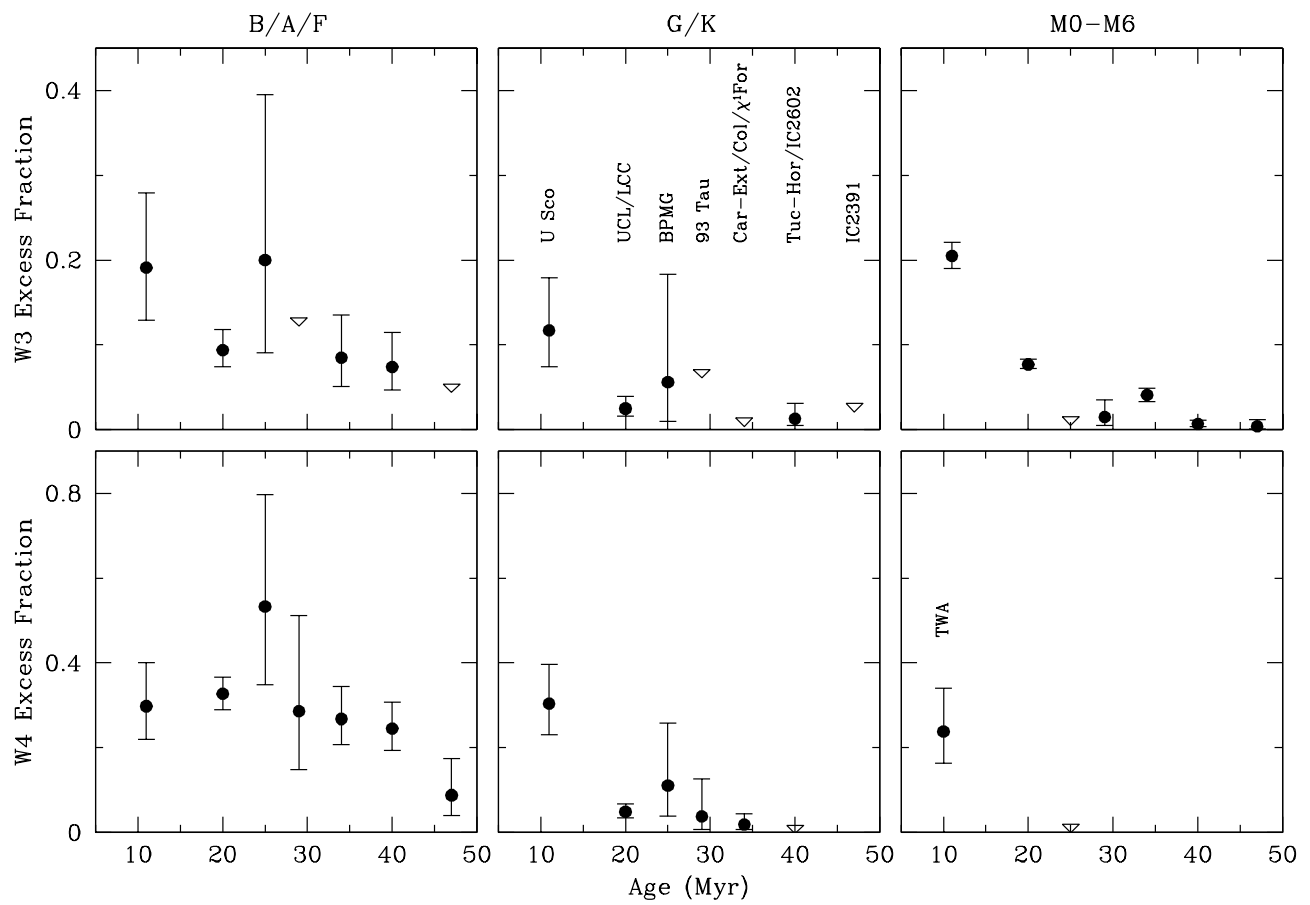


Figure 29. Excess fractions in W3 and W4 versus age for BPMG and other young associations (Table 6).